

André Marques Silva

Interface Improvement and Development of New Tools in the BobiSoft Software

Master's Thesis

September 2017



UNIVERSIDADE DE COIMBRA



FCTUC FACULDADE DE CIÊNCIAS
E TECNOLOGIA
UNIVERSIDADE DE COIMBRA

Interface Improvement and Development of New Tools in the BobiSoft Software

André Marques Silva

Coimbra, September 2017



Interface Improvement and Development of New Tools in the BobiSoft Software

Supervisor:

Professor Fernando J. T. E. Ferreira, Ph.D.

Jury President:

Professor Sérgio Manuel Ângelo da Cruz, Ph.D.

Jury Vowels:

Professor Paulo Jorge Carvalho Menezes, Ph.D.

Professor Fernando J. T. E. Ferreira, Ph.D.

Dissertation submitted in partial fulfillment for the degree of Master of Science in
Electrical and Computer Engineering.

Coimbra, September 2017

Acknowledgements

Os principais agradecimentos vão para a minha família: à minha mãe, pai, irmão e os meus queridos avós. Agradeço-vos todo o amor incondicional, que nunca ninguém poderá jamais substituir.

Aos meus amigos, aqueles me acompanham nos bons e maus momentos e me ajudam a seguir em frente. Sem eles sem sombra de dúvida nunca teria chegado até aqui! Inês Fonseca, Sandra Silva, Beatriz Oliveira, Jastin Soares, Diogo Vaz, João Mendes, Diogo Montes, João Coelho, Henrique Bastos e Renato Troca a todos vocês e aqueles que não nomeei o meu profundo agradecimento.

Ovviamente non potevano mancare i ringraziamenti ai miei amici Italiani. Tutti i momenti trascorsi insieme saranno sempre presenti nella mia memoria. Grazie, tutto è stato più semplice. Sino da quel momento ignorante del bagno per i deficienti! Silvia d'Angelo, Michele Roffi e Simone grazie mille. Luana Giliberto, senti.. mi basta solo dire una cosa: Bertelliii! Ci rivedremo cara, non smettere mai di essere quella che sei, grazie di cuore.

Finalmente, ao meu orientador o Professor Fernando Ferreira o meu muito obrigado pela oportunidade de desenvolver tal software e pela confiança que depositou em mim. A todos os professores que me ajudaram a crescer e tornar no engenheiro que serei, o meu obrigado. Ao professor Gabriel Falcão e ao investigador Manuel Rodrigues o meu muito obrigado por me ajudarem com a paralelização do código.

Resumo

Nesta dissertação, é apresentado o desenvolvimento da nova versão de um software de cálculo analítico, chamado BobiSoft, de projeto de enrolamentos estatóricos trifásicos.

O objetivo deste software é auxiliar e guiar a rebobinagem e projeto de enrolamentos de elevada qualidade e eficiência, sendo que a sua interface foi especialmente desenvolvida para o processo de rebobinagem. O software gera automaticamente 9 enrolamentos inteiros e simétricos, permitindo, porém, a implementação manual de quaisquer enrolamentos inteiros e fracionários, também eles simétricos. O software necessita de algumas informações relativas à geometria e tipo de enrolamento como dados de entrada. Com esses dados, o software apresenta resultados relevantes para a rápida avaliação da solução gerada.

O principal objetivo deste trabalho é o melhoramento do software para que este alcance um nível elevado de sofisticação e inovação, criando novas e importantes ferramentas para o projeto e avaliação de resultados. As ferramentas automáticas criadas têm o propósito de explorar ao máximo todas as oportunidades de melhoramento do projeto de enrolamento, deixando poucas possibilidades para mais melhoramentos. Em particular, foi desenvolvido um algoritmo iterativo que procura a melhor combinação de diferentes números de espiras por bobina e passo efetivo, de forma a minimizar o conteúdo harmónico da força magneto motriz do entreferro. Este algoritmo foi desenvolvido para poder ser paralelizado na CPU ou GPU, de modo a reduzir o tempo de execução. A redução do tempo de execução foi muito elevada.

Na parte final do trabalho, o software foi testado e os resultados formam bastante positivos, provando que as ferramentas foram corretamente desenvolvidas. Para além disto, foi realizada uma intervenção numa indústria de rebobinagem com o objetivo de a testar a robustez e a precisão do software numa situação real.

Palavras-chave: máquina de indução, software, projeto de enrolamentos, otimização de enrolamentos.

Abstract

In this thesis, the development of a new version of an analytical-based software named BobiSoft, for three-phase induction machine stator winding design, is presented.

The purpose of this software is to aid and guide the (re)designing of high-quality and high-efficiency windings, being specially designed for the rewinding task. The software automatically designs 9 integer winding configurations, but also allows the user to design free integer or fractional symmetric windings. It requires some basic information regarding the machine's stator geometry and winding as input data. The software then outputs relevant results which allow the user to quickly evaluate the computed solution.

The main goal of this work is to improve this software to a high level of sophistication and innovation, creating new and important features for winding designing and project evaluation. Innovative tools have been developed to exploit as much as possible the available opportunities for winding optimization, leaving only a few possibilities for further improvements. In particular, the development of an iterative algorithm that searches for the best combination of different number of turns per coil and effective coil pitch that minimizes the air-gap MMF harmonic content. In order to be fast, the algorithm was developed so it can be parallelized in the CPU or GPU. The speedup gain was huge.

In the last part of this work, the software was tested and the results were quite good, proving that the developed features are correct. In addition, an in-field test was successfully conducted in order to evaluate the software's robustness and accuracy in a real situation.

Keywords: induction machine, software, winding-design, winding-optimization.

It always seems impossible until it's done.

— Nelson Mandela

Contents

Acknowledgements	iii
Resumo	iv
Abstract	v
List of Acronyms	xii
List of Symbols	xiii
List of Figures	xvi
List of Tables	xviii
1 Introduction	1
1.1 Background	1
1.2 BobiSoft Overview	2
1.3 State of the Art	3
1.3.1 Final Considerations	8
1.4 Thesis Focus	9
1.5 Document Outline	9
2 Theoretical Foundations	10
2.1 Constructive Elements of Induction Machines	10
2.2 Electric Quantities of Induction Machines	15
2.3 Magnetic Saturation Analysis	18
2.4 Air-gap Magnetomotive Force and Winding Factors	20
2.5 Induction Machine Equivalent Circuit Parameters	22
2.5.1 Stator-Winding Resistance	22

2.5.2	The Magnetization Inductance	22
2.5.3	Stator Leakage Inductance	23
2.5.4	Stator Differential Leakage Inductance	24
2.5.5	Stator Slot Leakage Inductance	24
2.5.6	Zigzag Leakage Inductance	27
2.5.7	End-Winding Leakage Inductance	28
2.5.8	Referring the Rotor to Stator	28
2.6	Machine Parameters and Torque-Slip Curve	29
3	Routines and Algorithms	33
3.1	Automatic winding design	33
3.2	Main Computational Routine	36
3.3	Automatic Conductors Section Selection	37
3.4	Automatic Magnetic Flux Adaptation	38
3.5	Induction Motor Downsizing	39
3.6	Winding Optimization Tool	42
3.6.1	Formulation of the Winding Optimization Problematics	43
3.6.2	Proposed Algorithm	45
3.6.3	Iterative Method Limitations	48
3.6.4	Comparative Study	50
4	User's Interface	52
4.1	Data Input Interface	52
4.1.1	Winding Editing Tool Interface	53
4.2	Output Data Interface - Project Results	54
4.2.1	Machine Cross Section Diagram	54
4.2.2	Winding Pattern Schemes	55
4.2.3	MMF Air-gap Waveform Graph	57
4.2.4	Machine Parameters and Torque-Slip Curve Interface	58
4.3	Alternative Air-gap MMF Calculation	59
4.4	Core Loss Test Interface	60
4.5	Client Data Interface	61
4.6	Summary of BobiSoft 2.0 New Features	61

5	Experimental Validation	62
5.1	Machine Equivalent Circuit Parameters Test	63
5.2	Coil Pitch Optimization Test	64
5.3	In-field Test	66
5.3.1	Conclusions of the In-field Test	69
6	Conclusions and Future Work	71
	Bibliography	73
A	Experimental Magnetizing Curve	76
B	Air-gap Magnetomotive Force Analysis	79
C	Reference Values	84
C.1	Air-gap Induction Peak Reference Values	84
C.2	Current Density Reference Values	85
D	Rewinding Process	86

List of Acronyms

AC	Alternate Current
BLDC	Brushless DC motor
CPO	Coil Pitch Optimization
CDNTO	Coils with Different Number of Turns Optimization
DC	Direct Current
EMF	Electromotive Force
FEA	Finite Element Analysis
FEM	Finite Element Method
FFT	Fast Fourier Transform
MMF	Magnetomotive Force
NEMA	National Electrical Manufacturers Association
THD	Total Harmonic Distortion

List of Symbols

Symbol	Description	Unit
K_{active}	Active wire factor	
B	Air-gap induction peak	T
g	Air-gap length	m
\mathbb{F}_{peak}	Air-gap MMF peak	A.turn/m
THD	Air-gap MMF total harmonic distortion	
C_s	Carter's Coefficient	
τ_{coil}	Coil average pitch	slots
ζ_{coil}	Coil span	slots
C	Number of coils per phase	
S_{cond}	Conduction section	m ²
ρ_c	Conductor's density	kg/m ³
J	Current density	A/m ²
g'	Effective air-gap length	m
l_{si}	Effective stator core length	m
T_{em}	Electromagnetic torque	N.m
p	Machine's magnetic poles	
p_p	Machine's magnetic pole pairs	
s_n	Machine's slip of the n^{th} harmonic	
Ω_n	Magnetic field angular frequency	rad/s
ϕ	Magnetic flux per pole	Wb
τ_p	Magnetic poles' arc length	m
I_m	Magnetizing current	A
L_m	Magnetizing inductance	H
n_{pc}	Number of parallel groups	
m	Number of phases	

ω	Power source's electric angular frequency	rad/s
f	Power source's frequency	Hz
D_r	Rotor diameter	m
L_{lr}	Rotor leakage inductance	H
R_r	Rotor resistance	Ω /phase
K_s	Saturation coefficient	
τ_{slot}	Slot average pitch	m
w_{slot}	Slot average width	m
h_{slot}	Slot depth	m
K_{fill}	Slot fill factor	
w_{ss}	Slot opening width	m
w_{st}	Slot tooth width	m
S_{slot}	Slot useful section	m ²
Z	Number of slots	
D_{sb}	Stator bore diameter	m
P_w	Stator conduction Joule losses	W
l_{sc}	Stator core overall length	m
K_{sf}	Stator core stacking factor	
L_{ls}	Stator leakage inductance	H
L_{lds}	Stator differential leakage inductance	H
L_{les}	Stator end-winding leakage inductance	H
L_{lss}	Stator slot leakage inductance	H
L_{lzs}	Stator zigzag leakage inductance	H
R_s	Stator winding resistance	Ω /phase
n_s	Synchronous speed	rpm
W_s	Number of turns linked in series	
N_c	Number of turns per coil	
W_{ph}	Number of turns per phase	
μ_0	Vacuum permeability	Wb/(A.m)
I_w	Winding current	A
K_{wn}	Winding factor	
E_w	Winding voltage	V
σ_c	Wire conductor conductivity	S/m

l_w	Wire length per phase	m
M_w	Wire weight	kg
ceil	Upward rounding	
floor	Downward rounding	
mod	Remainder after division	

List of Figures

1.1	BobiSoft stator winding design computation process.	3
2.1	Slot Types.	11
2.2	Dimensions of a stator coil.	13
2.3	Carter's Effect [21].	14
2.4	Experimental normalized magnetization curve.	19
2.5	Magnetizing curve illustrating the formulation of the saturation factor [26].	19
2.6	Per-phase equivalent circuit of polyphase induction machines.	22
2.7	Leakage flux lines [23].	24
2.8	Stator slot magnetic field intensity of a two-layered winding [29].	25
2.9	Torque-slip curve, with the 5 th and 7 th parasitic torques [30].	29
2.10	Complete per-phase equivalent circuit including MMF spatial harmonic [23][31].	30
3.1	BobiSoft's 9 automatic winding designs.	34
3.2	Slot attribution array example ($Z = 12$, $p = 2$ and $m = 3$). Double-layer winding with a coil pitch of $\tau_{cp} = 5$	35
3.3	Flowchart of the eccentric/imbricated double-layer connection algorithm.	35
3.4	BobiSoft processing main routine (Compute Data).	36
3.5	Automatic selection of conductors section algorithm.	38
3.6	Average load factor by power range for electric motors in the EU, in the year 2000 [34][33].	39
3.7	Motor downsizing menu.	40
3.8	Constant power load type (torque-slip curve).	40
3.9	Coil pitch shortening optimization.	44
3.10	MMF symmetries.	44
3.11	Pole conductors symmetry. Number of turns attribution (N_0, N_1, \dots, N_k) [4].	44
3.12	Winding optimization algorithm flowchart.	46

3.13	Flowchart of the minimum MMF THD search algorithm (through the CDNTO).	47
3.14	Parallelization of the CDNTO algorithm on the CPU cores.	49
3.15	Parallelization of the CDNTO algorithm on the GPU cores.	49
3.16	CPO and CDNTO comparative performances.	50
4.1	Interface comparison between BobiSoft versions	53
4.2	(a) Winding editor menu. (b) Slot layering, U-upper, M-middle, and L-lower.	54
4.3	Machine cross section drawing procedures.	55
4.4	Winding pattern circular scheme drawing algorithm.	56
4.5	Winding pattern planar scheme.	56
4.6	Winding pattern planar scheme drawing algorithm.	57
4.7	MMF waveform graph.	58
4.8	Machine parameters and torque-slip curve interface.	58
4.9	Alternative air-gap MMF calculation interface.	59
4.10	Core loss test interface.	60
5.1	Coil pitch optimization experimental setup.	65
5.2	Frequency spectrum of the measured mechanical vibrations.	66
5.3	Uni-Motors motor parameters and torque-slip curve of the original and new projects.	69
A.1	Magnetizing curves of the 4 motors with different types of classes.	76
A.2	Stator cross section of the tested motors.	77
B.1	Current-sheet produced by N_{ck} conductors placed in the slot k	80
D.1	Rewinding process procedures - Part I.	87
D.2	Rewinding process procedures - Part II.	88
D.3	Different procedures of the winding's extraction: (a) mechanical procedure, and (b) heating procedure.	89

List of Tables

2.1	Slot useful section and depth formulas.	10
2.2	Machine's leakage reactances proportion of different motor classes [24].	31
3.1	Flux adjustment equations as function of the load type [33].	42
3.2	Winding characteristics.	50
5.1	Comparison between measured and simulated stator equivalent circuit parameters of IE1-4 induction machines.	63
5.2	BobiSoft projected windings' characteristics.	65
5.3	Coil pitch winding optimization experimental results.	65
5.4	SIMRIA rewinding project results.	67
5.5	Uni-Motors rewinding project results.	68
A.1	Magnetizing and B-I curves	78
B.1	Phase winding factors and direct, reverse factors relationship.	83
C.1	Air-gap induction peak reference values (EFACEC manufacturer, 2004).	84
C.2	Current density reference values (EFACEC manufacturer, 2004).	85
C.3	Current density correction factors (EFACEC manufacturer, 2004).	85

Chapter 1

Introduction

1.1 Background

Electric motors are indispensable components of any industrial facility across the world and by far the most important electric load. The power consumed by electric motors accounts for two-thirds of the total electrical energy used for commercial/industrial applications in the developed world. In Europe and the United States alone, the annual cost of energy consumed by these loads is estimated at over \$100 billion U.S. dollars. Therefore, any improvement of motor's efficiency may bring significant energy savings to the companies and increase the world's sustainability. In normal operating conditions, a motor's lifetime energy cost often surpasses the motor's acquisition price. Thus, due to rising energy costs over the past two decades, high efficiency motors may be preferable to cheaper, less efficient ones [1].

It is known that a single motor failure can negatively impact a company's short, medium, or even long term competitiveness and profitability. Therefore, effective maintenance and management strategies must be adopted to avoid or minimize those impacts. In addition, motors repaired or rewound by highly qualified professionals assure operation reliability and reduce maintenance costs. In fact, whenever the failure is the stator winding (30%–40% of all induction motor faults), the price of the rewinding service varies from 20% to 40% of the acquisition price for a new motor [2][3].

In consideration of the foregoing, rewinding services have great importance for a motor's maintenance, since, in general, induction motors over 4kW are rewound 2 to 4 times during their service life. Since the payback period to recover the extra cost of a new motor acquisition is, in most cases, more than 3 years, this repairing service is an interesting low-cost alternative for all efficiency classes [4].

During motor repair, some modifications can be made to increase its reliability and efficiency. On account of the largest loss share being associated with the stator winding

Joule losses, the winding redesign is an excellent opportunity for the machine's efficiency improvement. Thus, more complex winding can be designed and implemented, free of the limitations that large-scale, automated motor manufactures have. These optimizations may involve adapting the magnetizing flux to the motor's effective load, increasing the slot fill factor for better heat dissipation, and shortening the winding pole pitch in order to reduce the amount of conductor material needed and the magnetomotive force harmonic content [4]. In fact, winding electric quantities are almost only determined by the winding pattern. More specifically, winding factors (and the related MMF harmonic content), the back EMF harmonic distortion, currents, and magnetic flux densities. These quantities affect significantly the machine's dynamic and steady-state performances, efficiency, the increase of the machine's vibration, and noise levels [5].

Nowadays, most winding designs follow simple winding patterns that have been developed over many decades, and the principles of their development are commonly forgotten [6]. For most applications these designs work fine, though it might be possible that the winding is inadequate as well. For this purpose, and to help rewinders/technicians or engineers to project winding designs correctly and accurately, a software tool named BobiSoft was developed in 2004. The development of the newest version is the work presented in this document.

1.2 BobiSoft Overview

BobiSoft is an analytical software for induction machine stator winding design. It has been specifically developed for the rewinding design of three-phase windings of induction machines. For this reason, the software allows two different windings to be designed and evaluated simultaneously, for an easy and fast comparison, one belonging to the original winding pattern to be rewound (original project), and the other one corresponding to the replacement winding design (new project). The flowchart of figure 1.1 explains the software's computational process.

The main calculation routine of this program follows the following steps:

- Some basic data related to the machine's dimensions, winding data, and desirable preferences are entered by the user, so that the software can test its validity;
- The program computes the data and calculates key parameters, such as air-gap magnetic induction, conductor's current density, and slot fill factor;

- These parameters are then compared to reference values and warnings are emitted, whenever they exceed their limits;
- The routine finishes at this point. If a parameter does not respect the reference values, a permanent warning is shown to remind the user that the solution might not be adequate. Otherwise, if automatic tools are used, the routine is repeated until the project becomes valid, if possible.

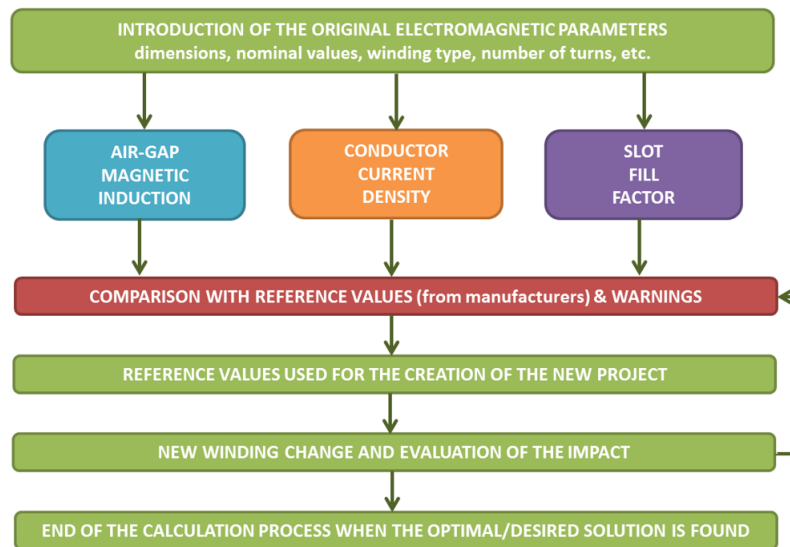


Figure 1.1: BobiSoft stator winding design computation process.

BobiSoft is also a didactic tool, since it can be used in technical/academic courses as well as in industrial training programs.

1.3 State of the Art

This section presents and discusses various innovative products/studies that are somehow related to the work developed in this dissertation. The following text is a list of some of the electric machine/motor design software available on the market. Please note that this list may not cover all the existing software, though it is the result of an exhaustive research.

- **AC Motor Design Software** by Softbit Technologies - This is an online design tool of three-phase squirrel cage induction motors, up to 50 hp. The software is compared to a specialized calculating tool created to assist preliminary designs of a motor, providing an intuitive interface and quick simulations. The user enters basic data of the AC electric motor, such as capacity (rated power), voltage, speed, power factor, and

required efficiency. Then, the design tool computes the solution automatically and the results are shown. Different results or optimizations can be generated by manually changing the input parameters, such as specific electric loading, specific magnetic loading, number of slots, current density, stator dimensions, and others, in order to suit the design's application. The software automatically designs single- and double-layer stator windings [7].

- **EMETOR** by EMETOR - This is the world's first online electric motor design software. It was developed during the years 2003-2008 at the Electrical Machines and Power Electronics lab of the Royal Institute of Technology in Stockholm, Sweden. The software is free and aims to make electric motor designs more efficient as well as to be a fast and intuitive analytical tool, while being accurate and powerful as a finite element tool. This tool deals with linear and non-linear materials, simulating magnetic saturation under load and no-load circumstances. The machines supported by EMETOR are Inner-/Outer-rotor surface-mounted permanent magnet machines, although it also offers a winding design tool, which designs AC distributed windings, suitable for other electric machines like induction motors. The winding design tool allows the user to find the optimal configuration for its electric motor winding. Many solutions can be investigated for integer, fractional (both single- and double-layer windings), and concentrated windings. The user can compare the maximum fundamental winding factor for different combinations of number of poles and number of slots. As outputs, the software displays winding layouts for different coil spans and barcharts of the MMF harmonic spectrum [8].
- **JMAG motor** by JSOL Corporation - It is an FEM analysis-based application for electromechanical designs specially adapted for electric motors. This software evaluates complex phenomena, such as heat generation, temperature distribution, eccentricity, stress, vibrations, radiated sound, magnetization, demagnetization, and skew effects. It also evaluates basic characteristics, such as induced voltage, torque, cogging torque, flux linkage, iron losses, coil losses, magnet loss, magnetic material permeance, and equivalent circuit model parameters extraction. The stator winding design can be automatically or manually edited for single- and double-layer windings. The user inputs basic winding data and the software outputs the winding pattern, respecting some specific requirements such as the maximum slot fill factor. There is no information regarding available automatic winding optimization tools [9].

- **MagneForce Simulation Suite** by MagneForce Software Systems Inc. - Is an FEA-based design tool with modules for synchronous generators, brushless and brush-commutated DC machines, and induction machines. The manufacturer claims the software is the first finite element development environment exclusively targeted for the design and simulation of electric motor and generator systems. The induction motor module (INDU) can simulate single- and polyphase winding designs. The software calculates key parameters, such as torque, torque-speed curve, iron losses, flux density distribution, machine power and efficiency. INDU's winding design tool has a large library of parameterized slot modules which is used to automatically generate the AC distributed winding pattern. Manual winding designs can be drawn from scratch. There are no automatic optimization tools for the stator winding [10].
- **MotorAnalysis** by Vladimir Kuptsov, Ph.D - MATLAB-based, it consists of a free three-phase induction motor design software. MotorAnalysis is based on FEA-simulations and establishes a complete set of tools for the design and analysis of induction motors. Regarding the stator winding editor, it automatically or manually designs single- and double-layer winding layouts. In addition, it allows the design of windings with coils with different number of turns. Optimizations are made to the machine/stator geometry, and the stator winding can be optimized manually attempt by attempt. The project data is computed at a speed defined by the user, depending on the speed/accuracy trade-off. Key parameters are generated, such as equivalent circuit parameters (based on no-load and load test simulations), power, torque, power factor, efficiency, losses for different operating points, and efficiency maps. The software estimates the temperature effects on winding resistances, as well as the nonlinear behavior of magnetizing inductance. In addition, SIMULINK models, based on the motor equivalent circuit parameters, are generated [11].
- **Motor-CAD** by Motor Design - Is an FEA-based electric machine design tool that computes electromagnetic and thermal fields. It supports the thermal analysis of brushless permanent magnet, induction, permanent magnet DC, switched reluctance, synchronous, and claw pole machines. Motor-CAD is a complete electric machine design software with a stator winding design tool that automatically designs single- and double-layer windings. Fractional winding patterns are also supported as well as windings with different turns number per coil. Manual patterns can be also implemented. There are no automatic stator winding optimization tools. Since Motor-CAD

is specialized in electromagnetic and thermal analysis, it offers, instead, many tools to optimize the stator teeth geometry and the conductors positioning inside slots. The results are presented in an easy-to-understand format and allow designing decisions to be taken efficiently by the user [12].

- **MotorSolve** by Infolytica Corporation - It is one of the most notorious software for electric machine design and analysis. It supports induction, synchronous, electronically- and brush-commutated machines. This software aims to aid the user in designing electric machines, and for this reason all machine parts are editable. It uses FEM algorithms to solve thermal and flux density fields and output key parameters related to machine performance, such as torque, efficiency, air-gap flux, cogging torque, and efficiency maps (chart of the motor's efficiency at different speeds and torque). This software is almost fully automatized, thus many complex operations like FEA-mesh refinements and post-processing are handled by the program itself. In MotorSolve the stator winding can be automatically or manually designed. The automatic design tool just needs basic input parameters, such as the pole, slot numbers, coil span, phase offsets, and the winding layout options are automatically generated. For each one of these layouts the back EMF, back EMF harmonics, and winding factors are immediately calculated. The manual winding design only allows the coils placement and the coils' turn number must be the same. During the simulation, the software considers the complex effects of the motor drive type, end winding geometry, layer positioning, slot and wire insulation. There are no automatic winding optimization tools [13].
- **Opera** by Vector Fields Software, Cobham - This is an FEA-based electric machine design software. Opera provides tools for designing electric machines with axial or radial flux topology and rotating or linear motion. The software aims to help engineers design highly efficient, reliable, and low cost electric machines. Parameterized templates allow designers to quickly establish and analyze motor and generator models. Opera has a dedicated winding tool which designs automatically single- and double-layer windings. It calculates, for each project, several winding patterns to be used. This tool provides optimal winding layout (circular and linear representation), star of slots representation, G6rges diagram, winding factors, and MMF harmonics. In addition, as a winding optimization tool, the built-in Winding Wizard can be used to set a range of slots and poles, in order to understand how a particular slot-pole combination of machine winding will optimize the machine's performance. The resulting data can

be used to help the designer choose the most suitable winding pattern [14].

- **Quick Field** by Tera Analysis - It is an FEA-based tool for electromagnetic, thermal, and stress design simulations. It has different available modules, such as DC-magnetics for DC, switched reluctance and synchronous motors, and AC-magnetics for induction motors. It was not possible to find relevant information about supported winding designs and automatic winding tools [15].
- **SmartFEM** by elmoCAD - This is a development system for electric machines that combines analytical calculations with numerical FEM. It uses professor Konrad Reichert's simulation package FEMAG, as an FEM solver. The software calculates some characteristics of the electric machine, such as back EMF, torque, cogging torque, inductance, dynamic behaviors, among others. The winding editor allows the automatic design of single- and double-layer integer/fractional windings. As default, the software computes automatically the winding scheme out of simple winding data (phase number, coils per slot, number of slots and poles, etc.). The impact of back EMF and fluxes is shown immediately. Fill factor, phase resistance, and the winding factors are calculated. The winding can be optimized by manually changing some parameters and comparing each result. SmartFEM supports winding configurations with coils with different number of turns [16].
- **SPEED** by CD-adapco - Analytical tool with FEA support for electric machine design. Speed supports brushless permanent magnet, induction, switched reluctance, DC commutator and universal motors. Developed by Prof. TJE Miller in the Speedlab at the University of Glasgow, SPEED has been acquired in 2011 by CD-adapco, a provider of CAE simulation tools for fluid dynamics and heat transfer, this software can be used with third party tools such as Motor-CAD. SPEED has several packages for different electric machine designs. The induction motor package, concerning the stator winding design, has an editor that allows the user to introduce integer and fractional single- and double-layer windings. There are no automatic optimization tools, though SPEED can be scripted into searching algorithms for a specific optimal solution. As an example, the work of Mario Jurkovic [17], where he created an algorithm, which linked MATLAB, SPEED, and Motor-CAD together in order to design a highly efficient ultra-light BLDC motor by changing the machine's constructive parts, for the propulsion of an ultra-light aircraft [18].

- **YES electric motor design software** by Yeadon Energy Systems Inc. - This is an analytical induction motor design software. It handles single- and polyphase motors, including capacitor start and split phase motors. Basic information about the motor, such as dimensions, material properties, and winding data is needed to compute the motor project design. This tool outputs the following results: magnetic circuit information (including flux densities and MMF drops), mechanical information (weights and inertias), winding information (including copper weight and slot fill), performance, speed-torque, current, losses, and efficiency. The winding pattern is inserted and optimized manually [19].
- **Software for Electric Machines Winding Design** created by Antonino Oscar Di Tommaso, Fabio Genduso, and Rosario Miceli, from the Department of Energy, Information Engineering and Mathematical Models of the University of Palermo, Italy. It consists of a MATLAB-based software developed for rotating electrical machine winding design. In order to design the stator winding, only a few elements are required, such as the numbers of slots, pole pairs, and number of phases. The software automatically designs integer and fractional winding patterns. Key results for the winding design quality evaluation are shown, such as the spectrum of winding factors, the spatial distribution of MMF and its relative harmonic content, the leakage coefficient, among others. The user can manually optimize the computed design by introducing simple and double-pitch shortening, phase belt shifting or interleaving, or other well-known techniques, in order to reduce the THD and the higher order harmonic slot coefficients of the EMF or MMF [5].

1.3.1 Final Considerations

Considering the tools mentioned in this list, it is clear that many softwares, based on finite element analysis, have been developed to solve the complex magnetic and thermal field problems in electric machines or power electronic drive systems. Without disregarding the importance of these analyses for the sake of high quality electric machine designs, it is clear that either stator winding design is being overlooked or designers deem it less important even though most electric machine designs rely on the fundamental flux wave theory, thus the achievement of a sinusoidal flux density distribution in the air-gap with the lowest possible harmonic content is necessary [20]. The software developed by the researchers at the University of Palermo is the only one that is fully developed for this purpose. SPEED

offers the potential to develop a general winding optimization tool that requires several days dedicated to the script's creation, but an algorithm for the creation of a general winding optimization tool was yet not developed. Other software from the presented list slightly tackle this issue with some specialized tools, but the computational efforts go mainly to geometry optimization. Finally, it is important to note that none of the presented software include a fully automated tool for winding optimization.

1.4 Thesis Focus

BobiSoft's previous version never had major updates, despite being used by hundreds of users across the world. Thus, there was a need to develop a new interface, to review some computing processes, and to create new important features to rewinding companies.

The focus of this work is BobiSoft's 1.1 renewing, reviewing, and improving all features in such a way that they become more intuitive and easy to use. There was a development of new automatic tools, for the sake of high quality and high efficient winding designs. The main goal of this work was the creation of a more powerful software that has sufficient tools to investigate more optimization opportunities. Therefore, BobiSoft was completely rewritten in the C++ language and redeveloped on Qt platform, thus creating BobiSoft 2.0.

1.5 Document Outline

The following is a brief description of the contents present in each chapter:

Chapter 2 presents the theoretical support of the developed calculation processes and algorithms used to compute the software's projects solutions.

Then, in chapter 3 the most complex algorithms and routines of the software are presented, from the algorithms behind the winding's representative schemes creation to the winding optimizing tools. This chapter uses the knowledge acquired in the previous chapter.

Chapter 4 describes the software's interface. Here, the software's input and output data methods are explained, as well as the most relevant new interfaces created and renewed.

Finally, chapter 5 presents the experimental tests performed to validate the software's quality and the simulations' accuracy. An in-field intervention was conducted in order to prove the software's applicability in the maintenance companies' reality.

Chapter 2

Theoretical Foundations

2.1 Constructive Elements of Induction Machines

This section presents the calculations used to determine the mechanical and magnetic quantities of induction machines.

Air-gap Length

The air-gap length g is defined as the distance between the rotor surface and the stator bore (eq. 2.1). The software only supports smooth and uniform rotor cores.

$$g = \frac{D_{sb} - D_r}{2} \quad (2.1)$$

Where D_{sb} is the stator bore diameter (mm), and D_r is the rotor diameter (mm).

Slot Useful Section and Depth

The slot's useful cross section is the available area for the conductors placement inside the slot. The software has five different types of slots, all represented in figure 2.1, which cover almost all standard stator slot geometries. In table 2.1, the formulas used to calculate the slot's useful section S_{slot} , and depth h_{slot} of the different 5 types of slots, are presented.

Table 2.1: Slot useful section and depth formulas.

Slot Type	Slot Useful Section (mm ²)	Slot Depth (mm)
A	$S_{slotA} = \frac{a^2\pi}{2} + d \cdot a + \frac{(d+2a+2c) \cdot b}{2} + \frac{c^2\pi}{2}$	$h_{slotA} = e + c + b + a$
B	$S_{slotB} = \frac{c^2\pi}{2} + \frac{(a+2c) \cdot b}{2}$	$h_{slotB} = d + c + b$
C	$S_{slotC} = \frac{c^2\pi}{2} + \frac{(a+2c) \cdot b}{2} + \frac{a^2\pi}{2}$	$h_{slotC} = d + c + b + a$
D	$S_{slotD} = \frac{(w_{ss}+e) \cdot c}{2} + \frac{(e+a) \cdot b}{2}$	$h_{slotD} = d + c + b$
E	$S_{slotE} = \frac{(w_{ss}+f) \cdot d}{2} + \frac{(f+2a) \cdot c}{2} + 2a \cdot b + \frac{a^2\pi}{2}$	$h_{slotE} = e + d + c + b + a$

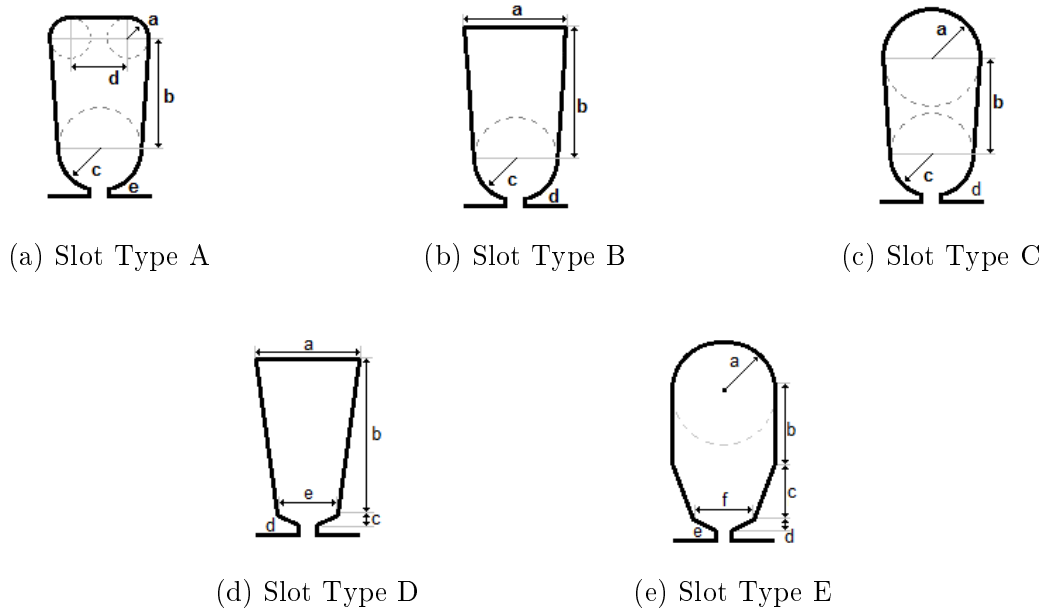


Figure 2.1: Slot Types.

Where w_{ss} is the slot's opening width (mm).

Slot Pitch

The slot pitch τ_s is defined by the arc length measured at the center of two adjacent slots. The stator slot pitch is calculated by equation 2.2:

$$\tau_s = \frac{\pi}{Z} \cdot (D_{sb} + h_{slot}), \quad (2.2)$$

where Z is the number of stator slots.

Slot Average Width

The average width of a slot w_{slot} is the quotient between its area and its depth. It is calculated, in mm, by equation 2.3:

$$w_{slot} = \frac{S_{slot}}{h_{slot}}. \quad (2.3)$$

Number of Turns per Phase

The number of turns per phase (W_{ph}) is the simple summation of the turns number of the coils belonging to the same phase. This number is equal to all phases, since the software only supports symmetric windings.

Weighted Average of Coil Pitch

The coil pitch τ_{coil} is defined as the peripheral length between two sides of a coil, measured in slots (eq. 2.4), where C is the number of coils per phase, ζ_c is the span of coil c in slots, N_c is the number of turns of coil c , and W_{ph} is number of turns per phase. Contrary to the previous version, the program does now support windings with different turn number per coil, thus not only the mean of the coil pitches is performed, but also the number of turns of each coil, affecting the weight of each coil pitch in the arithmetic average.

$$\tau_{coil} = \frac{\sum_{c=1}^C \zeta_c N_c}{W_{ph}} \quad (2.4)$$

Conduction Section

The conduction cross section S_{cond} is defined by the summation of the sections of all parallel conductors linked in series (eq. 2.5). The number of winding parallel groups (n_{pg}) does not affect the conduction section, but the current to which these conductors are submitted to.

$$S_{cond} = \sum_{k=1}^{n_{pc}} S_k \quad (2.5)$$

Where n_{pc} is the number of parallel conductors, and S_K is the section (mm²) of conductor index k 's.

Slot Fill Factor

The slot fill factor K_{fill} is the quotient between the total active conductor cross section and the slot useful section (eq. 2.6). It represents the difficulty of the rewinding task: the bigger this factor is, the more difficulty to implement the winding the rewinder will have. Because BobiSoft allows different number of turns per coil, the resultant slot fill factor corresponds to the most filled slot.

$$K_{fill} = \max \left\{ \frac{S_{cond} \cdot N_c}{S_{slot}} \right\}, c \in \{1, 2, \dots, C\} \quad (2.6)$$

Conductor Wire Length per Phase

The total wire length ($l_{w,ph}$) needed to wind a phase is the sum of all the coils wire lengths of a same phase (eq. 2.7). Each coil wire length is calculated on the basis of the dimensions of two layouts: rounded and triangular, being schematized in two dimensions in figure 2.2.

$$l_{w,ph} = \sum_{c=1}^C 2N_c [l_{sc} + l_{ad} \cdot K_{lw} \cdot l_{cs}], \quad (2.7)$$

where l_{sc} is the stator core overall length (mm), l_{ad} is the additional coil head length (l_{ad}) defined by the user as a percentage of the winding head,

$$l_{cs} = \tau_s \cdot \zeta_c,$$

and K_{lw} is the head shape's coefficient: $K_{lw} = \pi/2$ for rounded shape and $K_{lw} = \sqrt{2}$ for triangular shape.

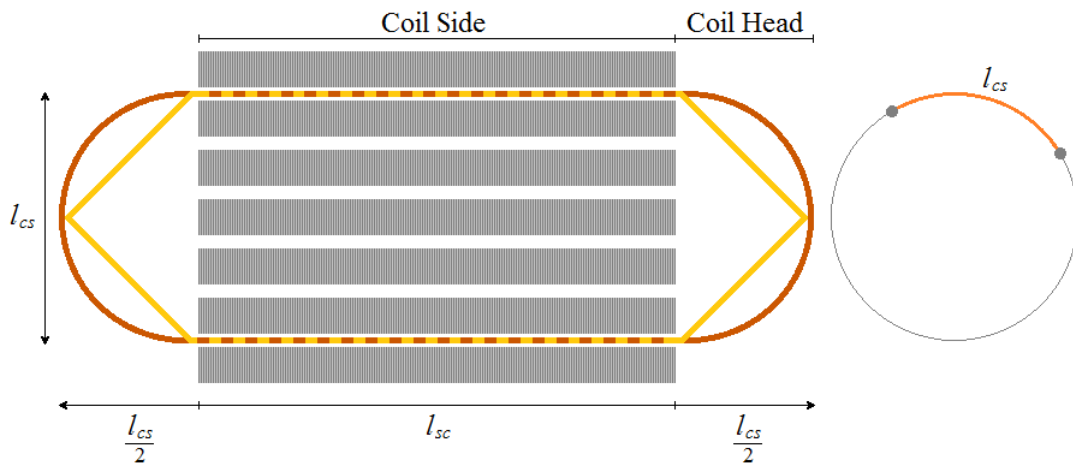


Figure 2.2: Dimensions of a stator coil.

Winding Conductors Weight

The winding conductors weight is determined through equation 2.8:

$$M_{wire} = m \cdot (\rho_c \cdot S_{cond} \cdot l_{w,ph}) \quad (2.8)$$

where ρ_c is conductors material density (kg/m^3) and m is winding number of phases.

Active Wire Factor

The active wire factor K_{active} is the relationship between the active wire length, which produces the useful air-gap electromagnetic torque and the wire total length (eq. 2.9). The bigger this factor is the more efficient is the winding, since the stator resistance and the end-winding leakage inductance are reduced.

$$K_{active} = \frac{l_{sc} \cdot W_{ph}}{l_{w,ph} - l_{sc} \cdot W_{ph}} \quad (2.9)$$

Effective Air-gap Length - Carter's Coefficient

Ideally, the magnetic flux is uniformly distributed along the air-gap. In a slotted armature, the effective area of flux path is considerably reduced because the magnetic flux tends to circulate inside low reluctance paths. Thus, slotted cores have uniform and high

flux density underneath the core teeth (iron - very high permeability), contrary to the flux distribution within the slot opening (air - very low permeability), as shown in figure 2.3.

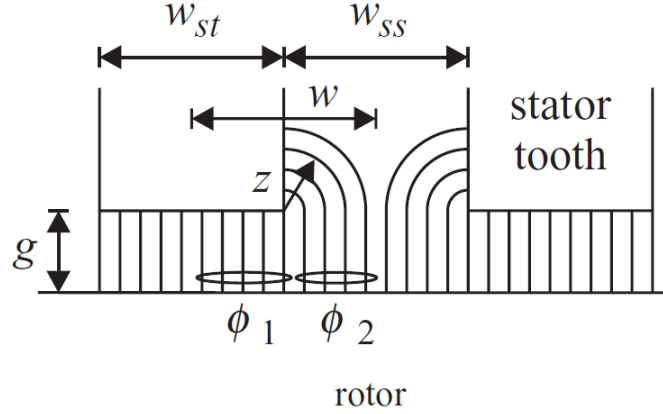


Figure 2.3: Carter's Effect [21].

The Carter's coefficient C_s incorporates this effect by replacing the physical air-gap g with a modified air-gap g' (eq. 2.10)[21]:

$$g' = g C_s. \quad (2.10)$$

In order to obtain the Carter's coefficient value, the flux inside a slot pitch is divided in two parts of the magnetic flux (fig. 2.3). Equation 2.11 mathematically represents this flux division:

$$\phi = \phi_1 + \phi_2. \quad (2.11)$$

Given the modified air-gap, assumptions of a uniformly distributed flux along the slot pitch may be considered. This way, the magnetic flux can be determined by equation 2.12:

$$\phi = \frac{\mu_0 \mathbb{F} w_{st} l}{2g'} (w_{ss} + w_{st}), \quad (2.12)$$

where w_{ss} is the tooth width of the slot, and w_{st} is the length of the air-gap opening.

Then, the corresponding terms for the different flux parts are expressed in equations 2.13 and 2.14:

$$\phi_1 = \frac{\mu_0 \mathbb{F} w_{st} l}{2g}, \quad (2.13)$$

$$\phi_2 = \frac{2\mu_0 \mathbb{F} l}{\pi} \ln \left(1 + \frac{\pi w_{ss}}{4g} \right). \quad (2.14)$$

By solving equation 2.11 through equations 2.12, 2.13, and 2.14, and solving it in order of g and g' , Carter's coefficient can finally be found (eq. 2.15). The complete analysis can be found in [21].

$$C_s = \frac{w_{ss} + w_{st}}{w_{st} + \frac{4g}{\pi} \ln(1 + \frac{\pi w_{ss}}{4g})} \quad (2.15)$$

2.2 Electric Quantities of Induction Machines

In this section, the machine electric quantities used by the program to compute the project's solution are defined.

Magnetic Field Synchronous Speed

The air-gap rotating magnetic field, created by a correctly distributed polyphase winding, revolves at a speed (n_s) given, in rpm, by equation 2.16:

$$n_s = \frac{120 \cdot f}{p} \quad (2.16)$$

where f is the voltage supply frequency (Hz), and p is the number of the machine's poles.

The direction of rotation of the magnetic field is imposed by the voltage supply sequence. Swapping the connections of two of the three phases will reverse the rotation direction.

Winding Voltage

The three-phase machines supported by the program have 6 terminals, which can only be wye or delta connected. The connection type will impose the voltage to each winding phase (E_w). In case of wye connection, the phase voltage is $\sqrt{3}$ times smaller than the line voltage. Otherwise, the phase voltage is equal to the line voltage.

The phase voltage of two- and single-phase machines is equal to the line voltage. For both cases the line voltage is inserted by the user as the nameplate rated voltage.

Winding Current

Similar to what happens with the winding voltage for three-phase machines, the winding current (I_w) also depends on how the winding is connected. In the case of wye connection, the phase current is equal to the line current. Otherwise, the phase current is $\sqrt{3}$ times smaller than the line current.

The phase current of two- and single-phase machines is equal to the line current. The line current is the nameplate rated current.

Current Density

The current density (J) is the electric current of a conductor cross section per unit area in A/mm² (eq. 2.17). The program does not take into account the skin effect, which may occur due to high frequency currents. Consequently, this result is always underestimated.

$$J = \frac{I_w}{S_{cond}}, \quad (2.17)$$

where I_w is the winding rated current.

It is known that the machine's heating is directly related to the winding current density. Therefore, this value is extremely important for the project's quality evaluation, being compared with typical values, so that it does not exceed them.

Winding Joule Effect Losses

The stator winding conduction losses, per phase ($P_{w,ph}$), are given by the equation 2.18:

$$P_{w,ph} = R_s I_w^2, \quad (2.18)$$

where R_s is the winding resistance.

Fundamental Magnetic Flux per Pole

The fundamental air-gap magnetic flux per pole and phase (ϕ_1), considering a machine with a smooth air-gap of length g , is given by equation 2.19 [22]:

$$\phi_1 = \frac{E_w}{\sqrt{2}\pi f W_s K_{w1}}, \quad (2.19)$$

where E_w is the winding per phase voltage, K_{w1} is the fundamental winding factor, and W_s is the number of turns linked in series per phase, defined as:

$$W_s = \frac{W_{ph}}{n_{pg}}.$$

Air-gap Magnetic Density Peak

The air-gap magnetic density peak is given in Tesla by equation 2.20 [22].

$$B_1 = \frac{\pi}{2\tau_p l_{si}} \phi_1, \quad (2.20)$$

where τ_p corresponds to the arc length of a magnetic pole (m). It is given by:

$$\tau_p = \frac{\pi D_s}{p},$$

and l_{si} is the effective active stator core length (m), which is calculated through:

$$l_{si} = l_{sc} \cdot K_{sf},$$

where K_{sf} as the core's stacking factor. Note that the product $\tau_p \cdot l_{si}$ is the effective area of a magnetic pole.

Air-gap Magnetomotive Force Peak

The air-gap magnetomotive force peak (A.turn/m) is given by equation 2.21 [22][23]:

$$\mathbb{F}_{peak} = \frac{K_s \cdot B_1}{\mu_0} \cdot g', \quad (2.21)$$

where K_s as the saturation factor.

Magnetization Current

For a polyphase machine the air-gap MMF peak produced by a phase winding is given by equation 2.22 [23]:

$$\mathbb{F}_{ph}(\theta, t) = \frac{4\sqrt{2}W_s I_m K_{w1}}{\pi p} \cdot \cos(\theta) \cos(\omega t - \varphi_p). \quad (2.22)$$

The magnetization current or the machine no-load current ($s \approx 0$), becomes simply the sum of the magnetizing current of all phases. For a symmetrical winding of m phases the supply voltages lag mutually by $2\pi/m$ ($\pi/2$ as for a two-phase winding) as well as for the displacement of the different winding phases. Consequently, the contribution of the winding phases to the MMF production becomes a vectorial summation of time and space terms [23]. So, for a three-phase machine, it results in the following equation:

$$\mathbb{F}_{peak} = \sum \mathbb{F}_{ph} = \frac{4\sqrt{2}W_s K_{w1}}{\pi p} \cdot I_m \left[\cos(0)\cos(0) + \cos\left(\frac{2\pi}{3}\right)\cos\left(\frac{2\pi}{3}\right) + \cos\left(\frac{4\pi}{3}\right)\cos\left(\frac{4\pi}{3}\right) \right],$$

which can be simplified to:

$$\mathbb{F}_{peak} = \frac{4\sqrt{2}W_s K_{w1}}{\pi p} \cdot \frac{3}{2} I_m.$$

Finally, the magnetization current for a three-phase machine is given by equation 2.23:

$$I_m = \frac{\pi p \cdot \mathbb{F}_{peak}}{6\sqrt{2}W_s K_{w1}} \quad (2.23)$$

Considering now the two-phase machine, the vectorial summation of the magnetomotive forces becomes:

$$\mathbb{F}_{peak} = \sum \mathbb{F}_{ph} = \frac{4\sqrt{2}W_s K_{w1}}{\pi p} \cdot I_m \left[\cos(0)\cos(0) + \cos\left(\frac{\pi}{2}\right)\cos\left(\frac{\pi}{2}\right) \right]$$

Therefore, the magnetization current for a two-phase machine is given by equation 2.24:

$$I_m = \frac{\pi p \cdot \mathbb{F}_{peak}}{4\sqrt{2}W_s K_{w1}} \quad (2.24)$$

MMF Total Harmonic Distortion

The Total Harmonic Distortion (THD) is the ratio of the sum of the powers of all air-gap MMF harmonic components to the power of the fundamental harmonic (eq. 2.25). In this analysis, the damping factor (K_n), due to the slot opening, is neglected ($K_n = 1$).

$$\text{THD} = \frac{\sqrt{\sum_{n=2}^{\infty} \left(\frac{K_{wn}}{n}\right)^2}}{K_{w1}} \quad (2.25)$$

The program considers the harmonic components up to the 42nd order.

2.3 Magnetic Saturation Analysis

In the BobiSoft's previous version the magnetic behavior of the machines' ferromagnetic cores is assumed to be linear. This assumption can be considered valid for low or even mild magnetic saturation levels [23]. BobiSoft generates automatic warnings to prevent the user from designing highly saturated machines, but there is no mechanism to avoid this possibility. Thus, in this case, the project results may have significant errors.

Magnetic saturation occurs when almost all the magnetic domains of a magnetic material have the same orientation. In this case, further increases of the magnetic flux intensity H will not cause further alignment of the magnetic domains. Consequently, the magnetic flux density B does not follow a linear proportionality to H , as it happens in the linear region. As a magnetic material becomes more saturated, its permeability decreases. Thus, some of the premises which support the basis of the analytic theory, here presented, become invalid. More specifically, the neglected permeability of the iron core, which is closely related to the air-gap induction function, should now be taken into account. Taking that into account, in [24] it is proposed the replacement of the saturated machine by an equivalent one, whose effective air-gap length is increased by a factor sufficient to absorb the magnetic potential drop in the iron of the saturated machine. Accordingly, the steel core of the equivalent machine has negligible reluctance and the previous assumption may still be valid.

In [25], the author deals with magnetic nonlinearity by adapting the machine's equivalent circuit parameters to the effective saturation level. The saturation curve is obtained by taking machine no-load current at different voltages below and above the rated voltage. Due to the very low slip at no-load the rotor branch impedance becomes very high, thus can be neglected, leaving the stator and magnetizing branches contributing to the excitation characteristics (the stator leakage flux path is mainly air and, for this reason, its associated reactance is practically linear). On the other hand, the magnetizing inductance has a

nonlinear behavior as imposed by the magnetic saturation characteristics of the steel core. Therefore, it is considered the only parameter affected by this phenomenon [25].

In this development, the magnetizing V-I curve is adapted to the normalized B-I magnetization curve¹ (fig. 2.4). So a generic magnetizing curve, independent of the machine's geometries, stator winding characteristics, and applied voltage, may be used in BobiSoft. In appendix A, the experimental procedures to obtain this curve are fully explained.

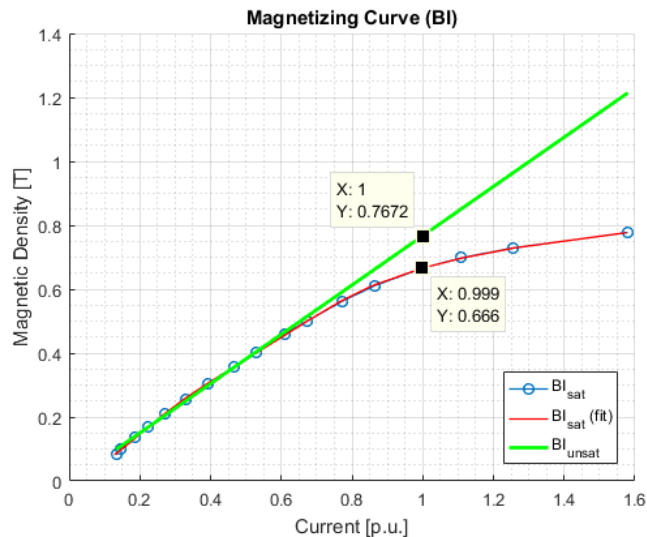


Figure 2.4: Experimental normalized magnetization curve.

The magnetizing reactance associated to any point P of the magnetizing curve is proportional to the slope of the line drawn from the origin through the point P and the slope of the linear magnetizing line (air-gap line or unsaturated line)[25] (fig. 2.5).

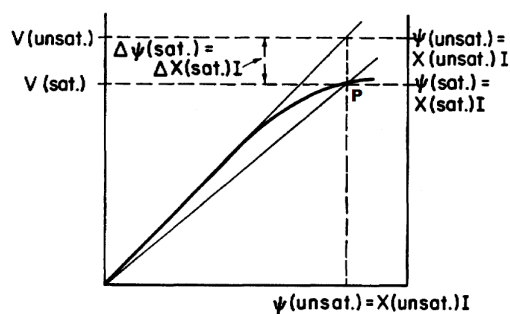


Figure 2.5: Magnetizing curve illustrating the formulation of the saturation factor [26].

¹As example: first step - calculate the air-gap induction peak ($B_{sat} = 0,666$); second step - extract the current I_p for that induction value using eq. 2.27 ($I_p(B_{sat}) = 1,00$ p.u.); third step - extract the unsaturated induction peak for that current from eq. 2.28 ($B_{unsat}(I_p) = 0,7672$); finally - calculate the saturation coefficient using eq. 2.26 ($K_s = 1,15$).

Thus, the saturated inductance, L_m , for any given point P on the magnetizing curve may be expressed as $L_m = L'_m/K_s$ (eq. 2.26) of the unsaturated inductance, L'_m [25], where:

$$K_s = \frac{B_{\text{unsat}}(I_p)}{B_{\text{sat}}(I_p)}. \quad (2.26)$$

Now that the solution is formulated, the software has to compute the B_{sat} and B_{unsat} flux densities. The flux B_{sat} is simply calculated through equation 2.20. Then, from the experimental magnetizing curve (fig. 2.4 - curve in blue) it has been performed a 5th order polynomial fitting, so the current I_p can be easily calculated analytically (fig. 2.4 - curve in red). The expression resulted in equation 2.27:

$$I_p(B) = 44.2977 \cdot B^5 - 73.9052 \cdot B^4 + 45.1486 \cdot B^3 - 11.7095 \cdot B^2 + 2.4083 \cdot B - 0.0000 \quad (2.27)$$

Finally, the air-gap line was drawn as a linear regression out of the points of the linear region of the magnetizing curve (fig. 2.4 - curve in green). The expression resulted in equation 2.28:

$$B_{\text{unsat}}(I_p) = 0.7672 \cdot I_p - 0.0000 \quad (2.28)$$

Note that both strategies lead to the same result. In fact, the magnetization inductance is inversely proportional to the air-gap length.

2.4 Air-gap Magnetomotive Force and Winding Factors

The used method to calculate the air-gap magnetomotive force is valid for any winding configuration. In this section, the simplified formulas to obtain the air-gap MMF waveform and the winding factors are presented. The full development can be found in Appendix B.

The resultant air-gap MMF of a winding with m phases is calculated through equation 2.29:

$$\begin{aligned} \mathbb{F}_r(\theta, t) = & \frac{I_A \sqrt{2} \sin(\omega t + \varphi_A)}{\pi} \sum_{n=1}^{\infty} \frac{K_n}{n} C_{n_A} \sin(n\theta - \theta_{n_A}) + \\ & \frac{I_B \sqrt{2} \sin(\omega t + \varphi_B)}{\pi} \sum_{n=1}^{\infty} \frac{K_n}{n} C_{n_B} \sin(n\theta - \theta_{n_B}) + \\ & \frac{I_C \sqrt{2} \sin(\omega t + \varphi_C)}{\pi} \sum_{n=1}^{\infty} \frac{K_n}{n} C_{n_C} \sin(n\theta - \theta_{n_C}) + \dots + \\ & \frac{I_m \sqrt{2} \sin(\omega t + \varphi_m)}{\pi} \sum_{n=1}^{\infty} \frac{K_n}{n} C_{n_m} \sin(n\theta - \theta_{n_m}), \end{aligned} \quad (2.29)$$

where

$$K_n = \frac{2}{n\beta} \sin\left(\frac{n\beta}{2}\right)$$

is the damping factor of the n^{th} space harmonic, due to the slot's opening β in degrees. The phase p magnetizing current is noted with I_p , being valid even before unbalanced m phase supply systems.

$$C_{np} = \sqrt{\left(\sum_{k=1}^{K_p} N_{ck} \cos(n\theta_k)\right)^2 + \left(\sum_{k=1}^{K_p} N_{ck} \sin(n\theta_k)\right)^2},$$

and

$$\theta_{np} = \text{arctg} \left(\frac{\sum_{k=1}^{K_p} N_{ck} \sin(n\theta_k)}{\sum_{k=1}^{K_p} N_{ck} \cos(n\theta_k)} \right),$$

where $\theta_k = \pi k \cdot p/Z$. The winding factors K_{wn} are obtained through equation 2.30:

$$K_{wn} = \frac{C_{np}}{2W_s}. \quad (2.30)$$

Equation 2.29 can be simplified into a system of two rotating vectors, revolving in the direct and reverse sense of the magnetic field, here defined with d and i , respectively. The simplified equation is presented in 2.31:

$$\mathbb{F}_r(\theta, t) = \frac{\sqrt{2}I}{\pi} \sum_{n=1}^{\infty} \frac{K_n}{n} [K_{nd} \sin(n\theta - \omega t + \varphi_d) + K_{ni} \sin(n\theta + \omega t + \varphi_i)], \quad (2.31)$$

where

$$K_{nd} = \sqrt{V_1^2 + V_2^2};$$

$$K_{ni} = \sqrt{W_1^2 + W_2^2};$$

$$\varphi_d = \text{arctg} \left(\frac{V_1}{V_2} \right);$$

$$\varphi_i = \text{arctg} \left(\frac{W_1}{W_2} \right);$$

and

$$V_1 = \frac{1}{2}[C_{n_A} \cos(n\theta_{n_A} + \varphi_A) + C_{n_B} \cos(n\theta_{n_B} + \varphi_B) + C_{n_C} \cos(n\theta_{n_C} + \varphi_C) + \dots + C_{n_N} \cos(n\theta_{n_N} + \varphi_N)];$$

$$V_2 = \frac{1}{2}[C_{n_A} \sin(n\theta_{n_A} + \varphi_A) + C_{n_B} \sin(n\theta_{n_B} + \varphi_B) + C_{n_C} \sin(n\theta_{n_C} + \varphi_C) + \dots + C_{n_N} \sin(n\theta_{n_N} + \varphi_N)];$$

$$W_1 = -\frac{1}{2}[C_{n_A} \cos(n\theta_{n_A} - \varphi_A) + C_{n_B} \cos(n\theta_{n_B} - \varphi_B) + C_{n_C} \cos(n\theta_{n_C} - \varphi_C) + \dots + C_{n_N} \cos(n\theta_{n_N} - \varphi_N)];$$

$$W_2 = -\frac{1}{2}[C_{n_A} \sin(n\theta_{n_A} - \varphi_A) + C_{n_B} \sin(n\theta_{n_B} - \varphi_B) + C_{n_C} \sin(n\theta_{n_C} - \varphi_C) + \dots + C_{n_N} \sin(n\theta_{n_N} - \varphi_N)].$$

An interesting characteristic of these two vectors is that the product of their amplitude $K_{nd,i}$ is zero for any harmonic order, whether the winding contains only pure space harmonics or if the winding is balanced [27]. This characteristic is used to verify the winding specified by the user.

2.5 Induction Machine Equivalent Circuit Parameters

In this section, the calculation of equivalent circuit parameters is explained. Figure 2.6 represents the steady-state equivalent circuit of a polyphase machine. The iron resistance (R_{fe}) is excluded from this analysis, due to the complexity and effort needed to obtain it, which is not worth since its impact on the electromagnetic torque can be neglected.

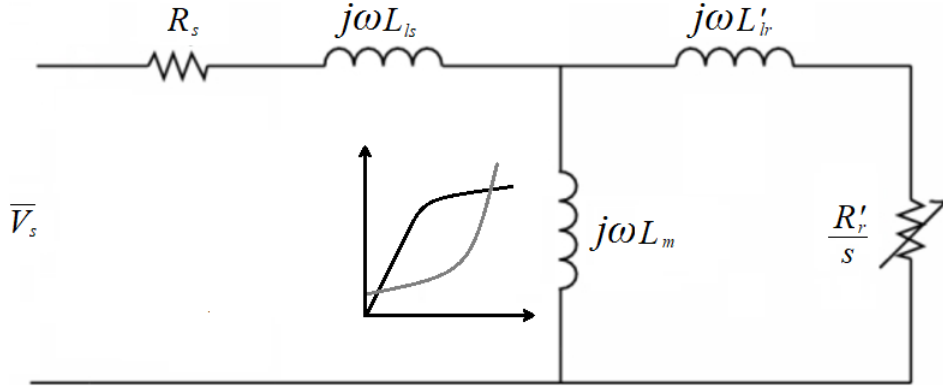


Figure 2.6: Per-phase equivalent circuit of polyphase induction machines.

2.5.1 Stator-Winding Resistance

The analysis starts with the basic stator winding resistance (R_s), given by equation 2.32:

$$R_s = \frac{1}{\sigma_c} \cdot \frac{l_{w,ph}}{S_{cond} \cdot n_{pg}^2}, \quad (2.32)$$

where σ_c is the wire conductor conductivity (S/m). The skin effect is neglected in this calculation, making the calculated resistance slightly smaller than its real value, considering the typical supply frequency of an induction machine.

2.5.2 The Magnetization Inductance

Considering a sinusoidal air-gap flux density at no-load, the air-gap flux amplitude is given by equation 2.33 [23]:

$$B_1 \approx \frac{\mu_0 \mathbb{F}_{ph}}{g' \cdot K_s}; \quad K_s \geq 1. \quad (2.33)$$

Now, the air-gap flux linkage ψ_{11h} , per phase, is

$$\psi_{11h} = W_s K_{w1} \phi_1,$$

where ϕ_1 is obtained from equations 2.33 and 2.20, resulting the following equation:

$$\psi_{11h} = \frac{2\mu_0 l_{si} \tau_p}{\pi g' \cdot K_s} W_s K_{w1} \mathbb{F}_{ph}.$$

Thus, the magnetization inductance of a phase L_{1m} , when all other phases and the rotor are open, is

$$L_{1m} = \frac{\psi_{11h}}{I_0 \sqrt{2}}.$$

Finally, for a three-phase induction machine, replacing its MMF peak value \mathbb{F}_{peak} (eq. 2.21) in the \mathbb{F}_{ph} of the air-gap flux linkage equation, the per-phase magnetization inductance (L_m) can be calculated by equation 2.34 [23]:

$$L_m = \frac{6\mu_0 (W_s K_{w1})^2}{\pi^2} \frac{l_{si} \tau_p}{p \cdot g' \cdot K_s}. \quad (2.34)$$

The same development can be applied for a two phase induction machine, thus the per-phase magnetization inductance becomes as in equation 2.35:

$$L_m = \frac{4\mu_0 (W_s K_{w1})^2}{\pi^2} \frac{l_{si} \tau_p}{p \cdot g' \cdot K_s}. \quad (2.35)$$

2.5.3 Stator Leakage Inductance

As in all magnetic circuits, some flux lines do not circulate inside the desirable paths, but encircle other parts of the magnetic circuit. These flux lines are called leakage flux. In induction machines, there are flux lines which encircle only the stator or only the rotor, that are characterized by equivalent leakage inductances L_{ls} and L_{lr} , respectively, because they do not contribute for the useful electromagnetic torque production. The various existing leakage flux lines can be categorized. Figure 2.7 schematizes the different types of possible flux leakage, which are also listed down below [23]:

- **Differential leakage inductance** (L_{lds}) - This inductance is related to the currents which produce space flux density harmonics in the air-gap. In some cases, the differential leakage inductance is included in the zigzag leakage inductance;
- **Slot leakage inductance** (L_{lss}) - Characterized by the flux lines which end-circle a single slot. It is highly dependent on slot geometry, rather than the teeth and back iron core saturation;
- **Zigzag leakage inductance** (L_{lzs}) - It characterizes the flux lines which touch both stator and rotor cores, but do not encircle both slots;

- **End-winding leakage inductance** (L_{les}) - Characterized by the flux lines which encircle the air and the materials surrounding the winding heads.

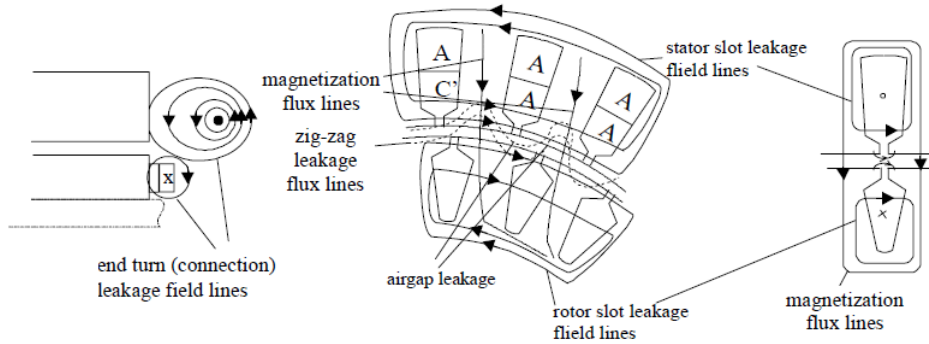


Figure 2.7: Leakage flux lines [23].

2.5.4 Stator Differential Leakage Inductance

In most cases, the machine's developed useful torque depends on the magnetization inductance of the fundamental harmonic of the stator winding MMF. Therefore, the differential leakage inductance may be defined as the flux produced by higher order terms [28]. In fact, to get the stator differential leakage inductance L_{ds} , it is sufficient to add all L_{mn} harmonics, except the fundamental, similar to what was done in equations 2.34 and 2.35. Consequently, L_{ds} for a three-phase winding is given by equation 2.36 [23]:

$$L_{ds} = \frac{6\mu_0\tau_p l_{si} W_s^2}{\pi^2 p \cdot g'} \sum_{n \neq 1}^{\infty} \frac{K_{wn}^2}{n^2 K_{sn}}. \quad (2.36)$$

For a two-phase winding the stator differential leakage inductance is given by equation 2.37:

$$L_{ds} = \frac{4\mu_0\tau_p l_{si} W_s^2}{\pi^2 p \cdot g'} \sum_{n \neq 1}^{\infty} \frac{K_{wn}^2}{n^2 K_{sn}}, \quad (2.37)$$

where K_{sn} is the saturation coefficient for higher order harmonics, taking the values in the interval [1; 1,2]. The higher the order, the closer this factor is to one. Since the pole pitch for the n^{th} harmonic is τ_p/n , the magnetic flux does not reach the back cores and thus these saturation factors are smaller than K_s [23].

2.5.5 Stator Slot Leakage Inductance

The stator slot leakage inductance can be obtained based on the magnetic energy stored in the slot (E_{ws}). This inductance is highly dependent on slot geometry and less on teeth and

back core saturation, thus its effect is neglected [23]. Generically, for a single-layer winding the energy stored is given by:

$$E_{ws} = \frac{1}{2} \mu_0 \cdot l_{si} \int_0^h H(x)^2 w(x) \cdot dx,$$

where h is the slot depth (m), $w(x)$ is the slot width (m) at the x -height and $H(x)$ is the magnetic field intensity, at the x -coordinate (A/m). For a double-layer winding the magnetic field intensities produced by each coil must be considered, $H(x) = H_1(x) + H_2(x)$, [29] (fig. 2.8).

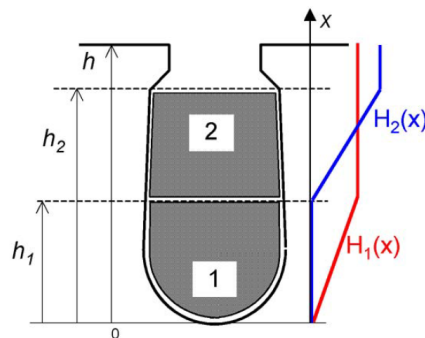


Figure 2.8: Stator slot magnetic field intensity of a two-layered winding [29].

The magnetic energy stored in an inductance can be calculated using the well-known equation:

$$E_{ws} = \frac{1}{2} L \cdot I^2.$$

Consequently, the slot leakage inductance can be defined as:

$$L_{lss} = 2E_{ws} \frac{1}{I^2}.$$

Thus, the magnetic energy stored in a slot is given by [29]:

$$E_{ws} = E_{ws1} + E_{ws2} + E_{ws12},$$

where

$$E_{ws1} = \frac{1}{2} \lambda_{slot,1} \cdot l_{si} \cdot i_{layer,1}^2,$$

$$E_{ws2} = \frac{1}{2} \lambda_{slot,2} \cdot l_{si} \cdot i_{layer,2}^2,$$

$$E_{ws12} = \lambda_{slot,12} \cdot l_{si} \cdot i_{layer,1} \cdot i_{layer,2}.$$

Note that for single-layer winding the stored energies E_{ws2} and E_{ws12} are null, because the second layer is nonexistent. The instantaneous currents, which circulate inside the layer conductors, may be defined as:

$$i_{layer,1} = \sqrt{2} I \cdot \cos(\varphi_1),$$

$$i_{layer,2} = \sqrt{2}I \cdot \cos(\varphi_2),$$

$$i_{layer,3} = \sqrt{2}I \cdot \cos(\varphi_3),$$

where φ_p is the shift angle between phases, including the current direction going in or out of the slot: $\varphi_{lag_p} + 0$ and $\varphi_{lag_p} + \pi$, respectively.

At last, the slot leakage coefficient can be found by:

$$\lambda_{slot} = \mu_0 \int_0^h H(x)^2 \cdot w(x) \cdot dx$$

In [29] is used a slot geometry independent algorithm to obtain this coefficient, in a way that can be easily programmed. However, in order to include windings with different number of turns per coil, some changes have been made. The algorithm is explained considering the most complex case, the double-layer winding. So, regarding figure 2.8, the slot is subdivided into N elementary thin layers of thickness $\Delta_x = h/N$, with h as the slot height. The elementary layers are numbered with the index i . The elementary height and width of the i^{th} layer are defined with x_i and w_i , respectively. The heights h_1 and h_2 correspond to the height reached by each layer inside the slot, and A_1 and A_2 are the conduction area of each layer.

The first step of the algorithm is to limit the areas belonging to each layer with the functions $p_1(x)$ and $p_2(x)$:

$$0 < x < h_1 \Rightarrow p_1(x) = 1; p_2(x) = 0$$

$$h_1 < x < h_2 \Rightarrow p_1(x) = 0; p_2(x) = 1$$

$$h_2 < x < h \Rightarrow p_1(x) = 0; p_2(x) = 0$$

The elementary areas are then calculated:

$$x_i = \left(i - \frac{1}{2}\right) \Delta_x,$$

$$A_{1i} = \Delta_x \cdot N_{c1} \cdot \sum_{k=1}^i p_1(x_k) w(x_k),$$

$$A_{2i} = \Delta_x \cdot N_{c2} \cdot \sum_{k=1}^i p_2(x_k) w(x_k),$$

where N_{cl} is the number of conductors of the l-layer.

After that, the following summations are computed:

$$l_1 = \sum_{i=1}^N \frac{A_{1i}^2}{w(x_i)} \Delta_x,$$

$$l_2 = \sum_{i=1}^N \frac{A_{2i}^2}{w(x_i)} \Delta x,$$

$$l_{12} = \sum_{i=1}^N \frac{A_{1i} A_{2i}}{w(x_i)} \Delta x,$$

Finally, the self- and mutual-inductance coefficients are calculated:

$$\lambda_{slot,1} = \mu_0 \frac{l_1}{A_1^2},$$

$$\lambda_{slot,2} = \mu_0 \frac{l_2}{A_2^2},$$

$$\lambda_{slot,12} = \mu_0 \frac{l_{12}}{A_1 A_2}.$$

At this point, all necessary data to calculate the k-slot leakage inductance has been gathered. Thus, a generic expression valid for single- and double-layer windings with m phases and different N_{ck} conductors per coil is given by equation 2.38:

$$L_{lss_k} = l_{si} [\lambda_{slot,1} \cdot \cos(\varphi_1)^2 + \lambda_{slot,2} \cdot \cos(\varphi_2)^2 + 2 \cdot \lambda_{slot,12} \cdot \cos(\varphi_1) \cdot \cos(\varphi_2)]. \quad (2.38)$$

Naturally, the stator slot leakage inductance is the sum of every k-slot leakage inductance of all coils linked in series belonging to the same phase (eq. 2.39):

$$L_{lss} = \sum_{k=1}^{p \cdot q / n_{pg}} L_{lss_k}. \quad (2.39)$$

2.5.6 Zigzag Leakage Inductance

As mentioned before, the zigzag flux circulates along the air-gap reaching both stator and rotor teeth. The zigzag leakage inductance presented here only characterizes the zigzag flux produced by the stator winding. This inductance is obtained by expressions 2.40 and 2.41 [23]:

$$L_{zls} \approx 2\mu_0 \frac{W_s^2 l_{si}}{pg} \lambda_{zs}, \quad (2.40)$$

where

$$\lambda_{zs} \approx \frac{5gC_s/w_{ss}}{5 + 4gC_s/w_{ss}},$$

and

$$L_{zls} \approx L_m \cdot \frac{\pi^2 p^2}{12Z^2} \left[1 - \frac{a(1+a)(1-1/C_s)}{2/C_s} \right], \quad (2.41)$$

where $a = w_{ts}/\tau_s$, τ_s as the stator slot pitch, measured at the teeth top.

In [23] this inductance is recommended to be the average of the values of equations 2.40 and 2.41. Since, equation 2.40 only includes the air-gap/slot opening, and in equation

2.41 the term between square brackets is a very small number and is highly dependent on the geometric parameters.

2.5.7 End-Winding Leakage Inductance

The three-dimensional character of the end-winding field and the materials that surround it make the calculating end-winding leakage inductance extremely difficult. In fact, many shapes of winding heads can be implemented, and because of that a unique expression to characterize this leakage flux is result of bold simplifications and assumptions. An approximate expression is given by equation 2.42 [23]:

$$L_{les} = 2\mu_0 \frac{W_s^2}{p} \cdot 0.34 \cdot (l_{es} - 0.64\tau_{coil} \cdot \tau_s), \quad (2.42)$$

where l_{es} is the average end-connection length (m).

2.5.8 Referring the Rotor to Stator

BobSoft 2.0 does not calculate rotor parameters because of the difficulty or even impossibility the user might face to obtain information of the rotor slots geometry and other data. Instead, if the user knows the rotor parameters referred to stator from the original project, or the motor's designing class, the software will be able to calculate and adapt them to the new project.

Bearing in mind that the real and the rotor resistance referred to stator have the same conduction losses, the following relationship is obtained, equation 2.43 [23]:

$$m_s R_r' I_r'^2 = m_r R_r I_r^2. \quad (2.43)$$

The same is applied to the rotor leakage reactance. Thus, from the leakage field energy conservation is obtained equation 2.44:

$$m_s \frac{L_{lr}'}{2} I_r'^2 = m_r \frac{L_{lr}}{2} I_r^2. \quad (2.44)$$

Consequently,

$$R_r' = R_r \frac{m_r}{m_s} \frac{1}{K_i^2}; \quad L_{lr}' = L_{lr} \frac{m_r}{m_s} \frac{1}{K_i^2}, \quad (2.45)$$

where

$$K_i = \frac{I_r'}{I_r} = \frac{m_r K_{w1r} W_r}{m_s K_{w1s} W_s}$$

is the current reduction factor [23].

From expression 2.45 the impedance correction from the old to the new project may be deduced (eq. 2.46):

$$Z'_{new} = Z'_{old} \cdot \frac{m_{new}}{m_{old}} \cdot \left(\frac{K_{w1_{new}} W_{s_{new}}}{K_{w1_{old}} W_{s_{old}}} \right)^2. \quad (2.46)$$

2.6 Machine Parameters and Torque-Slip Curve

In this section, the machine's torque slip curve computation is explained. The analysis of this curve can be an efficient way to evaluate the machine's performance at different operating points. In order to be more accurate in this analysis, the interference of parasitic torques is included in the torque-slip curve. The parasitic torques, caused by spatial MMF harmonics, are undesirable and unavoidable, as they exist due to the slotted structure of the stator. The associated negative effects manifest on the motor starting, the machine's efficiency, durability, acoustic noise, and vibration [30].

In figure 2.9, the influence of spatial harmonics on the developed electromagnetic torque is represented², proving the motor starting negative impact. Effectively, it can be observed that the torque produced by the 7th spatial harmonic, conjugated with a certain load level, may cause the machine to crawl at a speed of approximately 1/7 of the synchronous speed. In addition, the resultant torque is reduced due to the parasitic torques, which, at the motor rated operating point, are negative (braking effect), causing a slight increase of the motor slip and additional heating.

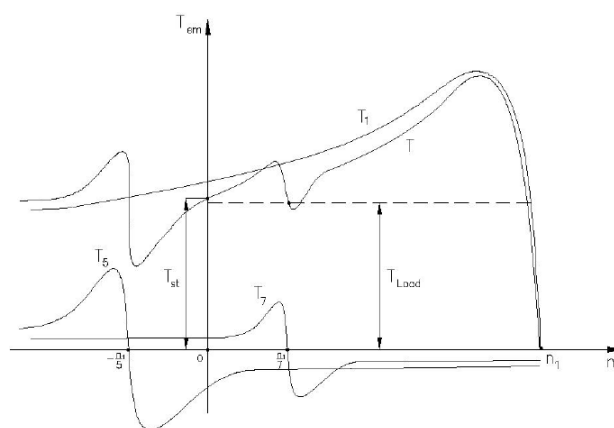


Figure 2.9: Torque-slip curve, with the 5th and 7th parasitic torques [30].

Since the conventional per-phase circuit of the polyphase machine was presented in figure 2.6, this schematic only includes the fundamental parameters that create a pure elec-

²The exaggerated amplitude of parasitic torques serve to emphasizes their effect on the resultant torque.

tromagnetic torque-slip curve. But the effect of the spatial harmonics can be modeled into the schematics of figure 2.10, resulting in the induction machine complete equivalent circuit.

This complete equivalent circuit is quite similar to what is conventional, but were added branches connected in series corresponding to each MMF spatial harmonic order. This is because the same stator current originates both the stator MMF fundamental and higher order harmonics [23].

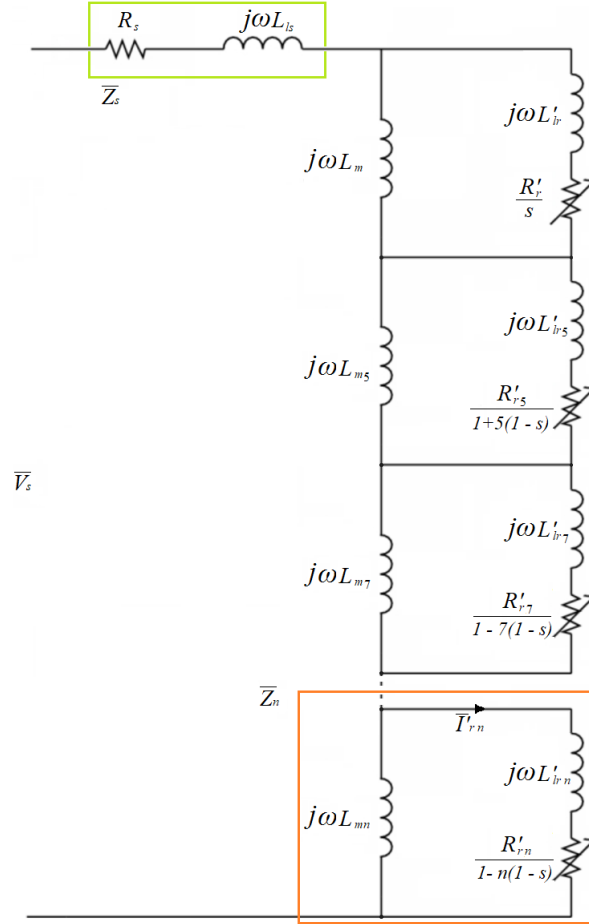


Figure 2.10: Complete per-phase equivalent circuit including MMF spatial harmonic [23][31].

The analysis starts with the definition of the synchronous speed of the n^{th} spatial harmonic (eq. 2.47) [23]:

$$\Omega_n = \frac{2\pi \cdot f \cdot \omega_1}{p \cdot n}. \quad (2.47)$$

Then, the slip of the n^{th} harmonic in relation to the fundamental torque is given by equation 2.48, where for the three-phase machine, $n = -5, +7, -11, +13, \dots$, generally $6n \pm 1$ ($n \in \mathbb{Z}^+$). The sign corresponds to the order sequence, negative or positive.

$$s_n = 1 - n(1 - s) \quad (2.48)$$

The slip for the n^{th} harmonic synchronism is calculated as $s_{sync_n} = 1 - \frac{1}{n}$. Therefore, the 5th and 7th harmonic slip are $s_{sync_5} = 1 - 1/(-5) = 6/5$ and $s_{sync_7} = 1 - 1/7 = 6/7$, respectively. The slip of all the other harmonics is comprised in

$$s_5 > s_n > s_7,$$

which means that the effect of all parasitic torques will be more visible within this interval.

The next step is to compute the parameters of the complete equivalent circuit. Starting with the magnetizing reactances X_{mn} (equations 2.49 or 2.50), whether the machine has a three- or two-phase winding, respectively [23][31][32]:

$$X_{mn} = \omega_1 \cdot \frac{6\mu_0\tau_p l_{si}}{\pi^2 p \cdot g' \cdot K_s} \left(\frac{K_{wn} W_s}{n} \right)^2, \quad (2.49)$$

$$X_{mn} = \omega_1 \cdot \frac{4\mu_0\tau_p l_{si}}{\pi^2 p \cdot g' \cdot K_s} \left(\frac{K_{wn} W_s}{n} \right)^2. \quad (2.50)$$

Then, the rotor resistance for the n^{th} harmonic can be calculated with equation 2.51 [31][32]:

$$R'_{rn} = R'_{r1} \cdot \frac{K_{wn}^2}{K_{w1}^2}. \quad (2.51)$$

Finally, the rotor leakage reactance for the n^{th} harmonic is calculated through equation 2.51 [31][32]:

$$X'_{lrn} = \omega_1 L'_{r1} \cdot \frac{K_{wn}^2}{K_{w1}^2}. \quad (2.52)$$

In case the rotor parameters are unknown, the program estimates their values. The rotor leakage reactance can be estimated from the standardized leakage reactances distributions of the design classes, defined in NEMA MG-1-2003 (table 2.2). Then, the rotor resistance is estimated through the shaft rated power at the rated slip.

Table 2.2: Machine's leakage reactances proportion of different motor classes [24].

Motor class	Description	Proportion (X_1/X_2)
A	Normal starting torque, normal starting current	1
B	Normal starting torque, low starting current	2/3
C	High starting torque, low starting current	3/7
D	High starting torque, high slip	1
Wound Rotor	Performance varies with the rotor resistance	1

Now, the analysis of the complete equivalent circuit can be done, so that the torque at the s slip may be extracted. First, the impedance of the n^{th} branch is given by equation 2.53:

$$\bar{Z}_n = \frac{jX_{mn} \cdot \left[\frac{R'_{rn}}{s_n} + jX'_{lrn} \right]}{\frac{R'_{rn}}{s_n} + j(X_{mn} + X'_{lrn})}. \quad (2.53)$$

Next, the impedance seen by the rotor parameters of each branch, when the voltage supply is short-circuited, is calculated through equation 2.54:

$$\bar{Z}_{tn} = \frac{jX_{mn} \cdot (\bar{Z}_s + \bar{Z}_{na} + \bar{Z}_{nb} + \dots + \bar{Z}_{nk})}{jX_{mn} + \bar{Z}_s + \bar{Z}_{na} + \bar{Z}_{nb} + \dots + \bar{Z}_{nk}}, \quad (2.54)$$

where the impedances \bar{Z}_{na} , \bar{Z}_{nb} , ..., \bar{Z}_{nk} are the impedances of all other branches of the k -harmonics considered.

Then, applying the Thévenin's Theorem to each branch in order to calculate the current of the n^{th} harmonic (I'_{rn}), the following expressions are used:

$$\begin{aligned} U_{thn} &= \left| \frac{jX_{mn}}{\bar{Z}_s + \bar{Z}_{na} + \bar{Z}_{nb} + jX_{mn}} \right| U_s, \\ R_{thn} &= \Re \{ \bar{Z}_{tn} \}, \\ X_{thn} &= \Im \{ \bar{Z}_{tn} \}. \end{aligned}$$

At last, the electromagnetic torque of the n^{th} harmonic, at s slip, is calculated with equation 2.55:

$$T_{em_n}(s_n) = \frac{R'_{rn}}{\Omega_n \cdot s_n} \cdot \frac{U_{thn}^2}{\left(R_{thn} + \frac{R'_{rn}}{s_n} \right)^2 + (X_{thn} + X'_{lrn})^2}. \quad (2.55)$$

Finally, the resultant electromagnetic torque is obtained by summing the torques of all harmonics and all phases (equation 2.56):

$$T_r(s_n) = m \cdot \sum_{n=1}^{\infty} T_{em_n}(s_n) \quad (2.56)$$

The program calculates, for the three-phase machine, the torques of the 5th and 7th harmonics, besides the fundamental torque. For the two-phase machine are considered the torques of the 3rd and 5th harmonics.

Chapter 3

Routines and Algorithms

In this chapter, the BobiSoft's most relevant algorithms and routines are presented.

3.1 Automatic winding design

The automatic winding pattern design is the most important and fundamental functionality of BobiSoft. Currently, 9 winding designs can be automatically generated (fig. 3.1), 5 being eccentric/imbricated and 4 being concentric patterns. This variety of designs is meant to cover almost all possible arrangements. Obviously, some configurations may be better, leading to savings of the conductor material, while others may be easier to assemble. The decision of the winding pattern to use is of the user's responsibility.

The algorithm used designs only integer and symmetric windings. It is known from the electric machine theory that an AC distributed winding has m windings shifted spatially by $2\pi/mp_p$ mechanical degrees (two-phase winding by $\pi/2p_p$). Each winding occupies $1/m$ of the number of stator slots. According to this theory, the basis of this algorithm is a vector Z_{conn} with Z elements, which attributes the phase and the coil side of the conductors inside a layer (l) of the k -slot. Therefore, the Z_{conn} vector of the l -layer is defined mathematically as:

$$Z_{conn_{u,m,l}} = [s_{s1} \cdot n_{s1}, s_{s2} \cdot n_{s2}, \dots, s_{sZ} \cdot n_{sZ}],$$

where

$$s_{sk} = \frac{\sin\left(\frac{\pi}{q} \cdot (k - 0.5 + \sigma_o)\right)}{\left|\sin\left(\frac{\pi}{q} \cdot (k - 0.5 + \sigma_o)\right)\right|},$$

is the coil side attribution to the k conductor, 1 as the incoming and -1 as the outgoing coil side. And

$$n_{sk} = 1 + [(k + \sigma_o) \bmod q] \bmod m,$$

as the phase correspondence. For example, for a three-phase winding ($m = 3$) n_{sk} can assume the values 1, 2 or 3.

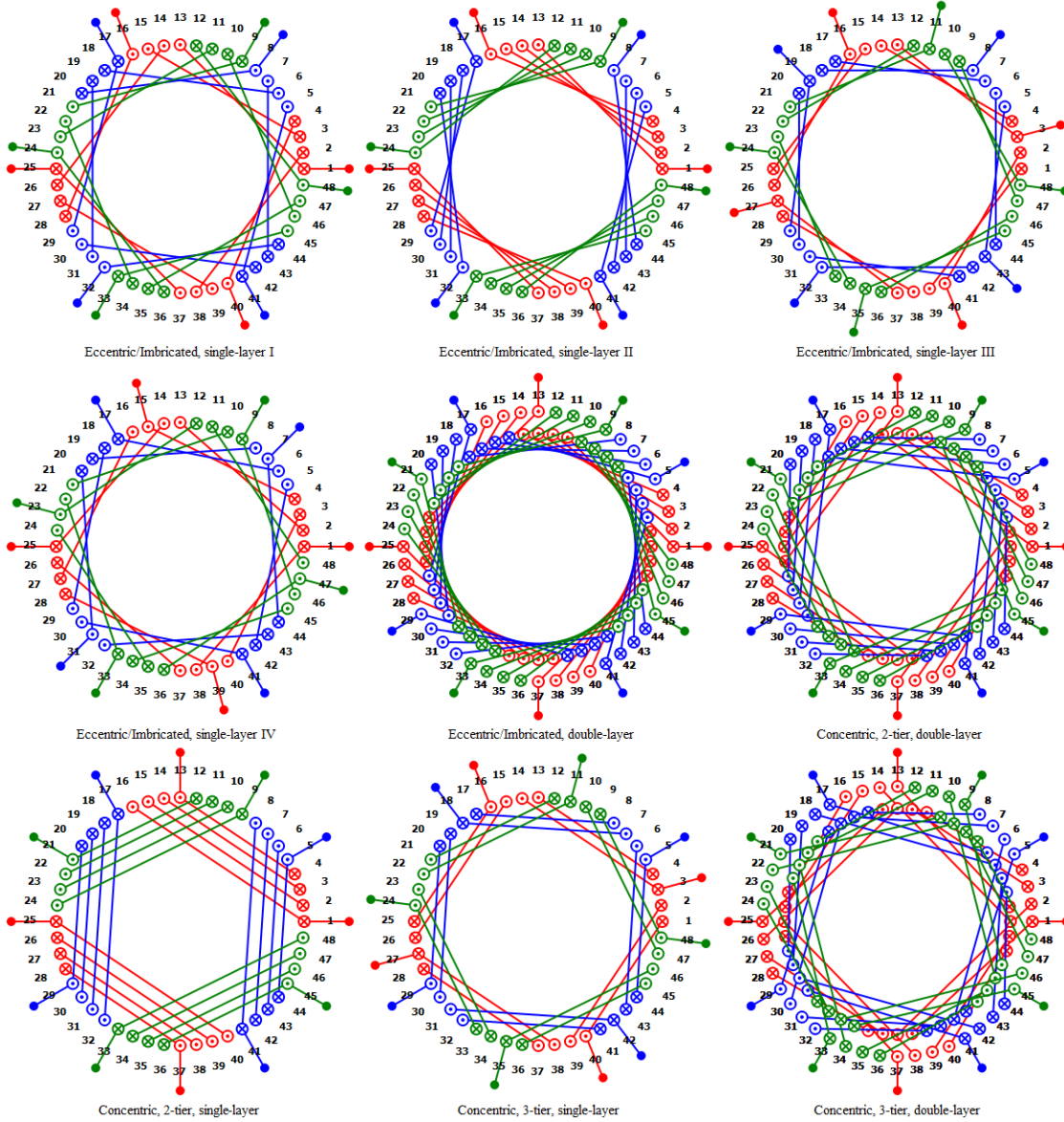


Figure 3.1: BobiSoft's 9 automatic winding designs.

In single-layer or full-pitched windings, the short-pitch variable σ_o is equal to zero. Double-layer windings are represented with two Z_{conn} vectors, where the vector correspondent to the upper layer Z_{conn_u} always defines $\sigma_o = 0$, and the vector of the lower layer Z_{conn_l} defines the short-pitch variable as:

$$\sigma_o = \frac{Z}{p} - \tau_{cp}, \quad \tau_{cp} \leq \frac{Z}{p},$$

where τ_{cp} is the effective coil pitch.

For the sake of a better understanding of this algorithm, figure 3.2 illustrates an example of a double-layer winding with an effective coil pitch of 5 slots (the machine has the

characteristics $Z = 12$, $p = 2$, and $m = 3$). In this example, the phase numbers 1, 2, and 3 were replaced by the letters a, b, and c, respectively, by virtue of clarity.

Slot	1	2	3	4	5	6	7	8	9	10	11	12
Z_{conn_U}	+a	+a	-b	-b	+c	+c	-a	-a	+b	+b	-c	-c
Z_{conn_L}	+a	-b	-b	+c	+c	-a	-a	+b	+b	-c	-c	+a
	0	$2\pi/3$				π	$4\pi/3$				2π	

Figure 3.2: Slot attribution array example ($Z = 12$, $p = 2$ and $m = 3$). Double-layer winding with a coil pitch of $\tau_{cp} = 5$.

At this point, the winding is partially completed, the last step is to connect the conductors of a phase in series and then split it into the desired number of parallel poles (n_{pg}). In this step, the coils are defined by the belonging phase, the incoming coil side (slot₁), the outgoing coil side (slot₂), their respective layers, the number of turns, and finally the terminals connection (only if the coil is not connected in series with other two coils). As an example, the connection algorithm of the eccentric/imbricated double-layer winding type is presented in figure 3.3.

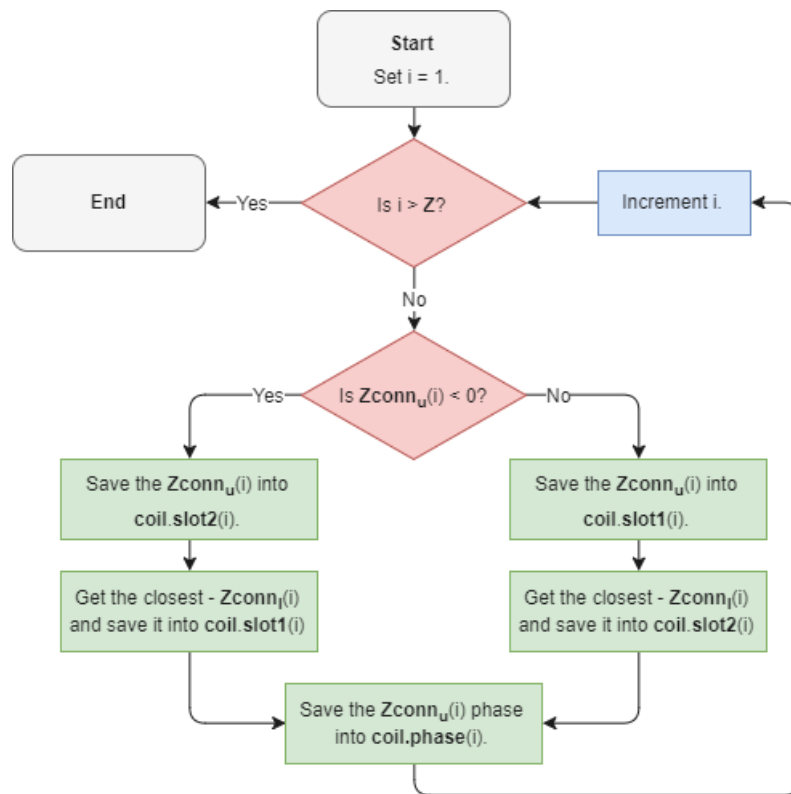


Figure 3.3: Flowchart of the eccentric/imbricated double-layer connection algorithm.

3.2 Main Computational Routine

The software computes the project solution once the Compute Data button is pressed. This action runs the routine of the flowchart in figure 3.4, which is the main processing sequence to generate the project solution.

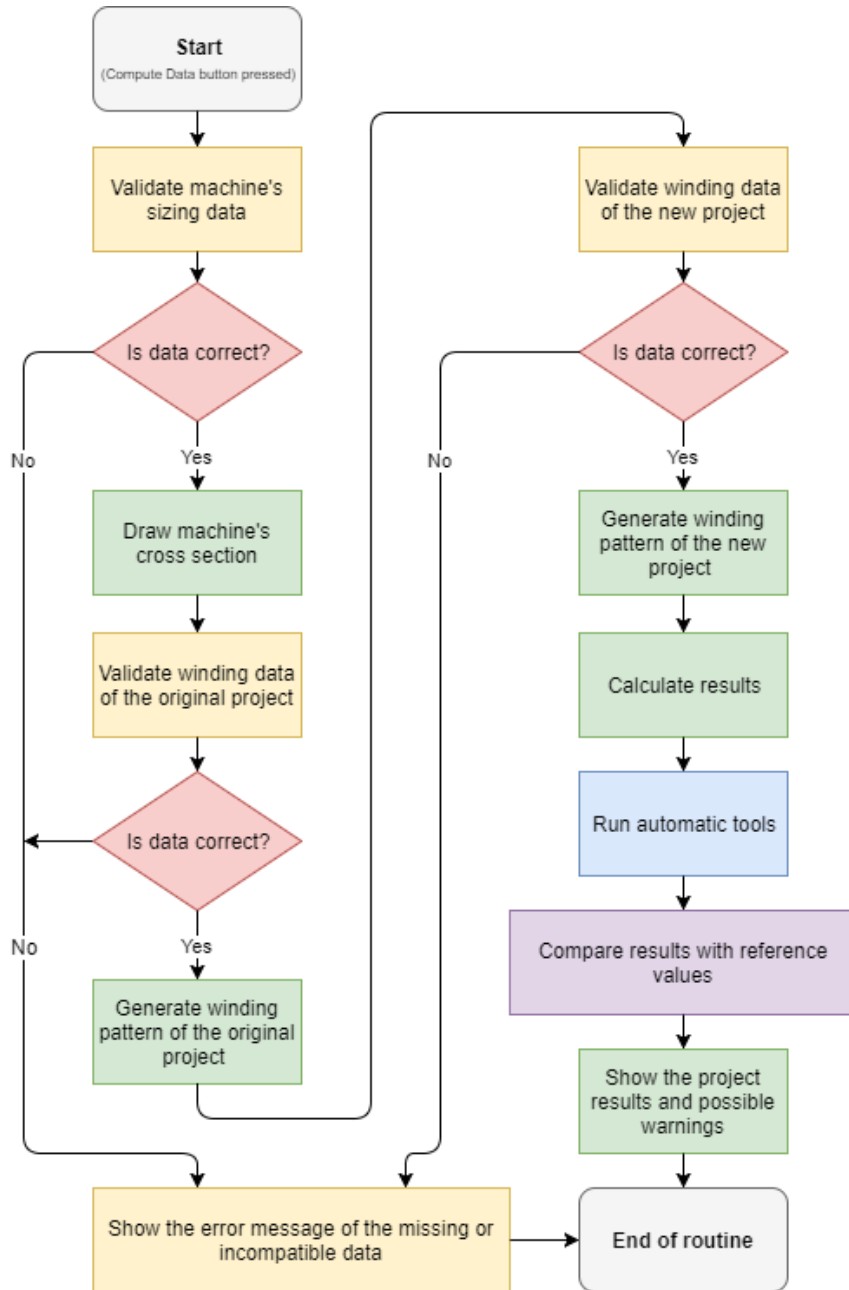


Figure 3.4: BobiSoft processing main routine (Compute Data).

The routine starts with the validation of the machine's structural dimensions, which are the stator core, slot dimensions, and the rotor core dimensions. If this data is physically compatible, the machine core cross section is drawn. Otherwise, and whenever the routine is interrupted, a warning message is shown, identifying the cause for its interruption.

Then, the winding data is prepared for the creation of the original project winding pattern. Firstly, it is verified if all winding data fields belonging to the original project are filled up. There is no need to check for invalid data because only preselected options for the automatic winding design can be entered. Only the number of slots per pole and phase number is evaluated, respectively $q = Z/p/m$. If q is an integer number and one of the 8 automatic winding designs is selected, the software is able to design the winding pattern, otherwise the routine stops. The software does not yet support the automatic design of fractional windings. Alternatively, free winding designs can be inserted manually in the winding editor. If the free winding type option is selected, the software validates the inserted pattern generating the winding if the data is compatible. Otherwise, the routine is halted.

The previous step is repeated for the new project winding data. At this point, the program has gathered all necessary information to calculate the quantities referred to in the chapter 2 and proceeds with their calculation.

The next step is to execute automatic tools. If no solution is found, the program keeps the solution found before the automatic tool was used. Then, the magnetic flux density and current density results are compared with typical values (see appendix C) and warning messages show whether these results are outside the reference boundaries. Finally, the results are shown and the printable reports become available for creation. The routine ends here.

3.3 Automatic Conductors Section Selection

The flowchart of figure 3.5 describes the algorithm which automatically selects the section and number of parallel conductors of the winding. This tool is only available for the new project.

The input parameters are the maximum section per wire and the maximum slot fill factor desirable (max K_{sff}). The first parameter is responsible for the creation of the n -parallel conductors, which will all have the maximum section inserted, except the last conductor, which will have sufficient section to satisfy the maximum slot fill factor condition. If no solution satisfies the mentioned conditions and the current density reference, the program will use the values inserted in the proper fields.

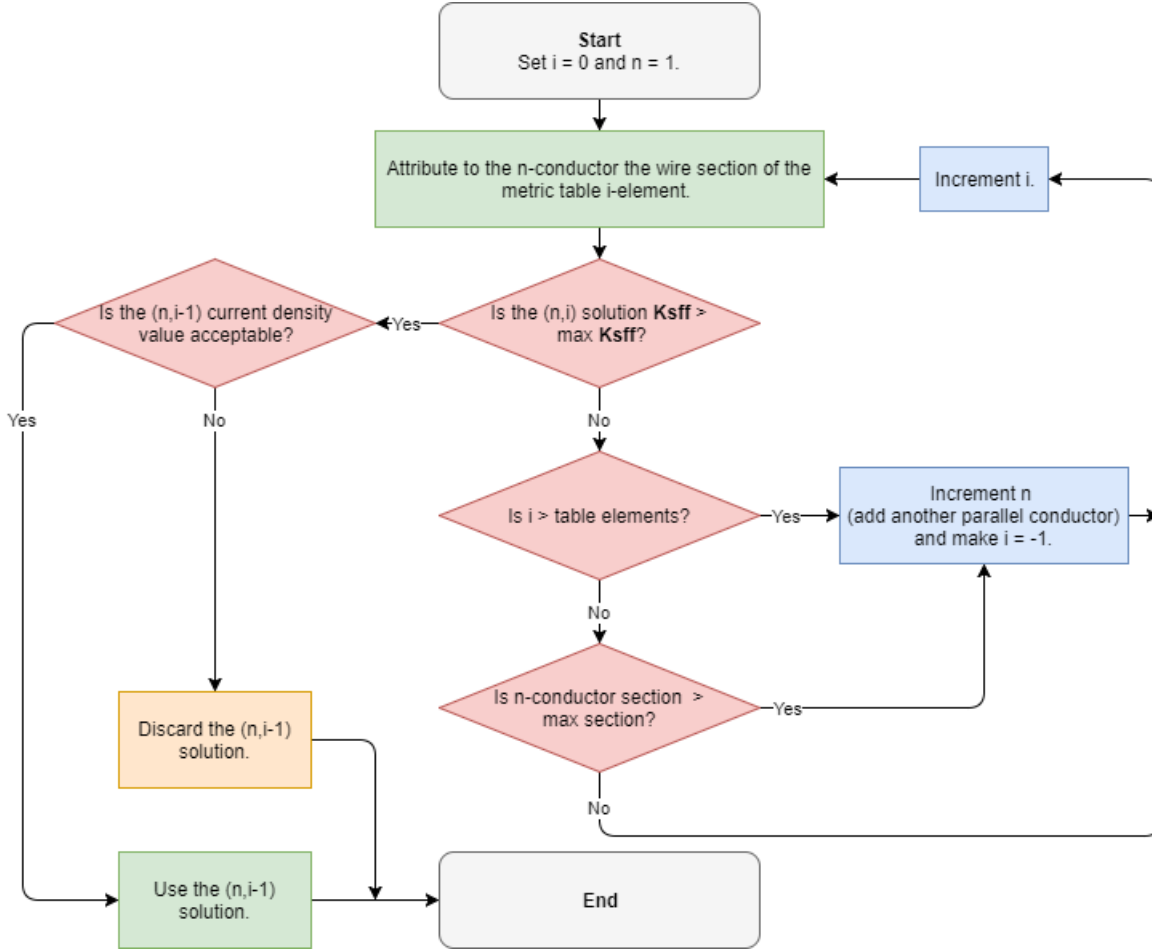


Figure 3.5: Automatic selection of conductors section algorithm.

3.4 Automatic Magnetic Flux Adaptation

During the rewinding project, there are various characteristics of the winding which may affect the magnetizing flux. It is desired that the magnetic flux keep constant, thus the rated torque and saturation level may still be equal to the original project.

Going back to the magnetic flux expression (equation 2.19, chapter 2) it is clear that the magnetic flux does not depend only on the winding configuration. Therefore, if any or all winding characteristics (number of parallel groups, winding factor, supply voltage and frequency) are modified the magnetic flux will not be kept the same. So, the last variable left, the number of turns W_{ph} , is adapted to obtain an approximate magnetic flux to the original project.

Equalizing the flux equations of both projects, the number of turns of the new project can be extracted (eq. 3.1):

$$W_{ph_{new}} = W_{ph_{orig}} \cdot \left[\frac{E_{w_{new}} \cdot n_{pg_{new}} \cdot f_{s_{orig}} \cdot K_{w1_{orig}}}{E_{w_{orig}} \cdot n_{pg_{orig}} \cdot f_{s_{new}} \cdot K_{w1_{new}}} \right]. \quad (3.1)$$

3.5 Induction Motor Downsizing

In the European Union (EU), the average of electric motors' load factor ($\zeta_{load} = P_{shaft}/P_{rated}$) is estimated to be less than 60%, in both industrial and tertiary sectors, for a wide power range of motors as is shown in figure 3.6 [33]. However, the average load factor per power range in some sectors can be as low as 25%. Motor oversizing is mainly due to poor motor system designs or gross overestimations of the mechanical power required by the load. The only advantage of having oversized motors is their longer lifetime, but at the cost of more power consumption. With this low load factor, both the motor's efficiency and power factor are low as well [34].

In [33], a strategy of motor downsizing in order to improve the motor's efficiency and power factor up to their maximum peaks, is proposed. This is achieved by means of magnetizing flux reduction. Frequently, the power factor improvement is underestimated, but the savings brought by the reduction of the upstream electrical installation losses, as a consequence of a higher power factor, can be quite significant. Consequently, the motor downsize has not only a local benefit on its efficiency, but also benefits the surrounding installation.

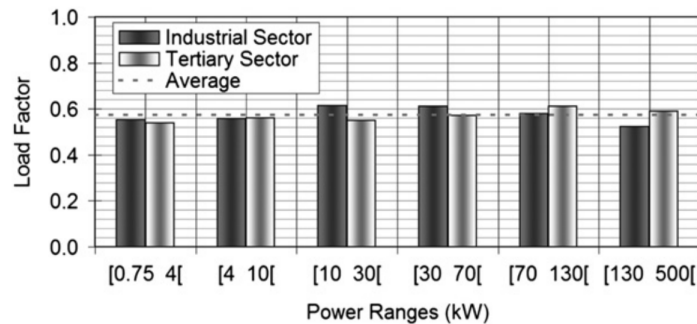


Figure 3.6: Average load factor by power range for electric motors in the EU, in the year 2000 [34][33].

For this purpose, the motor downsizing interface was created (fig. 3.7). In order to use this tool, the load type and the measured slip are required, while the remaining data serves to refine the optimization. The output is the new desired magnetic flux, which forces the actual machine's efficiency to reach its peak. Consequently, the new project number of turns per phase is calculated, thus the desired magnetizing flux is matched.

Motor Downsizing Optimization

Load Type Constant Power

Slip Measurement

Measured slip

Slip at maximum efficiency

Voltage Measurement

Measured voltage [V]

Power Measurement

Measured input Power [W]

Input Power at maximum efficiency [W]

Figure 3.7: Motor downsizing menu.

The analysis starts with the study of the machine's steady-state operation point imposed by the load. In [33], three load types are approached (constant, linear, and quadratic torque loads). In this tool, the constant power load type was added, whose development will be presented next. In figure 3.8 the machine's torque-slip curve and the constant power load curve are represented.

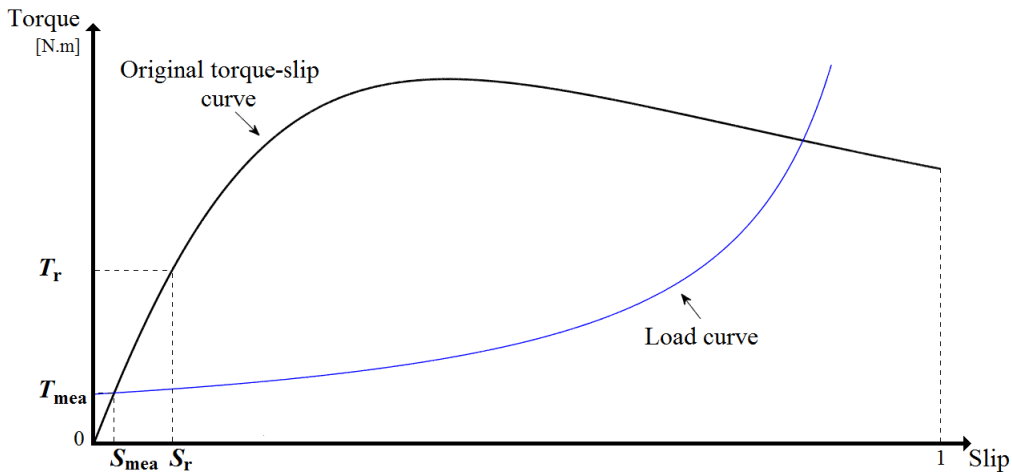


Figure 3.8: Constant power load type (torque-slip curve).

The system's steady-state operating point is defined by $(s_{mea}; T_{mea})$ and the rated efficiency operating point is defined as $(s_r; T_r)$, which, in most cases, corresponds to the machine's efficiency peak. Thus, the first step is to find the general equation that defines the load curve of figure 3.3:

$$T(s) = \frac{a}{1-s}; \quad T(s_{mea}) = T_{mea} \Rightarrow a = T_{mea} \cdot (1 - s_{mea}),$$

where $a = T_{mea} \cdot (1 - s_{mea})$, so this generic curve may be particularized to the motor's effective load. Then, the constant power load curve ($T \propto w^{-1}$) is defined by equation 3.2:

$$T_{load}(s) = \frac{T_{mea} \cdot (1 - s_{mea})}{1 - s}. \quad (3.2)$$

Now, considering that the machine electromagnetic torque follows a linear proportion in the interval $[0; s_r]$, the machine torque-slip curve, within this interval, can be obtained through equation 3.3.

$$T_{em}(s) = \frac{T_r}{s_r} \cdot s \quad (3.3)$$

Finally, inserting equation 3.3 with $s = s_{mea}$ in equation 3.2 and knowing the relationship between electromagnetic torque and the magnetic flux $T_{em} \propto \phi^2$, the flux adaptation expression for the constant power load type is obtained through:

$$\Phi_{new} \approx \Phi_{orig} \cdot \sqrt{\frac{s_{mea}}{s_r}} \cdot \sqrt{\frac{1 - s_{mea}}{1 - s_{new}}},$$

where s_{new} is the slip at maximum efficiency, which normally corresponds to the rated slip; and Φ_{new} and Φ_{orig} are the desired and the original magnetizing fluxes, respectively.

In the above expression, the term s_{mea}/s_r is identified in [33] as the approximated load factor, which can be approximated through equation 3.4:

$$\zeta_{load} = \frac{P_{shaft}}{P_r} \approx \frac{s_{mea} - s_{mea}^2}{s_r - s_r^2} \cdot \left(\frac{U_{mea}}{U_r}\right)^2 \approx \frac{s_{mea}}{s_r} \cdot \left(\frac{U_{mea}}{U_r}\right)^2. \quad (3.4)$$

The magnetizing flux reduction, caused by the voltage drop in the electric installation, is compensated by the factor U_{mea}/U_r , where the measurement of the actual voltage at the machine terminals is needed.

The final equation for the flux adaptation of constant power loads becomes equation 3.5:

$$\Phi_{new} \approx \Phi_{orig} \cdot \sqrt{\zeta_{load}} \cdot \sqrt{\frac{1 - s_{mea}}{1 - s_{new}}}. \quad (3.5)$$

In the cases where the machine's efficiency peak does not match the rated efficiency, the load factor can be estimated differently through equation 3.6 [33]. In this case, the actual (P_{shaft}) and maximum ($P_{r(\hat{\eta})}$) input power must be known, as well as the slip at maximum efficiency ($s_{r(\hat{\eta})}$).

$$\zeta_{\hat{\eta}} = \frac{P_{shaft}}{P_{r(\hat{\eta})}} \approx \frac{s_{mea} - s_{mea}^2}{s_{r(\hat{\eta})} - s_{r(\hat{\eta})}^2} \cdot \left(\frac{U_{mea}}{U_r}\right)^2 \approx \frac{s_{mea}}{s_{r(\hat{\eta})}} \cdot \left(\frac{U_{mea}}{U_r}\right)^2 \quad (3.6)$$

For the other load types, the equations in table 3.1 can be used for the magnetizing flux adaptation [33].

Table 3.1: Flux adjustment equations as function of the load type [33].

Load Type	$(T = f(w))$	Magnetizing Flux (ϕ)
Constant Power	$(T \propto w^{-1})$	$\Phi_{new} \approx \Phi_{orig} \cdot \sqrt{\zeta_{load}} \cdot \sqrt{\frac{1-s_{mea}}{1-s_{new}}}$
Constant Torque	$(T = const.)$	$\Phi_{new} \approx \Phi_{orig} \cdot \sqrt{\zeta_{load}}$
Linear Torque	$(T \propto w)$	$\Phi_{new} \approx \Phi_{orig} \cdot \sqrt{\zeta_{load}} \cdot \sqrt{\frac{1-s_{new}}{1-s_{mea}}}$
Quadratic Torque	$(T \propto w^2)$	$\Phi_{new} \approx \Phi_{orig} \cdot \sqrt{\zeta_{load}} \cdot \frac{1-s_{new}}{1-s_{mea}}$

3.6 Winding Optimization Tool

It is well-known that the winding pattern of an electric machine affects the MMF distribution and its performance. In fact, due to the slotted structure of the machine stator and rotor cores, MMF spatial harmonics are unavoidable. Therefore, an optimized winding design is necessary to mitigate the effects of the harmonic content, since many applications rely on smooth torque production, and attain the efficiency benefit [35].

The design of an induction motor, for example, can be summarized in usual procedures followed by designers. It all starts with the rating power and speed requirements, which automatically impose the machine's dimensions (stator, air-gap, and rotor dimensioning). For economic reasons, these dimensions are usually the smallest possible, so the material costs are reduced. The next decision to make is the choice of the stator slot number, which may be the lowest possible, because of the limited space available. Then, the winding layout can be finally designed, although many options have already been discarded by the low q ($q = Z/p/m$), due to the requirements for the number of poles and phases. Commonly, few attention is given to the winding design, with designers usually consulting tables of patterns to choose the solution that is, apparently, most suitable. For most standard machines this procedure is well-proven and works satisfactorily, but finding the best solution for a specific application is, inevitably, not a simple task [6].

In order to ensure the most suitable winding design, some sort of search algorithm is indispensable. The algorithm used must be extremely fast and efficient, because the space of winding layouts combinations may be very large, for machines with a large number of slots [6]. BobiSoft already had the basic winding data structures that may support such algorithm. Therefore, its creation was inherent to the software's new version.

Hereafter, winding optimization is defined as the reduction of the MMF spatial har-

monics in the air-gap field. In order to achieve the optimal MMF spatial THD reduction for a winding pattern, the algorithm presented in this section was added to BobiSoft.

3.6.1 Formulation of the Winding Optimization Problematics

The minimization of the spatial harmonic content of the air-gap magnetomotive force is the main goal of the winding optimizing algorithm (eq. 3.7):

$$\text{THD} = \frac{\sqrt{\sum_{n=2}^{\infty} \left[\frac{\left(\sum_{k=1}^{K_p} N_{ck} \cos(n\theta_k) \right)^2 + \left(\sum_{k=1}^{K_p} N_{ck} \sin(n\theta_k) \right)^2}{(2W_s \cdot n)^2} \right]}}{\sqrt{\frac{\left(\sum_{k=1}^{K_p} N_{ck} \cos(\theta_k) \right)^2 + \left(\sum_{k=1}^{K_p} N_{ck} \sin(\theta_k) \right)^2}{2W_s^2}}}. \quad (3.7)$$

In this equation it can be seen that the amplitude of the harmonics may be affected by the number of turns and the slot position of the k -conductors. Consequently, there are only two possibilities available to optimize the winding pattern, from the MMF spatial harmonics perspective: changing the coil pitch and/or the number of turns per coil.

As the most simple of two optimizing possibilities, the coil pitch may only be changed in double-layer windings, since for single-layer windings the position of the coil conductors is fixed. The optimization is made by simply shortening the coil pitch slot by slot until the effective coil pitch is shortened by q slots. It was verified, after exhaustive simulations, that the THD is commonly minimized at a coil pitch shorten by $\text{floor}(q/2)$ slots.

Figure 3.9 presents an example of coil pitch optimization, where the shortening of the coil pitch by one slot reduced the MMF THD by 12%¹.

The combination of different number of turns per coil for winding optimization is quite complex. Many candidates of the space of solutions may lead to an asymmetric winding layout. The following considerations must be taken into account for the sake of winding symmetry. Firstly, all phases must share the same combination of coils with different number of turns. Secondly, two consecutive slopes of the MMF waveform, ascendant and descendant, must mutually respect an even symmetry to a vertical axis placed at the slopes intersection point (figure 3.10 - even symmetry axis). Finally, every MMF slope must respect an odd symmetry to an axis placed at the intersection of the MMF curve with the x -axis (figure 3.10 - odd symmetry axis). The imbricated winding fails the last two conditions whenever the winding is double-layer and short pitched [4].

¹The winding in figure 3.9a with an effective coil pitch of 16 slots has a MMF THD of 4,953%. The winding in figure 3.9b with an effective coil pitch of 15 slots has a MMF THD of 4,355%.

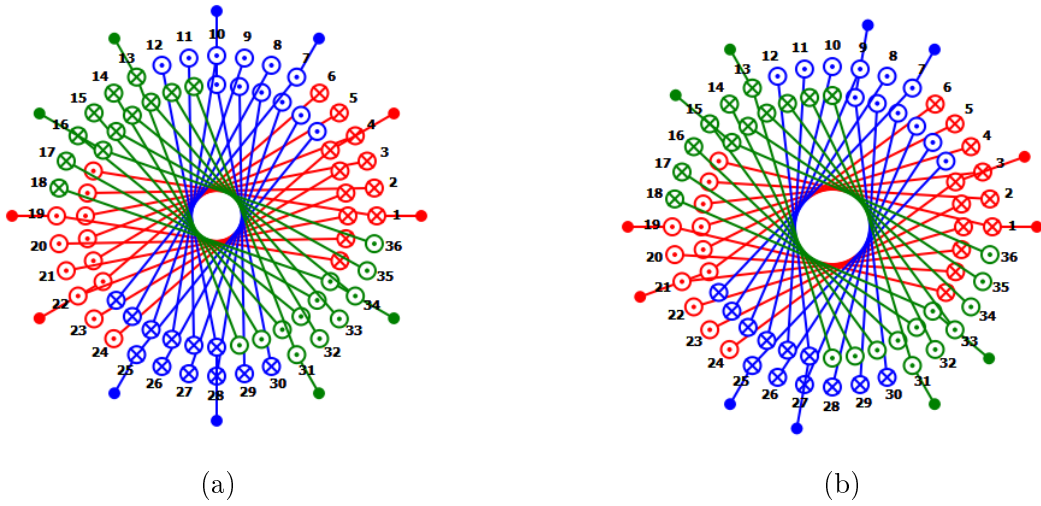


Figure 3.9: Coil pitch shortening optimization.

Therefore, this optimization is only valid for concentric winding and imbricated single-layer winding types.

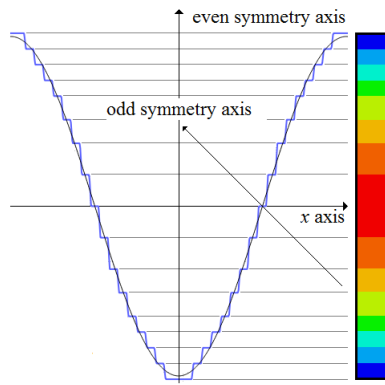


Figure 3.10: MMF symmetries.

Under these circumstances, the remaining solutions for this optimization approach are generalized in figure 3.11: the symmetry of the number of conductors inside each slot is from the center of the pole to its extremities, where two slots mutually distant for the pole's center may share the same number of conductors.

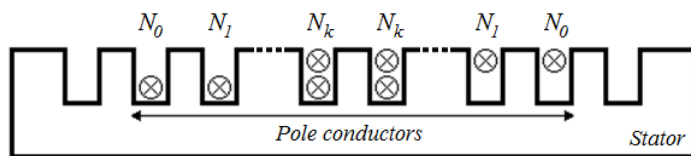


Figure 3.11: Pole conductors symmetry. Number of turns attribution (N_0, N_1, \dots, N_k) [4].

At this point, all possibilities for the winding pattern optimization have been discussed.

It seems easily understandable that the best solution found may produce an undesirable magnetic flux and the total amount of wire needed may not be economically and physically viable. Thus, these two design limitations must be taken into account when choosing the best solution.

3.6.2 Proposed Algorithm

As mentioned before in this section, the function to be minimized is the one that calculates the air-gap MMF THD (eq. 3.7). It was necessary to choose a method to solve this minimization problem. Two options were available, the nonlinear programming method and an iterative method. The chosen method was the iterative method, because of two main reasons: first, the finite space of solutions and the computational power available nowadays, which validates the use of an iterative method; second, nonlinear problems are extremely difficult to solve. Furthermore, it was not clear if this specific problem could have more than one feasible regions, and inside each region more than one valley may exist, possibly leading to false minimums. Therefore, the development a nonlinear programming method was not considered worth of the required work, due to time limitations.

The developed iterative method investigates all the space of solutions and the most adequate is imperatively chosen. Figure 3.12 presents the algorithm behind the winding optimization. Here, the two possibilities for the winding optimization may run alone or simultaneously. The user defines whether only the coils with different number of turns optimization (CDNTO) or the coil pitch optimization (CPO) should be used, respectively, by unchecking the coil pitch search check-box or checking it and making the turns search range (t_{rng}) equal to zero. If the two options are running simultaneously the CDNTO runs inside each iteration of the CPO. Inside the CPO, and whenever the CDNTO is executed alone, the procedures are exactly the same.

It all starts with the pre-processing routine, which prepares the data needed by the CDNTO to be executed efficiently. Its first procedure is to identify and group different coils of a phase, so the conditions for this optimization are fulfilled, in other words all poles of conductors follow the characteristics of figure 3.11. At the end of this procedure, the total number of groups of coils (N_{gc}), which effectively change their number of turns, is given by

$$N_{gc} = \text{ceil} \left(\frac{q + \frac{Z}{p} - \tau_{cp}}{2} \right),$$

where τ_{cp} is the effective coil pitch for double-layer windings. In case of single-layer or full-pitched windings $\tau_{cp} = Z/p$.

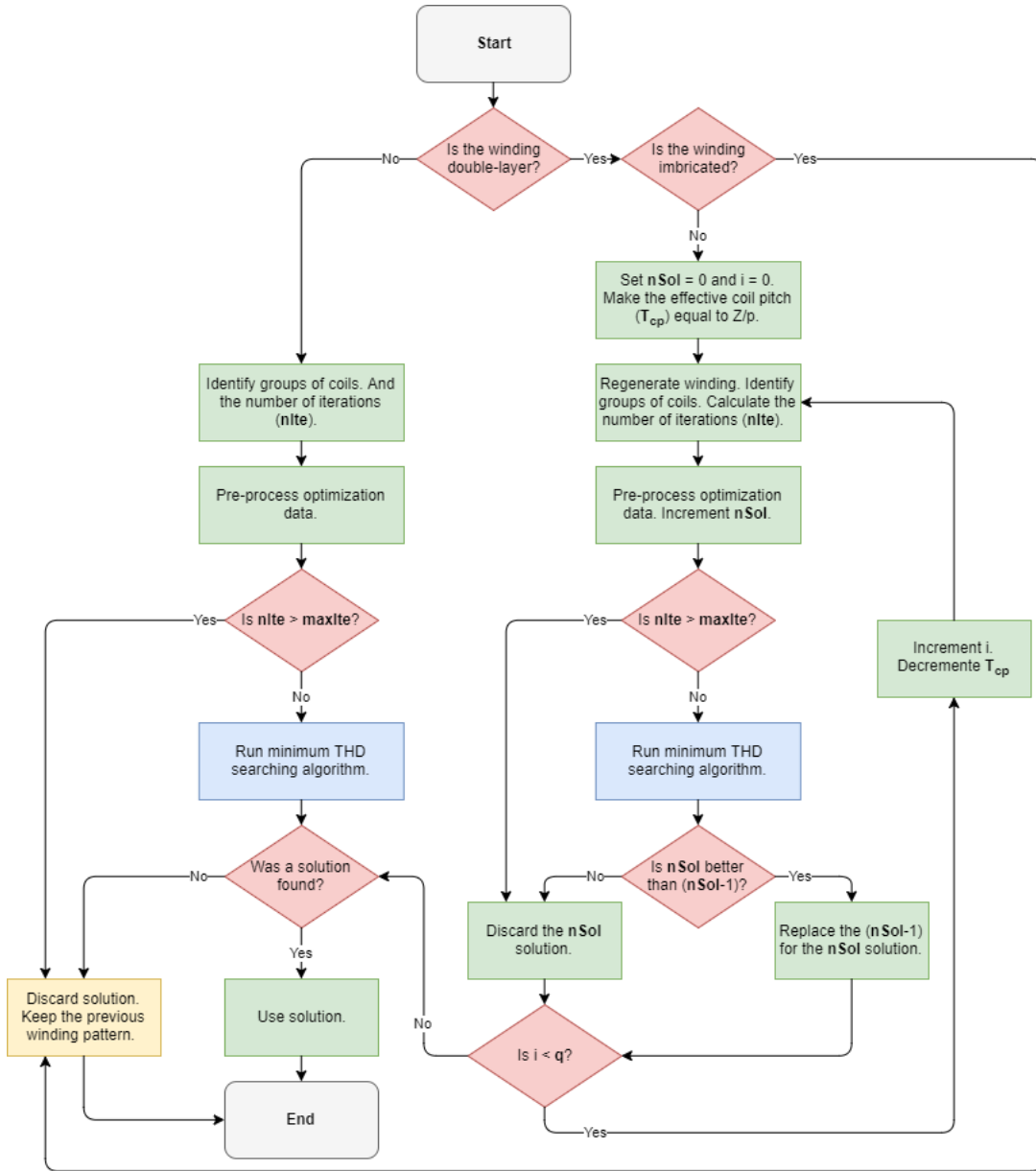


Figure 3.12: Winding optimization algorithm flowchart.

The next procedure is to calculate the maximum number of iterations, which is calculated through

$$n_{ite} = (2N_c \cdot t_{rng})^{N_{gc}}.$$

Finally, the last procedure of the pre-processing routine is the calculations of the wire length limit (L_{wu}) and the flux lower and upper limits (ϕ_l and ϕ_u , respectively). Each limit is set by the user. The wire length limit goes from a percentage of 70% to 130% of the new project's phase wire length. As for the magnetic flux, lower and upper limits can assume values from 95% to 100% and from 100% to 103% of the magnetic flux of the new project, respectively.

At this point the CDNTO may finally be executed. Figure 3.13 presents the CDNTO

algorithm. Here, the minimal MMF THD is found through the variation of the number of turns of the N_{gc} coils. Each variation is the result of the iteration number represented in a numeral system with radix equal to $2N_c \cdot t_{rng}$, where the least significant digit is the N_0 coil.

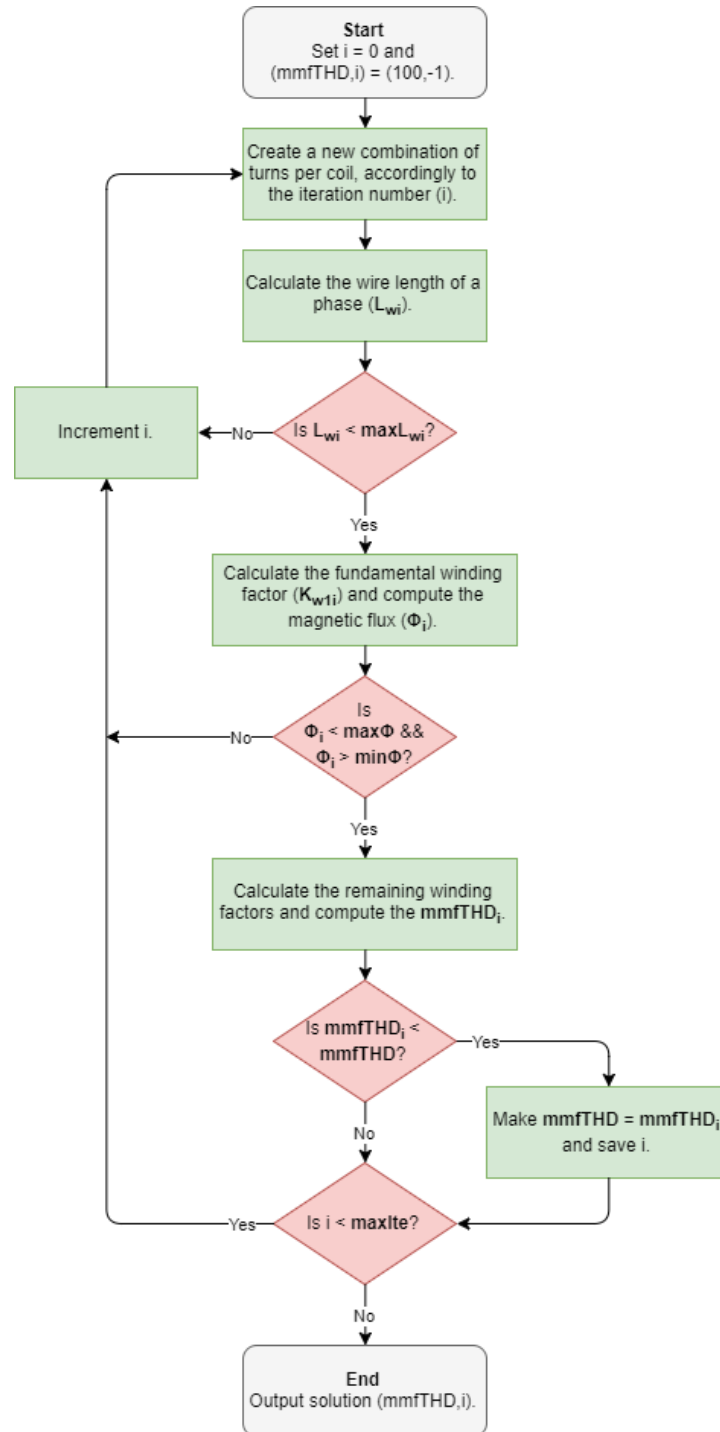


Figure 3.13: Flowchart of the minimum MMF THD search algorithm (through the CDNTO).

They all start with the same initial number of turns (N_{init}) equal to:

$$N_{init} = N_c \cdot t_{rng},$$

and finish with the same number of turns too (N_{end}) equal to:

$$N_{end} = N_c \cdot (1 + t_{rng}).$$

Then, the wire length (L_{wi}), winding factors (K_{wmi}), and magnetic flux (ϕ_i) of the i^{th} iteration are calculated by equations 2.7, 2.30, and 2.19, respectively (chapter 2).

The output of this algorithm is a structure of two variables, which saves the minimum THD found and the respective iteration number. This structure in the algorithm of the flowchart in figure 3.12 is defined as $nSol$.

3.6.3 Iterative Method Limitations

The unique limitation of the proposed iterative method is the computation time, which may increase proportionally with the number of iterations, in a worst case. The number of iterations is dependent of q , effective coil pitch, and the coils' number of turns. BobiSoft allows up to 2000 millions of iterations. As an extreme example, a CDNTO of 6 turns range of a three-phase machine with 180 slots, 2 poles, and a concentric double-layer winding short-pitched of 5 slots has 1839 million iterations to run. Thus, the machine in this example most likely does not exist. Nevertheless, the software should be able to use every available resource of the computer, so the algorithm may run within an acceptable time window.

The first strategy to speedup the algorithm was to optimize the code. In fact, at the current point of optimization the code runs approximately 200 times faster than the first attempt. Despite that, the huge speedup improvement will not be considered in the cumulative speedup, because it is independent of the machine resources. The strategy has mainly gone through the identification and replacement of the repeated calculations with variables containing the calculated value, which are determined before the algorithm is executed. Another strategy was the interruption of the current iteration if the wire length and magnetic flux limits were not exceeded.

After the code optimization, further speedups were only possible by means of hardware resources. Therefore, the first resource to use was the CPU, splitting the algorithm through all its cores (fig. 3.14). This was possible using the OpenMP API to solve this reduction problem. The speedup is approximately proportional to the number of CPU cores.

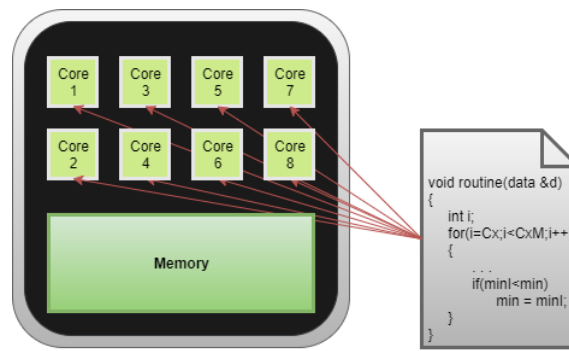


Figure 3.14: Parallelization of the CDNTO algorithm on the CPU cores.

The last available resource is the computer's graphic-card, which provides extreme parallel power due to the huge amount of processing cores used in the typical architecture. The algorithm was developed to run on Nvidia graphic-cards with CUDA cores. A separated program was created to handle the parallelization on the GPU. The speedup from an Intel core I3-5005U (with two cores 2GHz) for a NVIDIA GeForce 920M (with 384 CUDA cores 954 MHz) was about 12 times, however on the Nvidia GTX Titan X (with 3072 CUDA cores 1000 MHz) of the IT's NVIDIA research center (IT-Instituto de Telecomunicações, University of Coimbra) the speedup was about 150 times, running the 2000 millions of iterations in less than 15 seconds.

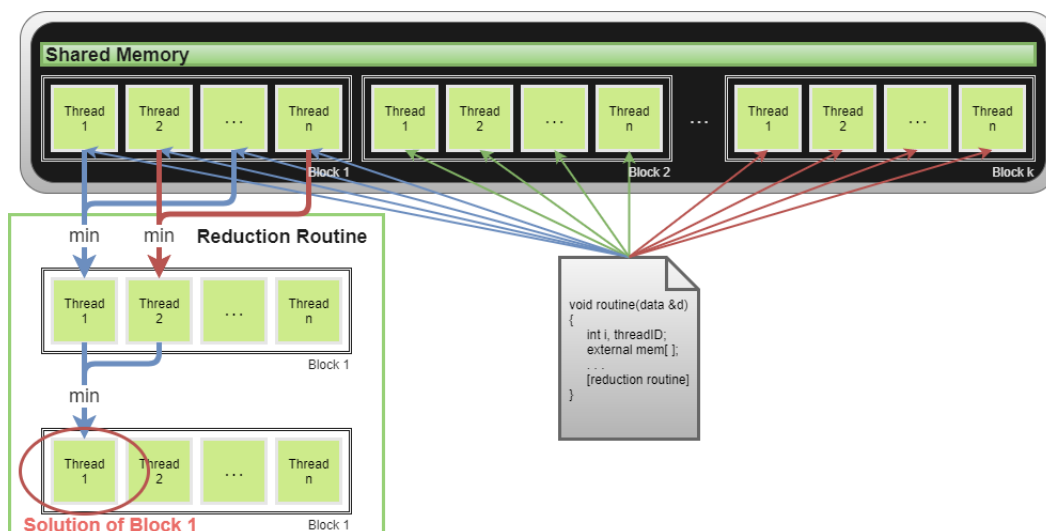


Figure 3.15: Parallelization of the CDNTO algorithm on the GPU cores.

Note that the code cannot be executed simultaneously on the CPU and the GPU. The user decides the platform to use. To conclude, after this speedup achievement the maximum number of iterations can perfectly be 10, 100, or even 1000 times higher. It can be increased if necessary.

3.6.4 Comparative Study

The example presented below establishes a comparative analysis between the CPO and CDNTO. For this example it was used a three-phase induction machine with 48 slots, 4 poles, and double layer winding ($q = 4$). The study consisted of varying the effective coil pitch of the winding and in each iteration was applied the CDNTO (limits defined: magnetic flux [98; 100]% and wire length below 100%). The air-gap MMF THD was calculated and the results are shown in the bar chart of figure 3.16:

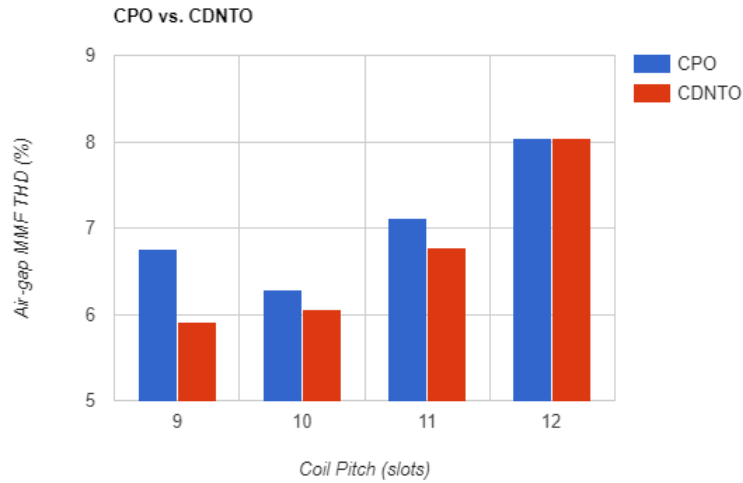


Figure 3.16: CPO and CDNTO comparative performances.

For each iteration the values of the air-gap induction peak, wire weight, and slot fill factor were registered on the table 3.2:

Table 3.2: Winding characteristics.

Quantities	Effective Coil Pitch:	9	10	11	12
B_1 (T)	CDNTO	0,587	0,590	0,590	0,594
	CPO	0,569	0,590	0,574	0,594
M_{wire} (kg)	CDNTO	8,52	8,37	8,28	8,48
	CPO	8,97	8,38	8,48	8,48
K_{fill} (%)	CDNTO	53,48	53,48	57,59	49,36
	CPO	53,47	49,36	49,36	49,36

From the above results, the CDNTO's best solution led to a reduction of the air-gap

MMF THD by 26,5%, a reduction of air-gap induction peak by 1,2%, an increase of 0,47% of the total wire weight, and an increase of the slot fill factor by 8,34%, comparatively to the original project (full pitch case). On the other hand, the CPO's best solution led to an air-gap MMF THD's reduction of 21,8%, a reduction of air-gap induction peak by 0,67%, and a reduction of 1,18% of the total wire weight.

In short, the CDNTO always improved the air-gap MMF distribution beyond the CPO used alone, as expected; except for the full pitch case, where was not found a solution within the specified boundaries. The greatest reduction of the air-gap MMF THD was achieved with the CDNTO for an effective coil pitch of 9 slots, despite the insignificant increase of the conductors' weight and the increase of the slot fill factor (which helps with the heating dissipation). This example proves the effectiveness of this algorithm and the additional jump in the winding's efficiency that can be achieved.

Additional examples can be found in [4].

Chapter 4

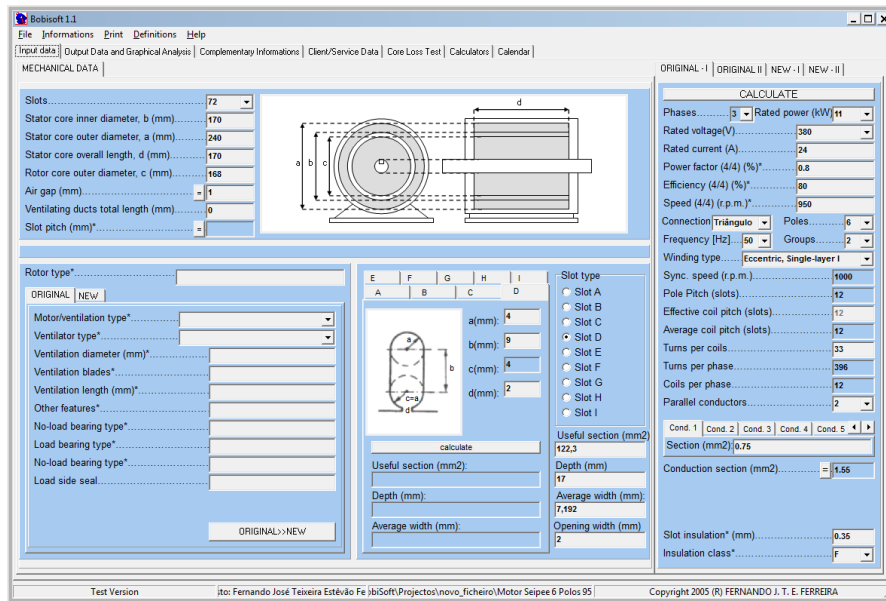
User's Interface

In this chapter, the program's interface is reviewed as well as the inherent routines used to design the projects' diagrams. In figure 4.1 the comparison between the old and new versions of BobiSoft is shown. Some modifications were done to the new version, so the user may find the software more intuitive and user friendly.

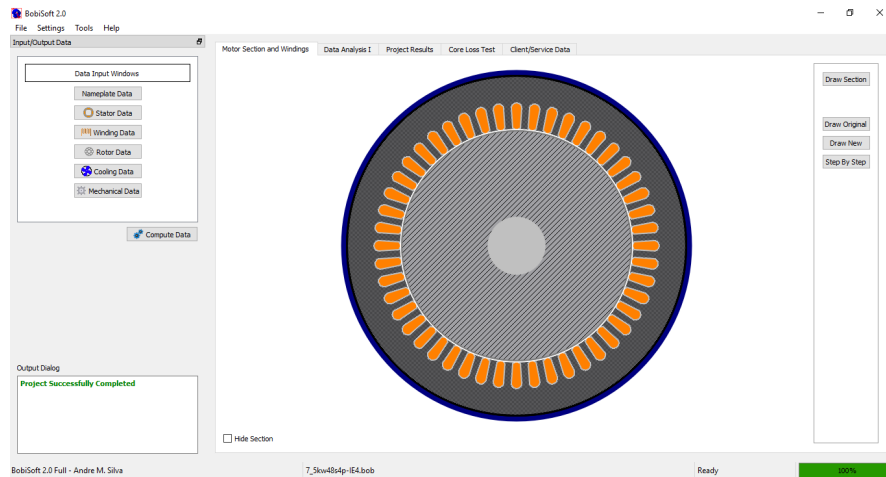
4.1 Data Input Interface

In the previous version, a dedicated multi-tabbed page was used as the interface for the data input. This way the data boxes were roughly packed into the tabs and disorganized. In order to make the interface less confusing and time consuming, two main changes were implemented. The first was to reorganize the data into families of the various machine parts, and the second was to create separated windows for these families. Therefore, the input windows of the nameplate, stator, winding, rotor, cooling, and mechanical data were created. These windows are permanently accessible through the dock area and each of them has two tabs, the original and new project pages, excluding the rotor data window. The winding data window has a third tab for the winding automatic tools setup. There is also a button that copies the data of the original project into the respective data boxes of the new project, which could accelerate the data insertion task.

In this version, the floating point of the numeric data is defined with the dot symbol, regardless of the user's region. The inserted data is validated at the beginning of the main computational routine. If invalid data is detected, a warning message is displayed locating the error.



(a) BobiSoft 1.1 interface



(b) BobiSoft 2.0 interface

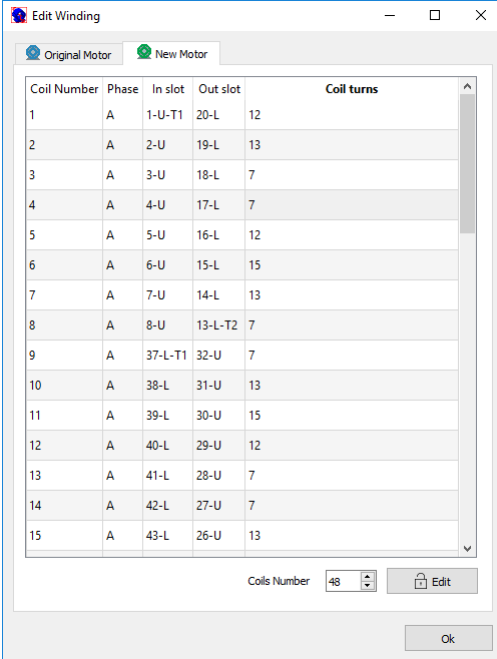
Figure 4.1: Interface comparison between BobiSoft versions

4.1.1 Winding Editing Tool Interface

The new version of BobiSoft allows the user to design its own winding pattern. For this purpose, the interface of figure 4.2a was created. With this tool the user is able to create any type of winding, including fractional windings, as long as it is symmetric. The number of turns of each coil can also be defined. In addition, this window can be opened next to a circular scheme of the winding, so it may guide the user.

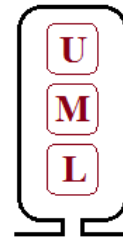
To use the winding editor the user just has to unlock the winding. Then, the winding can be fully editable, following simple rules: the slot layering must respect the order of figure 4.2b, the phase attribution is defined with the letters A,B, and C, and the winding terminals

are defined with T1 and T2.



Coil Number	Phase	In slot	Out slot	Coil turns
1	A	1-U-T1	20-L	12
2	A	2-U	19-L	13
3	A	3-U	18-L	7
4	A	4-U	17-L	7
5	A	5-U	16-L	12
6	A	6-U	15-L	15
7	A	7-U	14-L	13
8	A	8-U	13-L-T2	7
9	A	37-L-T1	32-U	7
10	A	38-L	31-U	13
11	A	39-L	30-U	15
12	A	40-L	29-U	12
13	A	41-L	28-U	7
14	A	42-L	27-U	7
15	A	43-L	26-U	13

(a)



(b)

Figure 4.2: (a) Winding editor menu. (b) Slot layering, U-upper, M-middle, and L-lower.

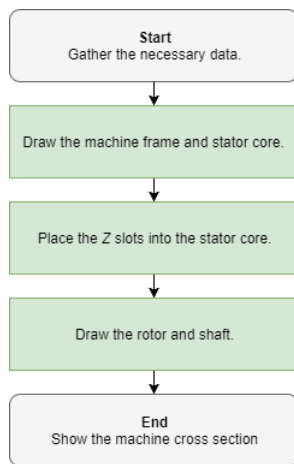
4.2 Output Data Interface - Project Results

In the software's new version, dedicated tabs are used to display the project results. The Data Analysis tab is used to show diagrams and schemes of the projects' windings, as well as the air-gap MMF wave and harmonics bar-charts. The Project Results tab shows the results carefully described in chapter 2, which may be used to evaluate the computed solution. The results of original and new projects are placed side-by-side, so the comparative analysis may be more efficient. Also, in this tab, the machine parameters and its torque-slip curve are displayed.

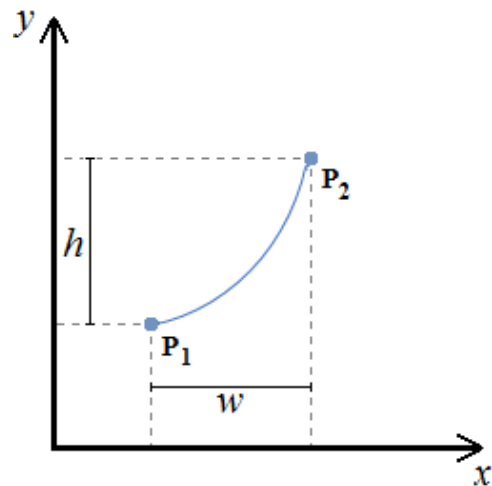
4.2.1 Machine Cross Section Diagram

The machine cross section diagram is displayed in the first tab of BobiSoft's main window (fig. 4.1b). This diagram may be extremely useful for the user to validate the stator and rotor geometric data, so the calculated solution is true to the real dimensions of the machine.

The following algorithm (fig. 4.3a) is used to generate the cross section diagram:



(a) Machine cross section drawing algorithm.



(b) Curve between points P1 and P2.

Figure 4.3: Machine cross section drawing procedures.

The slot drawing is based on the peripheral geometry subdivision. Thus, two geometric entities are identified, lines and curves. Lines are simply defined with two points; in this case, by the extreme points of the line. Curves are traced through trigonometric functions; for the example of figure 4.3b the n points of the curved are calculated with the following expressions:

$$P_n(x, y) \begin{cases} P_{x_n} = P_{1x} + w - w \cdot \cos\left(\frac{\pi}{2N} \cdot n\right) \\ P_{y_n} = P_{1y} + h \cdot \sin\left(\frac{\pi}{2N} \cdot n\right) \end{cases}$$

4.2.2 Winding Pattern Schemes

Understanding the winding pattern is not, in most cases, a quick and easy task. Mistakes can be easily made, so the representation of the winding pattern may be the simplest and containing the most information. The software offers several schemes to help the user quickly and fully understand each winding pattern.

The circular scheme (schemes represented in figure 3.1 of chapter 3) is probably the simplest and preferable scheme to quickly get the big picture of the winding pattern. In fact, the new version added the representation of the current direction in the slot for the going in current with \otimes , and, for the going out current with \odot , which identify the coil-sides.

The algorithm used to draw the circular scheme of the winding pattern is presented in figure 4.4.

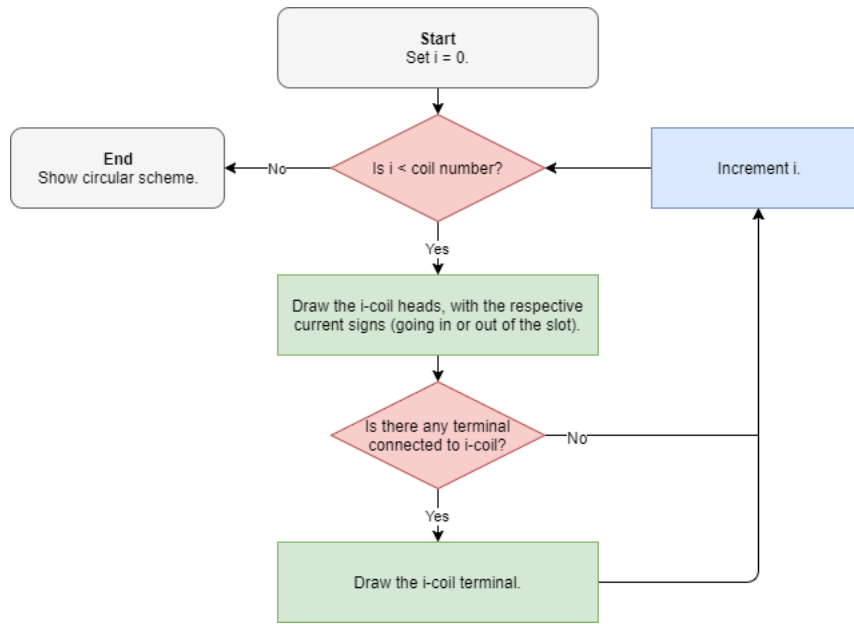


Figure 4.4: Winding pattern circular scheme drawing algorithm.

Another layout available is the planar scheme (fig. 4.5). Its understanding is more complex than the circular scheme, but it adds the inter-coils connection representation, making it the most complete scheme for the rewinder's guidance. In this version, the planar layout is fully represented, including the winding connection to the machine's terminals, being very similar to the planar scheme used by the WEG manufacturer. In fact, it was one of the requirements to obtain the WEG-Portugal official approval.

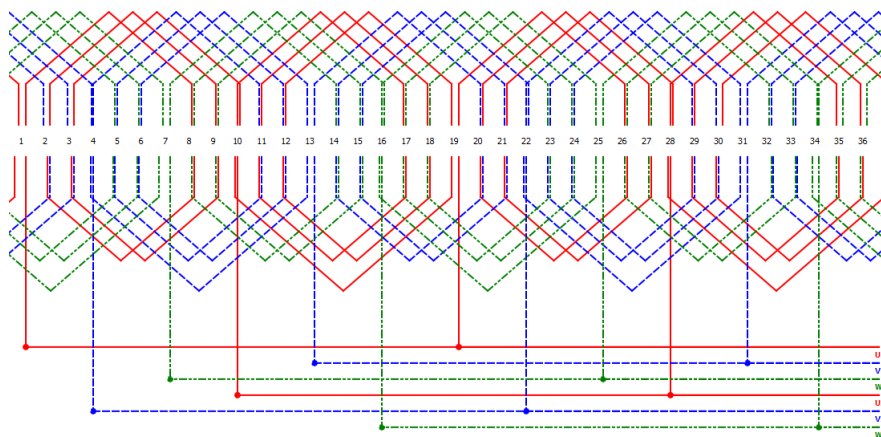


Figure 4.5: Winding pattern planar scheme.

The planar winding pattern layout is generated through the algorithm of figure 4.6.

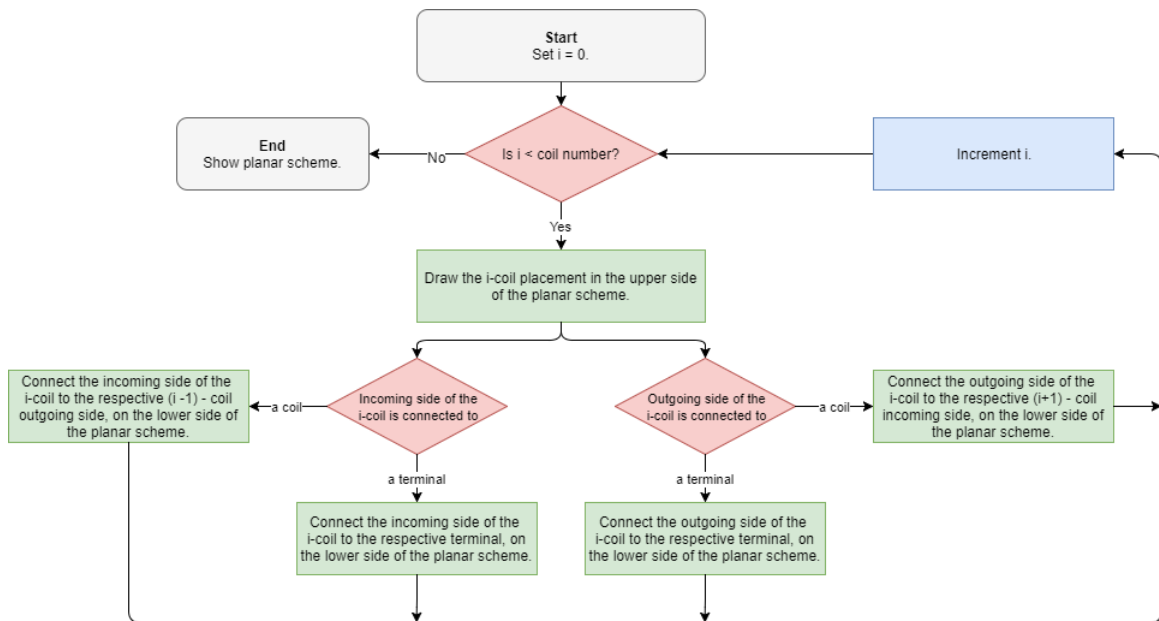


Figure 4.6: Winding pattern planar scheme drawing algorithm.

The software also provides textual forms of representing the winding layout, by the use of tables and lists (fig. 4.2a).

4.2.3 MMF Air-gap Waveform Graph

The MMF air-gap waveform graph is provided as an important project evaluation key (fig. 4.7). In the software's new version the amplitude of the waveform is given in A.turn/m. The fundamental MMF wave is also shown for the quick perception of the harmonic content improvement or degradation.

Because a snapshot of the MMF waveform is not sufficient to verify the correctness of the winding design, a new functionality was added to simulate the translation carried out by the MMF wave along the air-gap periphery. The options of phases' swap, phase current inversion, and phase shift of electrical 180° are included in the analysis, making the correct adaptations to the resultant MMF equation 2.29 (chapter 2). Therefore, the phases' swap changes the sequence order of the m phases of the winding, and for the phase current inversion and phase shift of electrical 180° it is enough to add the angle of 180° in the time and spatial terms of equation 2.29, respectively.

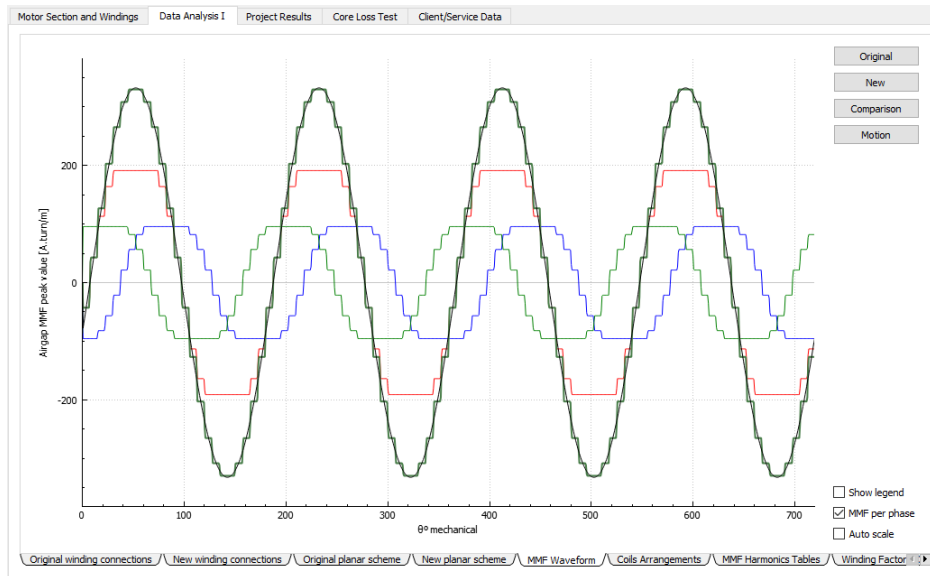


Figure 4.7: MMF waveform graph.

4.2.4 Machine Parameters and Torque-Slip Curve Interface

Many software for the designing of rotational electric machines output, among other results, the projected machine parameters and its torque-slip curve. These two results were perfectly possible to obtain with the data given by the user. So, a new interface was added to BobiSoft (fig. 4.8).

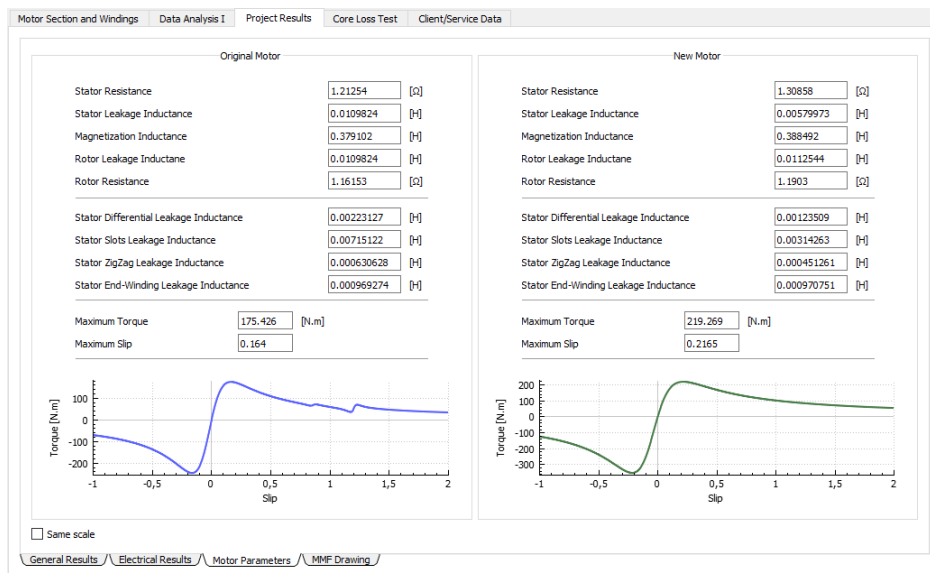


Figure 4.8: Machine parameters and torque-slip curve interface.

This interface gives the user the induction machine parameters of the equivalent circuit. One direct and important result that can be extracted from these parameters is the machine's torque-slip curve. In chapter 2, the theory behind the complete equivalent circuit, including

the interference of spatial harmonics, is explained, making the calculated curve a decisive result of the evaluation of the machine's performance at different points of operation.

Many other interesting results can be found from the machine's parameters, such as the efficiency maps (if the iron resistance (R_{fe}) is known).

4.3 Alternative Air-gap MMF Calculation

In BobiSoft 2.0, a new method to determine the winding factors from the air-gap MMF waveform was introduced. This procedure is purely didactic, since it calculates a result which has been previously calculated by the BobiSoft's main computational routine.

The air-gap MMF is firstly drawn through the slot's conductors positioning, the slot opening creates the transition slope between teeth (whenever the slot's opening is neglected this transition is a vertical line), thus creating the characteristic stepped waveform of the MMF distribution. This procedure is made to all phases, and finally all pulsating MMF waveforms are summed, resulting in the air-gap MMF waveform for a specific time. Finally, a FFT is applied to this waveform and the winding factors are retrieved. In figure 4.9 a comparison between the calculated and the retrieved winding factors is shown. The winding factors, calculated through this alternative method, are very close to those of the classic theory.

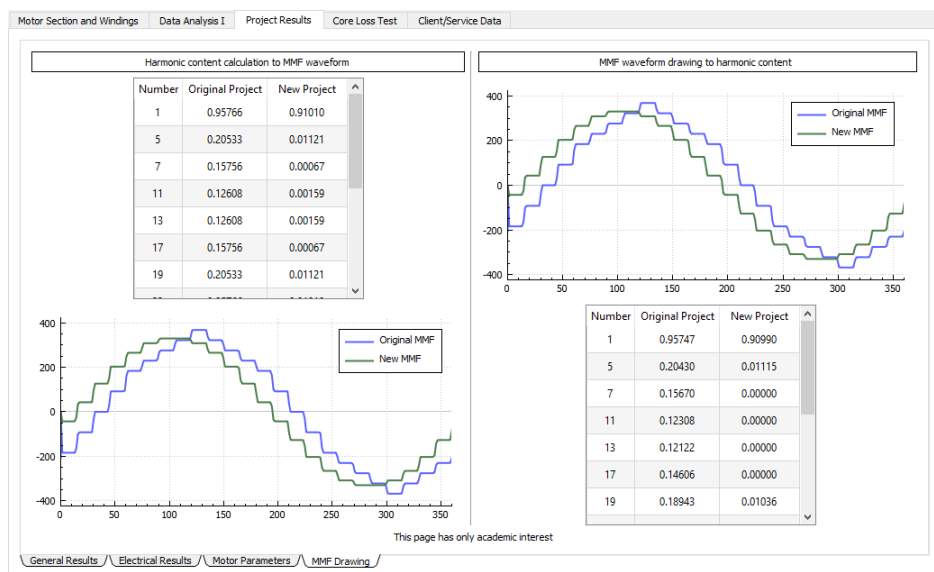


Figure 4.9: Alternative air-gap MMF calculation interface.

4.4 Core Loss Test Interface

The main cause of the electric motors' efficiency reduction, after the rewinding service, is the damage caused by the winding extraction process, which in most times is impossible to do without heating the stator. This has a negative impact on the stator core losses, since the insulation between the ferromagnetic sheets may be damaged.

The quality of stator core after the extraction can be evaluated with the core loss test, which has a specific interface in BobiSoft to help the user to perform the test (fig. 4.10).

The screenshot shows the following data in the 'Measurements' section:

Stator Core Temperature				
	Room	Start	End	Period
Before Extration	22	22	50	15
After Extration	22	22	53	15

Power			
	Voltage	Current	Power
Before Extration	230	2	300
After Extration	239	3	310

The 'Report' section contains the following text:

```

Report:
-Temperature Rise Before [°C]: _____ 28
-Temperature Rise After [°C]: _____ 31
-Power/weight Before [W/kg]: _____ 17.2493
-Power/weight After [W/kg]: _____ 17.318

Evaluation
Health index [Power]: _____ 0.967742
Health index [Temperature]:_ 0.903226
Final Evaluation: _____ Approved

```

Figure 4.10: Core loss test interface.

In this tab the user can quickly perform all calculations related to the Electrical Apparatus Service (EASA) guideline (EASA Tech. Note No. 17), in order to evaluate the stator core losses. This test is based on the variation of the stator core temperature and its losses under certain conditions before and after the winding extraction. For this test, the voltage source must be alternated and the amplitude the lowest as possible, in a way that the number of turns needed by the test coil is minimized. The minimum period of time necessary for each test is 15 minutes.

The test coil turn's number is automatically calculated by the software, as specified by the guidelines. It is not mandatory to fill up the values of voltage and current applied to the test winding, since their values are merely indicative. The final evaluation is merely qualitative, thus it helps the rewinder to decide whether the stator core is still acceptable for rewinding. The core loss test report can be printed.

4.5 Client Data Interface

The program has a dedicated menu for the registration of the client and service data. In this new version the user can upload images into the project file, such as the photos of the machine status before and after the repair is concluded. All this data can be printed and attached to other reports.

4.6 Summary of BobiSoft 2.0 New Features

The development of the new version of BobiSoft implicated the review of all calculations and algorithms. The following list summarizes the new main features added to BobiSoft:

- New Interface;
- Machine's cross section drawing;
- Improved circular and planar winding schemes;
- Free winding editor;
- Crossed winding heads avoidance tool;
- Eccentric groups of concentric windings creation tool;
- Automatic wire section selection tool;
- Automatic winding optimization tool;
- Automatic downsizing tool;
- Magnetic saturation effect;
- Machine parameters calculator (rotor parameters estimation);
- Stepped MMF waveform to winding factors calculator (academic interest only);
- Service photographic data registration;
- Wire material conversion calculator, in miscellaneous calculators;
- Option to export the project data to an EXCEL sheet (*CSV file creation);
- New automatic printable reports.

Additional and detailed information about the software interface can be found in the BobiSoft user's manual.

Chapter 5

Experimental Validation

This chapter presents the experiments performed to validate the software results.

A last version of BobiSoft 2.0 is being commercialized since May 2017 and several comments and suggestions have been given by the users. Therefore, so far, the software has been constantly updated and improved. In addition, new features have been created to satisfy BobiSoft's users.

The software's version 2.0 has been sold to universities, rewinding shops, and motor manufacturers across the world, such as: the Universidad Autónoma de Occidente, Cali, Colombia; the French research institute LAPLACE (Laboratoire Plasma et Conversion d'Énergie - Institut National Polytechnique de Toulouse); the EMS group (rewinding and maintenance), Australia; Universal Motors (motor manufacturer), Portugal; JJ Loughran (electric motors), Ireland.¹

Every day BobiSoft is being tested and used by hundreds of users all over the world, including those using the first versions. Consequently, constant attention is being paid to every feedback. During the development of the second version, the results of each calculation process have been compared to those of the original version, as a reference of validation. The final version of BobiSoft 2.0 has received the WEG-Portugal recommendation, after an internal technical evaluation. Many features had to be added and reviewed, so the software could pass their tests.

The above facts demonstrate the software's usefulness and quality. Nevertheless, some experimental tests have been carried out to confirm the effectiveness of some of the new tools added to this second version. It has also been conducted a supervision of the software's usage by a rewinder from the SindelTech company, based in Gafanha da Encarnação, Aveiro,

¹The Ph.D. student Victor Aguiar from the Federal University of Ceara, Fortaleza, Brazil, is currently using BobiSoft 2.0 for the development of his thesis (rewinding strategy as a solution to increase efficiency of industrial motors).

Portugal (July 2017). During this supervision two motors have been rewound following the project directives of the software.

5.1 Machine Equivalent Circuit Parameters Test

In this section, the machine's stator parameters, calculated by BobiSoft, are experimentally tested (rotor parameters are excluded from this test, because the program does not calculate them).

In [36], four induction machines are fully parameterized, following the IEEE 112 standards. The tested machines have the same rated power but different efficiency classes. The manufacturer provided the design detailed information, making it possible to simulate these machines in the software. In table 5.1, the measured and simulated parameters are compared.

Table 5.1: Comparison between measured and simulated stator equivalent circuit parameters of IE1-4 induction machines.

Motor Class	Parameter (Ω)	Measured	Simulated	Error (%)
IE1	R_s	2,20	2,20	+0,00
	X_{ls}	4,10	4,59	-11,28
	X_m	99,06	96,66	+2,45
IE2	R_s	2,20	2,20	+0,00
	X_{ls}	4,21	3,91	+11,82
	X_m	117,42	118,87	-1,23
IE3	R_s	1,61	1,61	+0,00
	X_{ls}	3,72	3,27	+12,88
	X_m	113,38	111,43	+1,73
IE4	R_s	1,25	1,25	+0,00
	X_{ls}	3,20	2,84	+11,92
	X_m	94,01	97,13	-3,26

Note: the wires materials' resistivity were adapted to the temperature of 40°C.

The results of table 5.1 show a fair accuracy of the simulated machines' parameters. The windings' resistance was intentionally forced to be approximate to the measured values,

so the winding heads' length could match those of the real winding². The simulated magnetizing reactance is extremely accurate to the measured values. On the other hand, the simulated stator leakage reactances' accuracy is not that accurate, but still quite satisfactory. Therefore, it is important to note that these parameters are highly dependent on the machine's geometry, and slight constructive deviations may affect them significantly. Other important aspect to be considered is the impossibility to separate, with this test, the stator from the rotor leakage inductances. Their values are obtained through standardized tables of the leakage inductances' distribution (table 2.2, chapter 2), which in reality may not correspond exactly as listed.

5.2 Coil Pitch Optimization Test

The test presented in this section has the purpose of validating the shortening pitch winding optimization.

For this test was assembled the experimental setup of figure 5.1. A three-phase induction machine was used ($Z = 36$ and $p = 4$, thus $q = 3$), with configurable coils assembled in an eccentric configuration (fig. 5.1-a). This machine has incorporated three test coils equally distanced (fig. 5.1-b). Electric measurements were obtained with the YOKOGAWA WT1800 power analyzer (fig. 5.1-c). The power source used was the PACIFIC 3300 AFX (30 kVA), which generates a free of harmonics, perfectly balanced three-phase voltage system (fig. 5.1-d). A data acquisition device of National Instruments (fig. 5.1-e) is used to acquire the mechanical vibrations signal measured with an accelerometer. Finally, to process the signal in real time, a Signal Express environment was developed (fig. 5.1-f), which outputs the mechanical vibration signal's FFT.

In BobiSoft, the machine's winding was reproduced. Three windings were created: full pitch, short pitch (one slot), and short pitch (two slots). The characteristics of these windings are shown in table 5.2. For each configuration, the magnetizing flux was kept constant, thus the supply voltage was adapted for each case.

²Additional head lengths used in the simulation: 21%, 23%, 18%, and 17%, for IE1-4, respectively.

Table 5.2: BobiSoft projected windings' characteristics.

Winding Type	Supply Voltage (V)	Winding Factor	MMF THD (%)
Full Pitch	400,0	0,9598	10,67
Short Pitch (1 slot)	393,9	0,9452	9,48
Short Pitch (2 slots)	375,9	0,9019	9,26

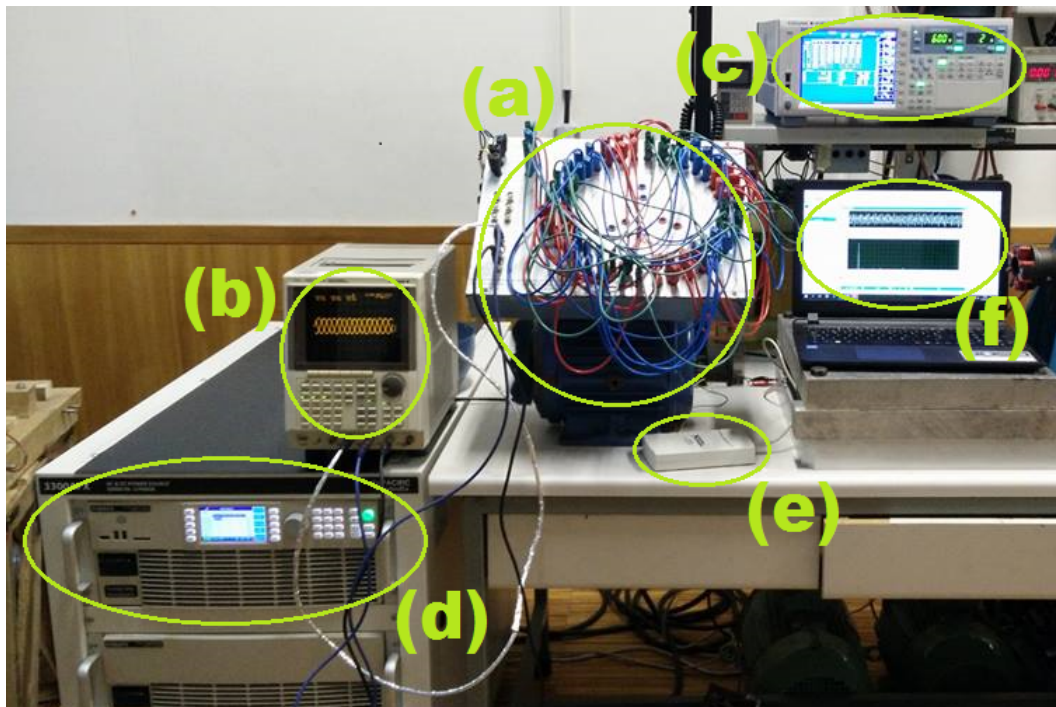


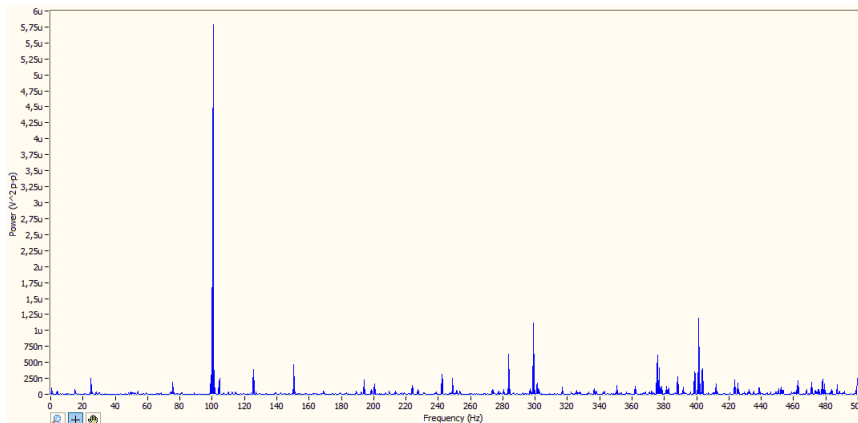
Figure 5.1: Coil pitch optimization experimental setup.

The experimental results are presented in table 5.3. The magnetizing flux was kept practically constant, despite the slight deviation in the full pitch case, therefore the flux adaptation equation is validated (eq. 3.1, chapter 3).

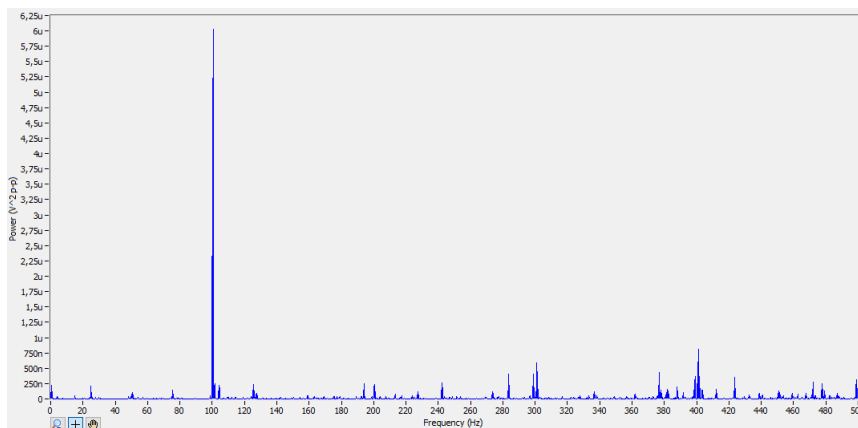
Table 5.3: Coil pitch winding optimization experimental results.

Measurement	Full Pitch	Shortened Pitch (1 slot)	Shortened Pitch (2 slots)
U_s (V)	400,08	393,92	375,90
I_s (A)	0,874	0,896	0,936
PF	0,111	0,108	0,111
I_{THD} (%)	0,332	0,298	0,259
Test Coil (V)	1,351	1,319	1,320

The reduction of the air-gap MMF THD could not be measured, however its effects are observed as expected in the line current, as its THD tends to be smaller when the winding is increasingly short-pitched. The rms value of these currents increases with the shortened pitch due to the reduction of the supply voltage. Regarding the vibration level (fig. 5.2), an attenuation with the shortened pitch was observed, as expected. For the full pitch case (fig. 5.2a) the vibration component of the 100 Hz was slightly lower than the two slots short-pitched winding case, but the remaining harmonic content is significantly higher. In fact, the vibration reduction was perceptible by the motor's acoustic noise. To conclude the CPO was verified, since the air-gap MMF THD, vibration, and acoustic noise were reduced.



(a) Full pitch.



(b) Shortened pitch of two slots.

Figure 5.2: Frequency spectrum of the measured mechanical vibrations.

5.3 In-field Test

The purpose of the in-field test was to identify possible errors and validate the effectiveness of the interface and results. The test was conducted at the SindelTech company, whose rewinder never had a previous contact with BobiSoft.

Two machines were available for rewinding. The supervisors asked for the first test to maintain the original winding layout, so they could confirm that the software was working properly and the results were the expected. Thus, BobiSoft was only used for the project's record and documentation. In this case, the machine to rewind was a pump of the sewage system of SIMRIA's water company, powered by an induction machine. The main characteristics of this machine and the project results are presented in table 5.4. The full process of this rewinding is documented in appendix D.

Table 5.4: SIMRIA rewinding project results.

Machine's Caracheristics	Original/New Project
Number of Slots	36
Slot Useful Section (mm ²)	82
Stator Bore Diameter (mm)	120
Stator Length (mm)	167
Air-gap (mm)	1
Slot Fill Factor (%)	52
Wire Weight (kg)	4,92 (4,73 extracted)
Winding Type	Concenctric, single-layer
Wires' Section (mm ²)	2x0,33 + 0,28
Number of Turns	45
Number of Poles	2
Number of Parallel Groups	2
Air-gap MMF THD (%)	6,36
Air-gap Induction (T)	0,62
Magnetizing Current (A/ph)	3,53
Winding Resistance (Ω /ph)	0,86 (0.91 measured)

This induction machine was not tested, apart from the measurement of the winding resistance, since its rotor could not be removed out of the sewage pipe.

In the second rewinding, the supervisors agreed to implement an optimized winding projected by the software. The machine's owner was aware of the situation and became very interested in the optimization, asking for the project's documentation, which was provided. This rewinding case was a vacuum system, powered by an induction machine (rated voltage:

400 V, rated current: 12,3 A, rated power: 5,5 kW, and rated speed: 720 rpm). The optimization consisted on the replacement of the damaged single-layer imbricated winding with a double-layer imbricated winding with an effective coil pitch of 5 slots. The characteristics of the machine and the project results are described in table 5.5.

Table 5.5: Uni-Motors rewinding project results.

Machine's Caracteristics	Original Project	New Project	Measurement
Number of Slots	48		
Slot Useful Section (mm ²)	92		
Stator Bore Diameter (mm)	200		
Stator Length (mm)	143		
Air-gap (mm)	0,6		
Slot Fill Factor (%)	52	54	
Wire Weight (kg)	6,1	5,8	6,2 / 5,8
Wires' Section (mm ²)	2x0,33 + 0,28	0,57 + 0,50	
Number of Turns	44	23	
Number of Poles	8	8	
Number of Parallel Groups	1	1	
Air-gap MMF THD (%)	15,6	13,9	
Air-gap Induction (T)	0,77	0,76	
Magnetizing Current (A/ph)	3,70	3,63	4,33
Winding Resistance (Ω /ph)	3,33	3,16	3,42 / 3,18

The machine's magnetizing current differs quite significantly from the simulated result, because the vacuum gum was coupled to the machine's shaft, which created much friction while spinning. The motor was surprisingly quiet, which made necessary to double check the supply voltage. The significant reduction of the winding weight was possible due to the rewinder's dexterity in reducing the head's length. The rewinder had some difficulty to assemble the winding, since the slot fill factor was increased by two percentage points. Nonetheless, the rewinding was performed within the usual timing. The rewinder suggested the use of more parallel wires of reduced section, so the winding could have been easier to assemble.

In figure 5.3 this machine's parameters and the torque-slip curve of both projects are

presented. The reduction of the air-gap MMF THD was beneficial to the stator leakage reluctance (it was reduced by 32%). Consequently, the maximum torque was increased and the nominal slip was reduced. In the torque-slip curve of the new project the practical parasitic torques' elimination can be observed.

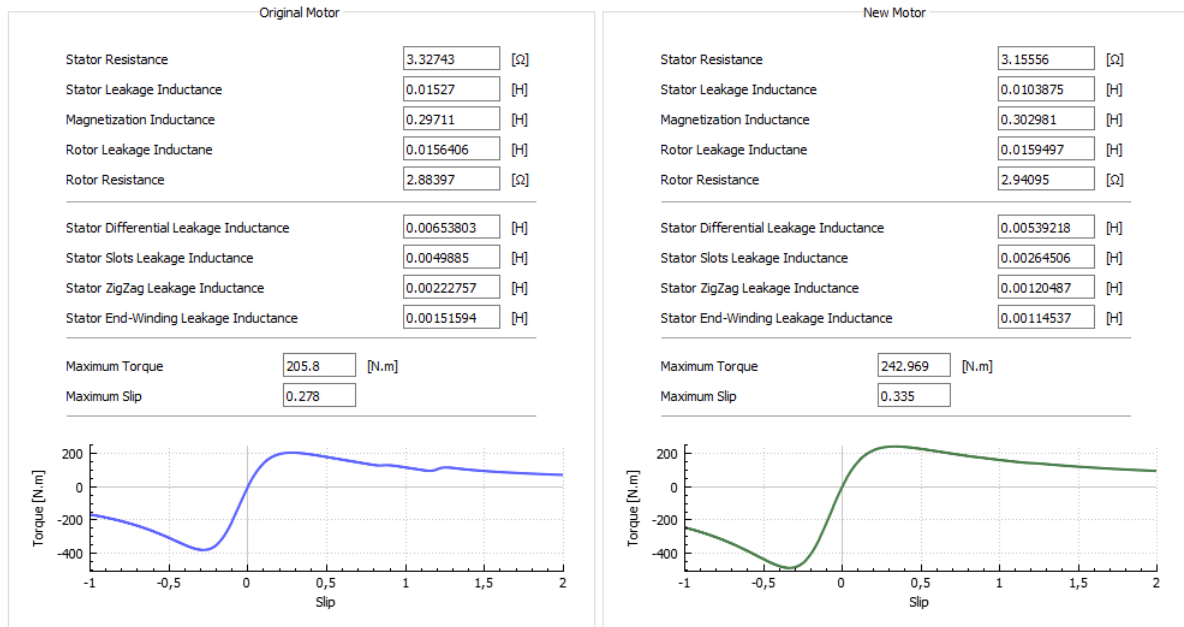


Figure 5.3: Uni-Motors motor parameters and torque-slip curve of the original and new projects.

5.3.1 Conclusions of the In-field Test

BobiSoft fulfilled all the expectations for this test. The rewinder was surprised by the quick output of solutions and the theoretical support that the software provides. For example, the determination of winding's number of turns per coil was a mystery to him. He uses an empirical formula given to him by his mentor which is not totally correct.

In the rewinder's opinion, the interface was very clear and intuitive, although many results were beyond his comprehension, and, therefore, useless to the rewinding task. The two results that the rewinder found extremely interesting were the air-gap induction (machine's saturation) and current density (machine's heating), for which BobiSoft emits a warning if their values be outside the typical/acceptable boundaries. Thus, the rewinder realized the material savings he could achieve if he pushed the machines to their limit during the rewinding process.

To conclude, the winding's circular scheme was, in the rewinder's opinion, the best representation for winding pattern's. Due to his experience he needed only a few seconds

to understand the winding pattern (different winding patterns were presented to him and were quickly recognized or understood). The only aspect he would change is the one-phase circular scheme representation, since for more complex windings the representation of other phases may make it more confusing.

Chapter 6

Conclusions and Future Work

BobiSoft's new version was successfully created during the development of this master's thesis. The software was completely rewritten, the interface was renewed, and new important features with practical and academic interest were developed.

Firstly, a copy of BobiSoft's previous version was programmed. All results have been exhaustively compared, in order to validate not only their correctness but also the robustness of the software's structures.

Secondly, all winding schemes were improved. The winding editor was added to this new version allowing the design of fractional and any other type of symmetric windings. Then, there was a need to make the software capable to handle two-phase induction machines as well. Thus, all calculation processes and routines were reviewed and generalized to support two- and three-phase induction machines (some of these calculations are already generalized to any phase number, as seen in chapter 2).

Thirdly, the development of more relevant features brought a higher notoriety to BobiSoft. The most relevant one is the automatic winding optimizing tool, which is a unique search algorithm that finds the combination of different turns per coil conjugated with shortened pitch which minimizes the air-gap MMF harmonic content. This algorithm uses the fastest available resources of the user's computer to determine the best solution, dividing the computational efforts into the available CPU or GPU units, providing to the users an additional opportunity to design less noisy and more efficient machines (this last benefit is expected, but not tested yet). Another important feature is the automatic downsizing tool that allows the user to increase the efficiency of oversized induction motors, adapting only the winding's number of turns. Lastly, the analytical calculation of the machine's equivalent circuit parameters gives the possibility to evaluate the machine's performance, such as the torque-slip curve.

Finally, the experimental tests performed showed good results, validating almost all

BobiSoft 2.0 functionalities. In addition, the in-field test endorsed the quality and applicability of this unique software, proving, as well, its easy to use interface, the expedite winding's creation, and the easy communicability of complex technical information.

To conclude, since May 2017 BobiSoft 2.0 is being commercialized and universities, research centers, motor manufacturers, and motor maintenance companies have acquired this version. This demonstrates interest from many sectors of the electric motor industry for this software.

BobiSoft can still be much more developed. The list bellow presents work that can be developed:

- Conducting experimental tests to validate or rebuff the efficiency benefits expected from the CDNTO;
- Investigation of a nonlinear programming method to solve the CDNTO's problematics (alternative to the iterative method);
- Expand and generalize the program to handle windings with m-phases and n-layers;
- Expand and generalize the program to design windings of single-phase induction machines;
- Development of fractional winding automatic design tool;
- Add efficiency maps to project outputs;
- Creation of new project's nameplate output interface;
- Creation of a BobiSoft's expansion pack for the full design of rotational electric machines with distributed windings, including the rotor design and analysis;
- Integration of FEA in the program, in order to solve magnetic and thermal field problems.

Bibliography

- [1] A. o. E. Electrical Apparatus Service Association and M. Trades, “The Effect Of Repair/Rewinding On Motor Efficiency,” *EASA/AEMT Rewind Study and Good Practice Guide to Maintain Motor Efficiency*, pp. 1–3, 2003.
- [2] S. Nandi, H. A. Toliyat, and X. Li, “Condition monitoring and fault diagnosis of electrical motors—a review,” *IEEE Transactions on Energy Conversion*, p. 719–729, 2005.
- [3] A. T. de Almeida and F. J. T. E. Ferreira, “Actions to promote energy-efficient electric motor repair,” *Inter. Journal of Energy Technology and Policy*, pp. 302–314, 2003.
- [4] F. J. T. E. Ferreira, A. M. Silva, and A. T. de Almeida, “Software tool for fast and optimized design of three-phase stator windings of induction motors,” *EEMODS2017*, 2017.
- [5] A. O. Di Tommaso, F. Genduso, and R. Miceli, “A new software tool for design, optimization, and complete analysis of rotating electrical machines windings,” *IEEE transactions on magnetics*, 2015.
- [6] A. C. Smith and D. Delgado, “Automated ac winding design,” *Proc. 5th IET Int. Conf. Power Electron., Mach. Drives (PEMD)*, pp. 1–6, 2010.
- [7] softBit, accessed 2017-04-10. [Online]. Available: <http://www.softbitonline.com/index.html>
- [8] Emetor AB, accessed 2017-04-10. [Online]. Available: <https://www.emetor.com/>
- [9] JSol Corp., accessed 2017-04-11. [Online]. Available: <http://www.jmag-international.com/>
- [10] MagneForce, accessed 2017-04-11. [Online]. Available: <http://www.magneforcess.com/>
- [11] Vladimir Kuptsov, accessed 2017-04-11. [Online]. Available: <http://motoranalysis.com/>

-
- [12] MotorDesign, accessed 2017-04-11. [Online]. Available: <https://www.motor-design.com/>
- [13] Infolytica Corp., accessed 2017-04-15. [Online]. Available: <https://www.infolytica.com/en/products/motorsolve/>
- [14] Vector Fields Software, accessed 2017-04-17. [Online]. Available: <http://operafea.com/motor-design-software/>
- [15] Tera Analysis, accessed 2017-04-17. [Online]. Available: <http://www.quickfield.com/>
- [16] elmoCad, accessed 2017-04-10. [Online]. Available: <http://www.elmocad.de/products-3/smartfem-2/>
- [17] M. Jurkovic and D. Zarko, "Optimized design of a brushless dc permanent magnet motor for propulsion of an ultra light aircraft," *Journal Automatika*, pp. 244–254, 2012.
- [18] CD-adapco, accessed 2017-04-17. [Online]. Available: <http://www.speed-emachine-design.com/>
- [19] Yeadon Energy Systems Inc., accessed 2017-04-17. [Online]. Available: <http://www.yeadoninc.com/>
- [20] G. Maier, H. Kdfler, and J. Bacher, "The use of pitch factor in calculations of ac-machines with concentrated windings," *Proc. Eur. Power Electron. Drives Assoc. (EPE)*, pp. 1–6, 2005.
- [21] P. Krause, O. Wasynczuk, S. Sudhoff, and S. Pekarek, *Analysis of Electric Machinery and Drive Systems, Third Edition*, 2013.
- [22] B. J. Chalmers and A. C. Williamson, *A.C. Machines: Electromagnetics and Design*, 1991.
- [23] I. Boldea and A. S. Nasar, *The induction machines design handbook, second edition*, 2010.
- [24] A. E. Fitzgerald, C. J. Kingsley, and D. S. Umans, *Electric Machinery, Sixth Edition*, 2003.
- [25] F. DeMello and G. W. Walsh, "Reclosing transients in induction motors with terminal capacitors," *Trans. AIEE (Power App.Sys.)*, vol. 80, pp. 1206–1213, 1961.

- [26] T. A. Lipo and A. Consoli, "Modeling and simulation of induction motors with saturable leakage reactances," *IEEE Transactions on Industry Applications*, VOL. IA-20, pp. 180–189, 1984.
- [27] M. V. Cistelecan, F. J. T. E. Ferreira, and M. Popescu, "Three phase tooth-concentrated multiple-layer fractional windings with low space harmonic content," *Energy Conversion Congress and Exposition, IEEE*, pp. 1399–1405, 2010.
- [28] T. A. Lipo, *Analysis of Synchronous Machines, Second Edition*, 2012.
- [29] A. Boglietti, A. Cavagnino, and M. Lazzari, "Computational algorithms for induction-motor equivalent circuit parameter determination—part i: Resistances and leakage reactances," *IEEE transactions on industrial electronics*, VOL. 58, NO. 9, pp. 3723–3733, 2011.
- [30] X. Liang and Y. Luyi, "Harmonic analysis for induction motors," *IEEE CCECE/CCGEIJ, Ottawa*, pp. 172–177, 2006.
- [31] J. Vinay and N. K. Deshmukh, "Determination of iron loss considering spatial harmonics and tooth pulsation effects for cage motor," *ICRERA, Milwaukee*, pp. 348–353, 2014.
- [32] H. Wayne Beaty and L. K. James, *Electric Motor Handbook*, 1998.
- [33] F. J. T. E. Ferreira and A. T. de Almeida, "Induction motor downsizing as a low-cost strategy to save energy," *Journal of Cleaner Production*, pp. 117–131, 2012.
- [34] ———, "Method for in-field evaluation of the stator winding connection of three-phase induction motors to maximize efficiency and power factor," *IEEE Trans. Energy Convers.*, pp. 370–379, 2006.
- [35] C. C. Hwang, S. P. Cheng, and P. L. Li, "An automatic winding layout technique for permanent magnet machines," *IEEE IEMDC*, pp. 766–769, 2007.
- [36] H. Silva, *Simulação e comparação dos parâmetros do circuito equivalente por fase de motores de indução trifásicos com rotor em gaiola de esquilo de diferentes classes de rendimento*. Universidade de Coimbra, 2016.
- [37] M. G. Say, *Performance and design of AC machines*, 1970.

Appendix A

Experimental Magnetizing Curve

The experimental procedures to obtain the magnetizing curve, as function of the air-gap magnetic flux density, are explained in this appendix. Four different classes of motors were tested (IE1 to IE4), in order to verify if there was an accentuated variation between their magnetizing curves.

Initially, it was performed a no-load test on each motor, at different voltages, below and above their rated voltages, and the line current was measured [36]. This way, the magnetizing curves were obtained (fig. A.1).

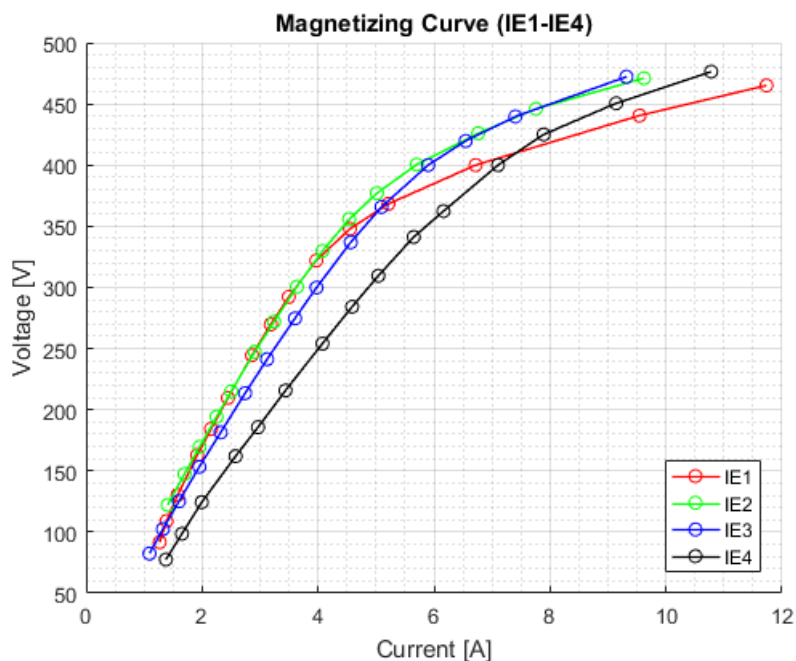


Figure A.1: Magnetizing curves of the 4 motors with different types of classes.

It seems evident that the higher the motor class, the lower is the degree of saturation at the motor's rated voltage. In addition, the magnetizing curves are quite similar, particularly

in the linear region, despite the different saturation degrees, and core steel sheets material and thickness (IE1: 1100-60SP, 0.6 mm of thickness; IE2-4: 550-50SP, 0.5 mm of thickness). The IE4 curve is slightly shifted to the right because of its mechanical friction and ventilation losses are the highest of all tested motors, thus, in this case, more current is absorbed by the rotor.

Next, the magnetizing curve to be chosen should better reflect the effective magnetization current. In other words, the current driven by the rotor and the iron equivalent resistance must be minimal. Therefore, the IE3 motor was chosen, which has the less mechanical and iron losses [36].

Now, the magnetizing curve must be transformed into a B-I curve. Thus, the voltage at the machine's magnetizing branch needs to be determined, in order to calculate the air-gap magnetic field density. The magnetization voltage can be calculated through

$$E_w = |\bar{U}_s - \bar{I}_s \cdot \bar{Z}_s|,$$

where $Z_s = 4.05 + j3,719 (\Omega)$ [36]. The field density B was calculated with BobiSoft. The machine's dimensions were given by the manufacturer (fig. A.2), with an air-gap of 0.6 mm.

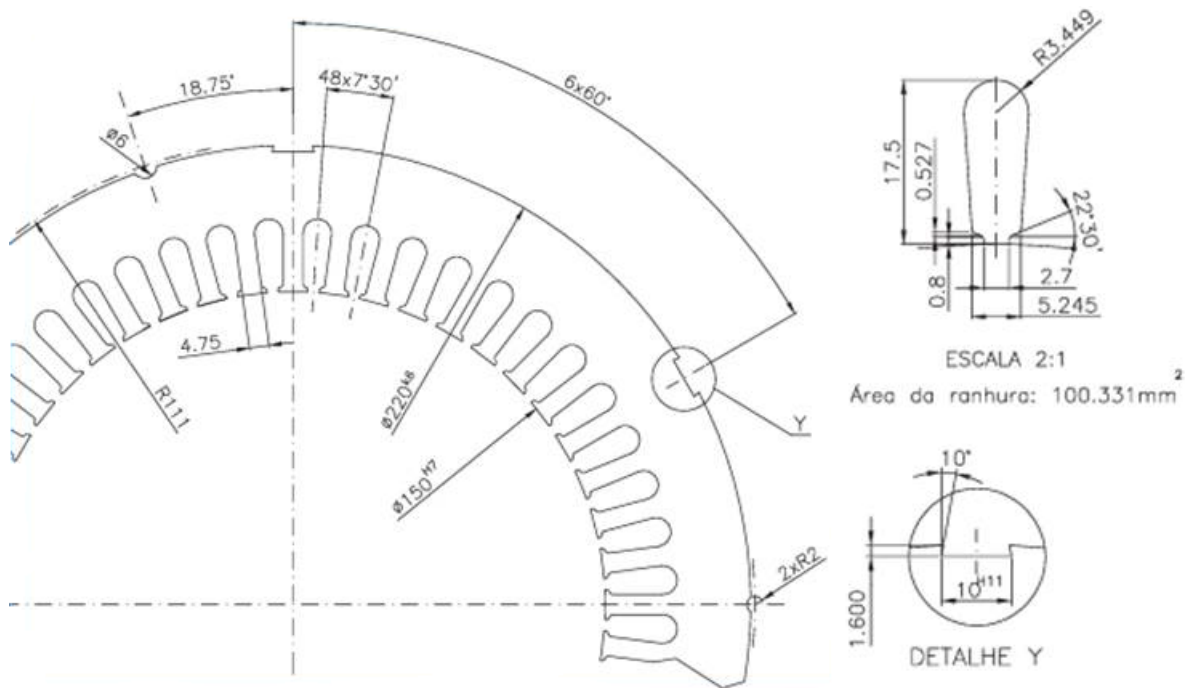


Figure A.2: Stator cross section of the tested motors.

The resultant B-I curve is listed in table A.1. The current can be present in p.u., whose reference is the no-load current at the rated voltage.

Table A.1: Magnetizing and B-I curves

Voltage (V)	Current (A)	E_w (V)	B (T)
472,2	9,318	450,4081	0,777
439,7	7,403	422,3867	0,729
419,7	6,545	404,3933	0,698
400	5,899	386,2041	0,666
365,8	5,096	353,882	0,611
336,9	4,564	326,2262	0,563
299,8	3,974	290,506	0,501
274,7	3,603	266,2737	0,46
241,3	3,123	233,9963	0,404
213,5	2,743	207,085	0,357
181,4	2,321	175,9719	0,304
153,3	1,953	148,7325	0,257
125,1	1,602	121,3534	0,21
102,4	1,326	99,2989	0,171
82,4	1,094	79,84147	0,138
59,5	0,857	57,49574	0,099

Appendix B

Air-gap Magnetomotive Force Analysis

This appendix discusses a general approach to compute the magnetomotive force in the machine's air-gap, valid for any phase number and any type of winding. In this development, it is considered that the armature has Z slots uniformly distributed along the stator core, numerated as $k = 1, 2, \dots, Z$. The subset of slots containing conductors belonging to a given phase, p , are noted as $\{K_p\}$. These conductors are carrying a sinusoidal current $I_w = \sqrt{2}I \sin(\omega t)$.

The analysis is based on the current-sheet concept. In figure B.1 it is represented a slot with N_{ck} conductors belonging to a phase placed at the angle θ_k measured from an arbitrary slot, which is numerated as k_1 . The angular opening of the slot is β , which is supposed to be equal for all slots, and the stator bore radius is defined as R .

The current-sheet of this slot can be defined as follows:

$$A_k(\theta, t) = \begin{cases} \frac{N_{ck} I \sqrt{2} \sin(\omega t)}{\beta} & , \theta \in [\theta_k - \frac{\beta}{2}, \theta_k + \frac{\beta}{2}] \\ 0 & , \theta \notin [\theta_k - \frac{\beta}{2}, \theta_k + \frac{\beta}{2}] \end{cases}$$

The approach starts with the analysis of the classic Fourier sine series for the slot current-sheet curve (eq. B.1):

$$f(x) = \frac{1}{2}a_0 + \sum_{n=1}^{\infty} \left[a_n \cos\left(\frac{n\pi x}{L}\right) + b_n \sin\left(\frac{n\pi x}{L}\right) \right], \quad (\text{B.1})$$

where

$$a_0 = \frac{1}{L} \int_0^{2L} f(x) dx$$

$$a_n = \frac{1}{L} \int_0^{2L} f(x) \cos\left(\frac{n\pi x}{L}\right) dx$$

$$b_n = \frac{1}{L} \int_0^{2L} f(x) \sin\left(\frac{n\pi x}{L}\right) dx$$

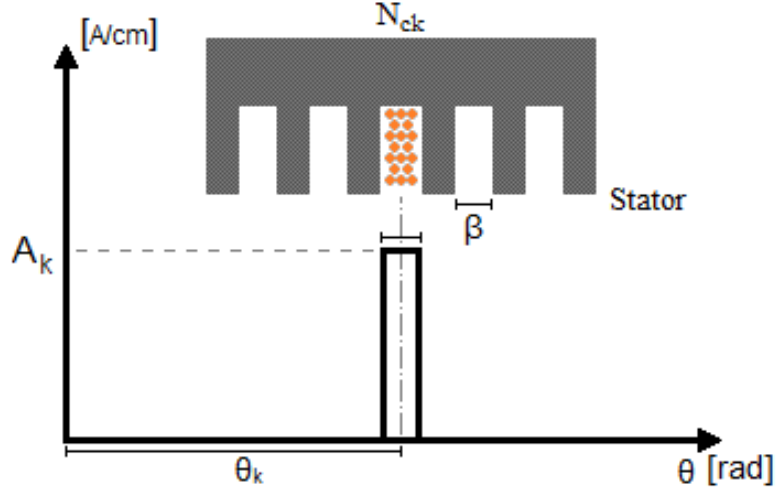


Figure B.1: Current-sheet produced by N_{ck} conductors placed in the slot k .

The Fourier coefficients are calculated as follows:

$$a_n = \frac{1}{\pi} \int_0^{2\pi} A_k(\theta) \cos\left(\frac{n\pi\theta}{\pi}\right) d\theta = \frac{2A_k}{n\pi} \cos(n\theta_k) \sin\left(n\frac{\beta}{2}\right),$$

$$b_n = \frac{1}{\pi} \int_0^{2\pi} A_k(\theta) \sin\left(\frac{n\pi\theta}{\pi}\right) d\theta = \frac{2A_k}{n\pi} \sin(n\theta_k) \sin\left(n\frac{\beta}{2}\right),$$

$$a_0 = \frac{1}{\pi} \int_0^{2\pi} A_k(\theta) d\theta = \frac{\beta A_k}{\pi}.$$

Now, applying the above coefficients to equation B.1:

$$A_k(\theta) = \frac{A_k}{\pi} \left[\frac{\beta}{2} + \sum_{n=1}^{\infty} \frac{2}{n} \cos(n\theta_k) \sin\left(n\frac{\beta}{2}\right) \cos(n\theta) + \frac{2}{n} \sin(n\theta_k) \sin\left(n\frac{\beta}{2}\right) \cos(n\theta) \right]$$

Finally, the simplified generic slot current-sheet expression is obtained (eq. B.2) [27]:

$$A_k(\theta, t) = \frac{N_{ck} I \sqrt{2} \sin(\omega t)}{R\pi} \left[\frac{1}{2} + \sum_{n=1}^{\infty} K_n \cos(n(\theta - \theta_k)) \right], \quad (\text{B.2})$$

where

$$K_n = \frac{2}{n\beta} \sin\left(\frac{n\beta}{2}\right)$$

If the slot's opening is negligible the K_n coefficient tends to 1, the ideal case:

$$\lim_{\beta \rightarrow 0} \frac{2}{n\beta} \sin\left(\frac{n\beta}{2}\right) \stackrel{0}{=} \lim_{\beta \rightarrow 0} \frac{2n \cos\left(\frac{n\beta}{2}\right)}{2n} = 1$$

In fact, the effect of slot opening on the produced MMF is considered through this factor, K_n . It reflects the reduction of the harmonics amplitude by the slots opening. Thus, it would be correct to design stator slots with the biggest opening possible, for the purpose of reducing the harmonic content, but so the fundamental term is reduced.

The next step is to sum the current-sheet produced by all conductors of phase p , resulting in the equation B.3.

$$A_p(\theta, t) = \sum_{k=1}^{K_p} A_k(\theta, t) = \frac{I\sqrt{2}\sin(\omega t)}{R\pi} \left[\frac{1}{2} \sum_{k=1}^{K_p} N_{ck} + \sum_{n=1}^{\infty} K_n \sum_{k=1}^{K_p} N_{ck} \cos(n(\theta - \theta_k)) \right] \quad (\text{B.3})$$

The relationship between the MMF and the current-sheet, produced by a winding phase, is given by equation B.4 [27].

$$\frac{\partial \mathbb{F}_p}{\partial \theta} = A_p(\theta)R \Leftrightarrow \mathbb{F}_p = R \int A_p(\theta) d\theta \quad (\text{B.4})$$

Applying equation B.3 in the expression above it is obtained the MMF produce by the phase p (eq. B.5) [27].

$$\begin{aligned} \mathbb{F}_p(\theta, t) &= \frac{I\sqrt{2}\sin(\omega t)}{\pi} \sum_{n=1}^{\infty} \frac{K_n}{n} \sum_{k=1}^{K_p} N_{ck} \sin(n(\theta - \theta_k)) \\ \mathbb{F}_p(\theta, t) &= \frac{I\sqrt{2}\sin(\omega t)}{\pi} \sum_{n=1}^{\infty} \frac{K_n}{n} C_{np} \sin(n\theta - \theta_{np}), \end{aligned} \quad (\text{B.5})$$

where

$$C_{np} = \sqrt{\left(\sum_{k=1}^{K_p} N_{ck} \cos(n\theta_k) \right)^2 + \left(\sum_{k=1}^{K_p} N_{ck} \sin(n\theta_k) \right)^2},$$

and

$$\theta_{np} = \text{arctg} \left(\frac{\sum_{k=1}^{K_p} N_{ck} \sin(n\theta_k)}{\sum_{k=1}^{K_p} N_{ck} \cos(n\theta_k)} \right),$$

where $\theta_k = \pi k \cdot p/Z$. The winding factors, K_{wn} of the phase p , are calculated through equation B.6. Note that C_{np} is the exact vectorial summation of the MMF produced by each coil of the phase p .

$$K_{wn} = \frac{C_{np}}{2W_s} \quad (\text{B.6})$$

Note that if there is more than one parallel path only the slots/phase/path are considered. The resulting air-gap MMF is then calculated as the vectorial sum of the pulsating MMF of each phase:

$$\vec{\mathbb{F}}_r = \vec{\mathbb{F}}_A + \vec{\mathbb{F}}_B + \vec{\mathbb{F}}_C + \dots + \vec{\mathbb{F}}_N$$

So, developing the above sum it becomes (eq. B.7):

$$\begin{aligned}
\mathbb{F}_r(\theta, t) = & \frac{I_A \sqrt{2} \sin(\omega t + \varphi_A)}{\pi} \sum_{n=1}^{\infty} \frac{K_n}{n} C_{n_A} \sin(n\theta - \theta_{n_A}) + \\
& \frac{I_B \sqrt{2} \sin(\omega t + \varphi_B)}{\pi} \sum_{n=1}^{\infty} \frac{K_n}{n} C_{n_B} \sin(n\theta - \theta_{n_B}) + \\
& \frac{I_C \sqrt{2} \sin(\omega t + \varphi_C)}{\pi} \sum_{n=1}^{\infty} \frac{K_n}{n} C_{n_C} \sin(n\theta - \theta_{n_C}) + \dots + \\
& \frac{I_N \sqrt{2} \sin(\omega t + \varphi_N)}{\pi} \sum_{n=1}^{\infty} \frac{K_n}{n} C_{n_N} \sin(n\theta - \theta_{n_N})
\end{aligned} \tag{B.7}$$

The development above is valid even under unbalanced currents. But, assuming a supply of symmetric currents, $I = I_A = I_B = I_C = \dots = I_N$, the resultant air-gap MMF can be simplified into the following expression (eq. B.8).

$$\begin{aligned}
\mathbb{F}_r(\theta, t) = & \frac{\sqrt{2}I}{\pi} \sum_{n=1}^{\infty} \frac{K_n}{n} [V_1 \cos(n\theta - \omega t) + V_2 \sin(n\theta - \omega t) + \\
& W_1 \cos(n\theta + \omega t) + W_2 \sin(n\theta + \omega t)],
\end{aligned} \tag{B.8}$$

where

$$\begin{aligned}
V_1 &= \frac{1}{2}[C_{n_A} \cos(n\theta_{n_A} + \varphi_A) + C_{n_B} \cos(n\theta_{n_B} + \varphi_B) + C_{n_C} \cos(n\theta_{n_C} + \varphi_C) + \dots + C_{n_N} \cos(n\theta_{n_N} + \varphi_N)]; \\
V_2 &= \frac{1}{2}[C_{n_A} \sin(n\theta_{n_A} + \varphi_A) + C_{n_B} \sin(n\theta_{n_B} + \varphi_B) + C_{n_C} \sin(n\theta_{n_C} + \varphi_C) + \dots + C_{n_N} \sin(n\theta_{n_N} + \varphi_N)]; \\
W_1 &= -\frac{1}{2}[C_{n_A} \cos(n\theta_{n_A} - \varphi_A) + C_{n_B} \cos(n\theta_{n_B} - \varphi_B) + C_{n_C} \cos(n\theta_{n_C} - \varphi_C) + \dots + C_{n_N} \cos(n\theta_{n_N} - \varphi_N)]; \\
W_2 &= -\frac{1}{2}[C_{n_A} \sin(n\theta_{n_A} - \varphi_A) + C_{n_B} \sin(n\theta_{n_B} - \varphi_B) + C_{n_C} \sin(n\theta_{n_C} - \varphi_C) + \dots + C_{n_N} \sin(n\theta_{n_N} - \varphi_N)].
\end{aligned}$$

Equation B.8 can be further simplified with linear combinations of sines and cosines, resulting in the air-gap MMF expression (eq. B.9) [27]:

$$\mathbb{F}_r(\theta, t) = \frac{\sqrt{2}I}{\pi} \sum_{n=1}^{\infty} \frac{K_n}{n} [K_{nd} \sin(n\theta - \omega t + \varphi_d) + K_{ni} \sin(n\theta + \omega t + \varphi_i)], \tag{B.9}$$

Where

$$\begin{aligned}
K_{nd} &= \sqrt{V_1^2 + V_2^2}, \\
K_{ni} &= \sqrt{W_1^2 + W_2^2}, \\
\varphi_d &= \arctg\left(\frac{V_1}{V_2}\right), \\
\varphi_i &= \arctg\left(\frac{W_1}{W_2}\right).
\end{aligned}$$

The factor K_{nd} (direct) is associated with the pulsating MMF harmonics, which create a rotating wave that revolves in the same direction as the rotating magnetic field. On the

other hand, the factor K_{ni} (revers) is associated with the pulsating MMF harmonics, which create a rotating wave that revolves in the opposite direction of the rotating magnetic field. Therefore, considering a three-phase system, the $(6n+1)$ harmonics of the MMF belong to the K_{nd} factor and the $(6n-1)$ harmonics belong to the K_{ni} factor. In table B.1 a representative situation of this fact computed by the program is presented.

Table B.1: Phase winding factors and direct, reverse factors relationship.

Order	Kwd	Kwi	Phase A	Phase B	Phase C
1	0,9577	0,0000	0,9577	-0,9577	-0,9577
2	0,0000	0,0000	0,0000	0,0000	0,0000
3	0,0000	0,0000	0,6533	0,6533	0,6533
4	0,0000	0,0000	0,0000	0,0000	0,0000
5	0,0000	0,2053	0,2053	0,2053	-0,2053
6	0,0000	0,0000	0,0000	0,0000	0,0000
7	0,1575	0,0000	-0,1575	0,1575	-0,1575

An interesting characteristic of these factors is that their product verifies whether the winding pattern is symmetric or not. Thus, if only pure space harmonics exist (case of symmetric winding) the the product of K_{nd} and K_{ni} is zero ($K_{nd} \cdot K_{ni} = 0$), for any harmonic order, [27]. Otherwise, the winding pattern is asymmetrical. This condition is used to validate the winding pattern introduced manually by the user.

Appendix C

Reference Values

This appendix presents the EFACEC's typical values for air-gap induction peak and current density for induction machines. These reference values are used in BobiSoft versions 1.1 and 2.0, and their purpose is to prevent the designing of underrated machines or, in case of a rewinding, to detect atypical winding designs and avoid their replication.

C.1 Air-gap Induction Peak Reference Values

Table C.1 provides the typical values for the air-gap induction peak. They are function of the machine's poles number and rated power (P_r in kW).

Table C.1: Air-gap induction peak reference values (EFACEC manufacturer, 2004).

Poles Number	Function
2	$0,00001 \cdot P_r^2 - 0,0037 \cdot P_r + 0,8041$
4	$0,000003 \cdot P_r^2 - 0,001 \cdot P_r + 0,9036$
6	$-0,0009 \cdot P_r + 1,001$
≥ 8	$-0,0004 \cdot P_r + 1,1004$

In [23][37] the average values for the air-gap induction peak are comprised in the interval $[0,65; 0,82](T)$, which does not deviate much from the listed values.

C.2 Current Density Reference Values

Table C.1 provides the typical values for the current density. They are function of the machine's poles number and rated power (P_r in kW).

Table C.2: Current density reference values (EFACEC manufacturer, 2004).

Poles Number	Function
2	$-0,0362 \cdot P_r + 8,9149$
4	$-0,0221 \cdot P_r + 7,6481$
6	$-0,0220 \cdot P_r + 11,024$
≥ 8	$-0,0157 \cdot P_r + 12,017$

A correction factor, due to the machine's cooling type, is then multiplied to the reference values (table C.3).

Table C.3: Current density correction factors (EFACEC manufacturer, 2004).

Cooling Type	Correction Factor
Open without ventilation	0,66
Closed without ventilation	0,66
Open with auto-ventilation	1,33
Closed with auto-ventilation	1,00 (ref)
Open with forced ventilation	2,33
Closed with forced ventilation	2,00

Appendix D

Rewinding Process

In this appendix, the typical procedures of the rewinding process are explained. The motor here presented is part of a pump in the sewage system of the water company SIMRIA.

The first step of the rewinding process is to verify if the stator's winding is truly damaged. In this case, the three-phases were short-circuited (fig. D.1-1). So, the winding should be removed out of the stator core. Both crowns (winding heads agglomerate) are cut off (the crown with terminals is saved for the original project winding reference). The rewinder uses a collection of steel blades with different angulations, and the correct tool is chosen to minimize the damage to the steel sheets (fig. D.1-2). In this process, one sheet was damaged and removed (fig. D.1-3). During the rewinding task the effective core length may be shortened, thus the machine's performance is slightly affected. Next, the conductors that remained inside the slots are pushed in by hammering them with a steel rod (fig. D.1-4) and then pulled out (fig. D.1 - 5). Depending on the wedges used in the previous winding, the slots may be more or less damaged; in this case were used wooden wedges (fig. D.1-6). Then, the stator is cleaned with diluent sprayed by a high-pressure washer (fig. D.1-7). Sharp stator teeth are smoothed in order to prevent the conductors' insulation to be damaged - this procedure may increase the slots opening (fig. D.1-8). Finally, the stator is painted - this procedure is optional (fig. D.1-9).

At this point, the stator can receive the new winding. First, the original project is extracted from the saved crown, and from it are identified the winding type, the number of parallel groups and conductors, and the coils' number of turns (fig. D.1-10). The diameter of the wire(s) without insulation is measured with the device in figure D.1-11. The slot's insulation paper is then inserted (fig. D.1-12)

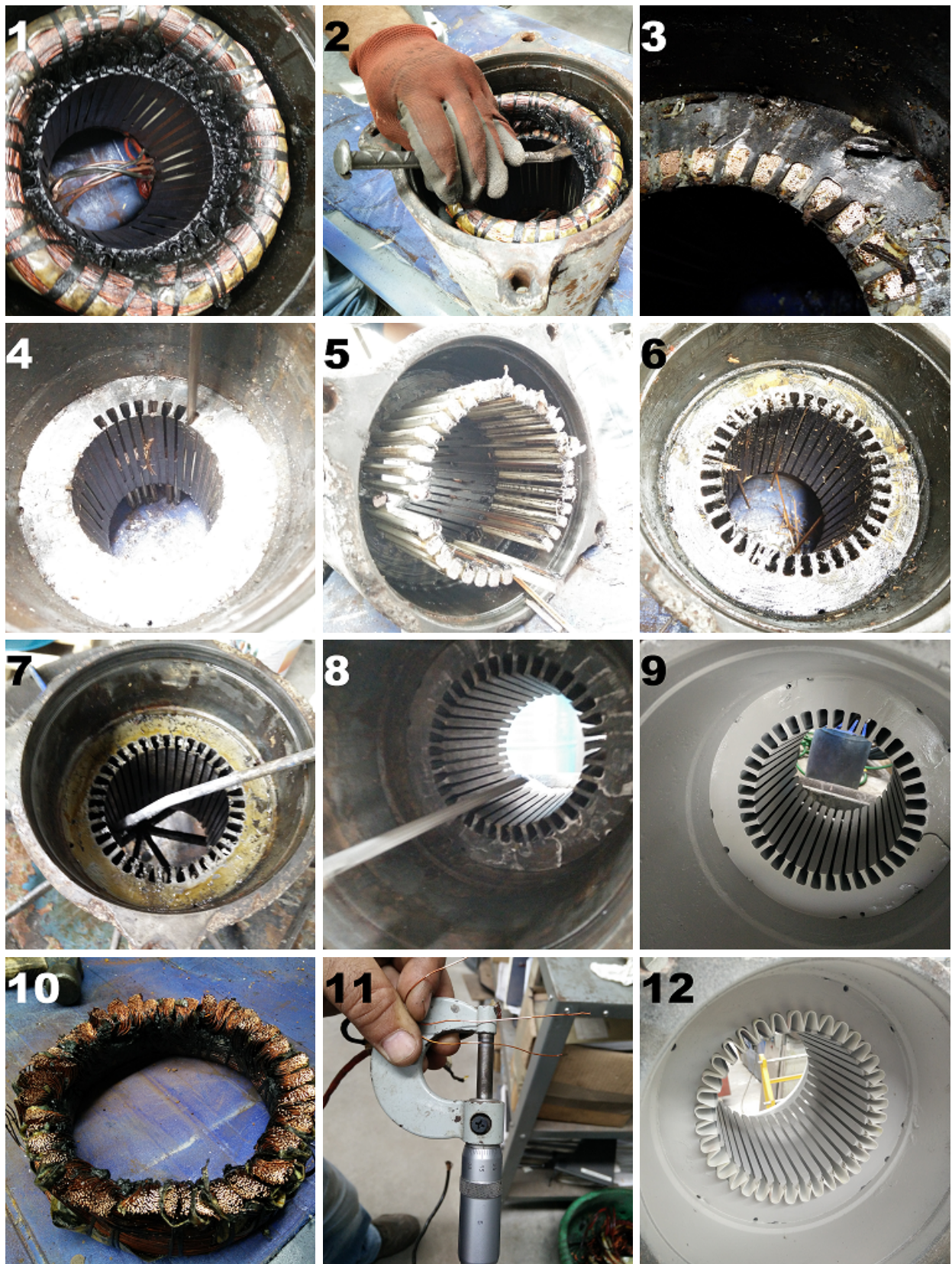


Figure D.1: Rewinding process procedures - Part I.

After gathering all data regarding the original project, the new winding project is made. Due to economic reasons, it is important that a solution is found quickly. This task is almost impossible to perform without a software such as BobiSoft, which means that many

projects are actually copies of previous windings and/or gross mistakes tend to be made.

After deciding what winding is going to be assembled, the coils are made and held by cotton threads (fig. D.2-13). The mold is set with a piece of wire wound with one turn and adjusted to core's slots. Then the coils are inserted and the heads are insulated with a special tape (fig. D.2-14). In double-layer windings the two layers are separated by a piece of insulation paper. All coils placed, the slots are closed with the wedges (fig. D.2-15). Next, the heads are compacted by a plastic hammer and the cotton threads are removed. The heads of the opposite side of the terminals are held with a special synthetic thread (fig. D.2-16). Now, on the terminals' side, the coils in series and parallel groups are arranged properly (fig. D.2-17) and soldered together (fig. D.2-18).

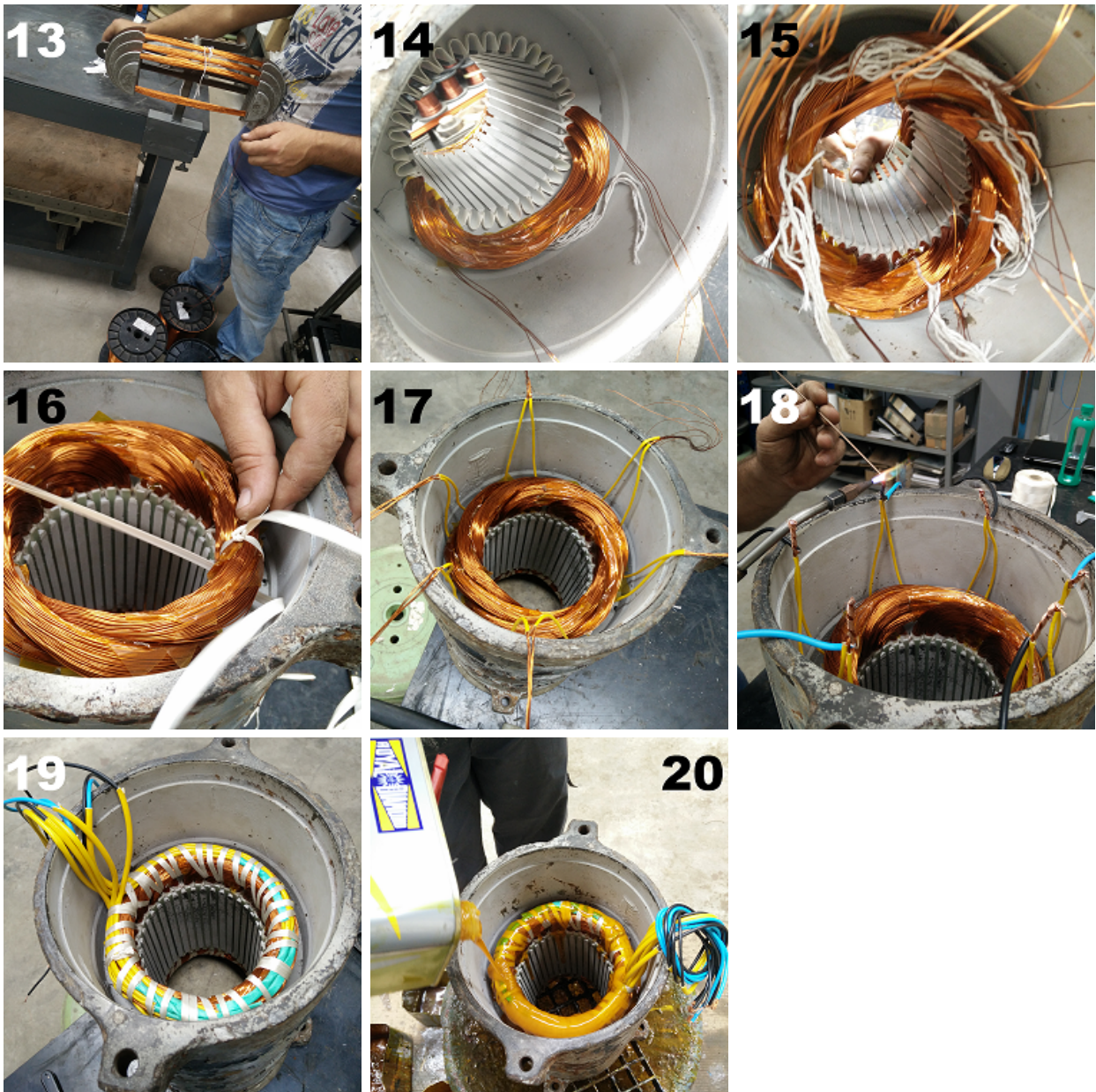
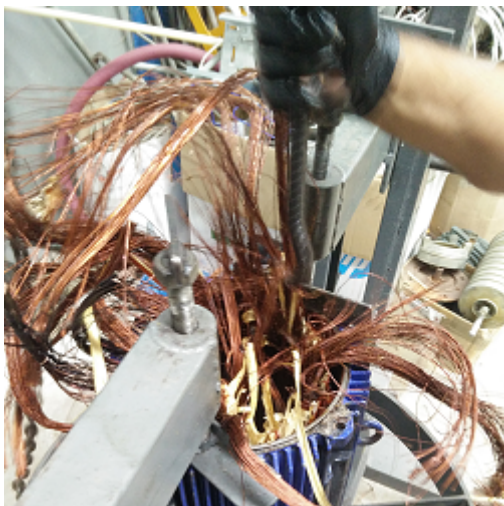


Figure D.2: Rewinding process procedures - Part II.

Then, the machine's terminals are added and the winding resistance is measured as a control test (fig. D.2-19). Finally, a heat resistant varnish is applied, covering the whole winding, in order to glue the heads together, so they become resistant to mechanical vibrations (fig. D.2-20). The motor is dried inside an oven. The rewinding process finishes at this point.

Different procedures of winding extraction are used by this company. The fastest and less damaging one is the mechanical procedure, whereby one crown is cut off and, with a mechanic press, the conductors are pulled out (fig. D.3a). This process submits the stator core to extreme axial forces, thus the applied force should be limited, so the stator is not broken or even pulled out of the frame. If the conductors cannot be mechanically removed, the stator core is heated in order to break the varnish, so the conductors may be removed easily (fig. D.3b). This technique should only be used as a last resource, since heat destroys the laminations' oxide, and consequently the iron losses are highly increased. The quality of the stator core can be evaluated through the core loss test, mentioned in the chapter 4.



(a)



(b)

Figure D.3: Different procedures of the winding's extraction: (a) mechanical procedure, and (b) heating procedure.